NASA/TM—2020-220306

SAE Technical Paper 2019–01–2027
DOT/FAA/TC–19/28

Summary of the High Ice Water Content (HIWC) RADAR Flight Campaigns

Thomas P. Ratvasky
Glenn Research Center, Cleveland, Ohio

Steven D. Harrah
Langley Research Center, Hampton, Virginia

J. Walter Strapp
Met Analytics Inc., Aurora, Ontario, Canada

Lyle E. Lilie
Science Engineering Associates, Inc., Tolland, Connecticut

Fred H. Proctor
Langley Research Center, Hampton, Virginia

Justin K. Strickland and Patricia J. Hunt
Analytical Mechanics Associates, Hampton, Virginia

Kristopher M. Bedka, Glenn S. Diskin, and John B. Nowak
Langley Research Center, Hampton, Virginia

Thaopaul V. Bui
Ames Research Center, Moffett Field, California

Aaron Bansemer
National Center for Atmospheric Research, Boulder, Colorado

Christopher J. Dumont
FAA William J. Hughes Technical Center, Atlantic City, New Jersey

April 2020

NASA STI Program . . . in Profile

Since its founding, NASA has been dedicated to the advancement of aeronautics and space science. The NASA Scientific and Technical Information (STI) Program plays a key part in helping NASA maintain this important role.

The NASA STI Program operates under the auspices of the Agency Chief Information Officer. It collects, organizes, provides for archiving, and disseminates NASA's STI. The NASA STI Program provides access to the NASA Technical Report Server—Registered (NTRS Reg) and NASA Technical Report Server—Public (NTRS) thus providing one of the largest collections of aeronautical and space science STI in the world. Results are published in both non-NASA channels and by NASA in the NASA STI Report Series, which includes the following report types:

- TECHNICAL PUBLICATION. Reports of completed research or a major significant phase of research that present the results of NASA programs and include extensive data or theoretical analysis. Includes compilations of significant scientific and technical data and information deemed to be of continuing reference value. NASA counter-part of peer-reviewed formal professional papers, but has less stringent limitations on manuscript length and extent of graphic presentations.

- TECHNICAL MEMORANDUM. Scientific and technical findings that are preliminary or of specialized interest, e.g., "quick-release" reports, working papers, and bibliographies that contain minimal annotation. Does not contain extensive analysis.

- CONTRACTOR REPORT. Scientific and technical findings by NASA-sponsored contractors and grantees.

- CONFERENCE PUBLICATION. Collected papers from scientific and technical conferences, symposia, seminars, or other meetings sponsored or co-sponsored by NASA.

- SPECIAL PUBLICATION. Scientific, technical, or historical information from NASA programs, projects, and missions, often concerned with subjects having substantial public interest.

- TECHNICAL TRANSLATION. English-language translations of foreign scientific and technical material pertinent to NASA's mission.

For more information about the NASA STI program, see the following:

- Access the NASA STI program home page at http://www.sti.nasa.gov

- E-mail your question to help@sti.nasa.gov

- Fax your question to the NASA STI Information Desk at 757-864-6500

- Telephone the NASA STI Information Desk at 757-864-9658

- Write to:
  NASA STI Program
  Mail Stop 148
  NASA Langley Research Center
  Hampton, VA 23681-2199

NASA/TM—2020-220306

SAE Technical Paper 2019–01–2027
DOT/FAA/TC–19/28

Summary of the High Ice Water Content (HIWC) RADAR Flight Campaigns

Thomas P. Ratvasky
Glenn Research Center, Cleveland, Ohio

Steven D. Harrah
Langley Research Center, Hampton, Virginia

J. Walter Strapp
Met Analytics Inc., Aurora, Ontario, Canada

Lyle E. Lilie
Science Engineering Associates, Inc., Tolland, Connecticut

Fred H. Proctor
Langley Research Center, Hampton, Virginia

Justin K. Strickland and Patricia J. Hunt
Analytical Mechanics Associates, Hampton, Virginia

Kristopher M. Bedka, Glenn S. Diskin, and John B. Nowak
Langley Research Center, Hampton, Virginia

Thaopaul V. Bui
Ames Research Center, Moffett Field, California

Aaron Bansemer
National Center for Atmospheric Research, Boulder, Colorado

Christopher J. Dumont
FAA William J. Hughes Technical Center, Atlantic City, New Jersey

Prepared for the
SAE International Conference on Icing of Aircraft, Engines, and Structures
sponsored by the Society of Automotive Engineers
Minneapolis, Minnesota, June 17–21, 2019

National Aeronautics and
Space Administration

Glenn Research Center
Cleveland, Ohio 44135

April 2020

Acknowledgments

Many people contributed to the success of these flight campaigns and the authors are grateful to all who helped. Special recognition is due to the entire NASA DC–8 team—particularly Adam Webster, Tim Moes, Ken Norlin, and pilots Nils Larson, Wayne Ringelberg, Dave Fedors, and Frank Batteas—for the safe flight operation, to the Federal Aviation Administration (FAA)—particularly Tom Bond, Jim Riley, and Stephanie DiVito—for their sustained financial and technical support, and to Matt Grzych from Boeing and Ben Bernstein from Leading Edge Atmospherics for their forecast support and real-time tactical guidance. Thanks also are extended to NASA Langley Research Center's satellite team, Louis Nguyen and Chris Yost, for adapting to the many changes within this project and to Julie Haggerty from the National Center for Atmospheric Research (NCAR) for implementation of algorithm for predicting high ice water content areas (ALPHA), the data archive, and instrumentation support. The research was sponsored by NASA's Advance Air Vehicles Program through the Advance Air Transport Technology (AATT) and the Aerosciences Evaluation and Test Capabilities (AETC) projects and by the FAA's Aviation Weather Research Program.

This work was sponsored by the Advanced Air Vehicle Program
at the NASA Glenn Research Center

Level of Review: This material has been technically reviewed by technical management.

Available from

NASA STI Program
Mail Stop 148
NASA Langley Research Center
Hampton, VA 23681-2199

National Technical Information Service
5285 Port Royal Road
Springfield, VA 22161
703-605-6000

This report is available in electronic form at http://www.sti.nasa.gov/ and http://ntrs.nasa.gov/

Summary of the High Ice Water Content (HIWC) RADAR Flight Campaigns

Thomas P. Ratvasky
National Aeronautics and Space Administration
Glenn Research Center
Cleveland, Ohio 44135

Steven D. Harrah
National Aeronautics and Space Administration
Langley Research Center
Hampton, Virginia 23681

J. Walter Strapp
Met Analytics Inc.
Aurora, Ontario, Canada L4G 4Y1

Lyle E. Lilie
Science Engineering Associates, Inc.
Tolland, Connecticut 06084

Fred H. Proctor*
National Aeronautics and Space Administration
Langley Research Center
Hampton, Virginia 23681

Justin K. Strickland and Patricia J. Hunt
Analytical Mechanics Associates
Hampton, Virginia 23666

Kristopher M. Bedka, Glenn S. Diskin, and John B. Nowak
National Aeronautics and Space Administration
Langley Research Center
Hampton, Virginia 23681

Thaopaul V. Bui
National Aeronautics and Space Administration
Ames Research Center
Moffett Field, California 94035

Aaron Bansemer
National Center for Atmospheric Research
Boulder, Colorado 80307

Christopher J. Dumont
FAA William J. Hughes Technical Center
Atlantic City, New Jersey 08405

*Distinguished Research Associate

Summary

NASA and the Federal Aviation Administration (FAA) conducted two flight campaigns to quantify onboard weather radar measurements with in situ measurements of high concentrations of ice crystals found in deep convective storms. The ultimate goal of this research was to improve the understanding of high ice water content (HIWC) and develop onboard weather radar processing techniques to detect regions of HIWC ahead of an aircraft to enable tactical avoidance of the potentially hazardous conditions. Two HIWC RADAR campaigns utilized the NASA DC–8 Airborne Science Laboratory equipped with a Honeywell RDR–4000 weather radar and in situ microphysical instruments to characterize the ice crystal clouds. The purpose of this report is to summarize how these campaigns were conducted and highlight key results.

The first campaign was conducted in August 2015 with a base of operations in Ft. Lauderdale, Florida. Ten research flights were made into deep convective systems that included mesoscale convective systems (MCSs) near the Gulf of Mexico and Atlantic Ocean, and Tropical Storms Danny and Erika near the Caribbean Sea. The radar and in situ measurements from these 10 flights were analyzed and correlations defined. Key results included (1) derived relationships between radar reflectivity factor (RRF), ice water content (IWC), and ice particle size distribution (PSD), (2) characterization of HIWC conditions at the –50 °C and other flight levels, and (3) verification of pilot observations, such as low RRF and pitot and total air temperature (TAT) anomalies. This data set also enabled new pilot radar HIWC detection algorithms to be developed and tested.

A second campaign was conducted in August 2018 to test proposed HIWC radar detection algorithms within a new set of storm systems. Seven research flights were conducted from bases of operations in Ft. Lauderdale, Florida, Palmdale, California, and Kona, Hawaii. Flights were made into convective systems over the Gulf of Mexico and into an eastern Pacific tropical system that developed into Hurricane Lane. Using a new, NASA-developed radar processing technique called Swerling, regions of HIWC were identified, and estimates of IWC were produced, at distances up to 60 nmi ahead of the NASA DC–8. Subsequently, the DC–8 flew through these regions to acquire the in situ measurements to verify the radar-based IWC estimates.

Introduction

In 2003, the Federal Aviation Administration (FAA) chartered an Aviation Rulemaking Advisory Committee (ARAC) called the Engine Harmonization Working Group (EHWG) to evaluate the effects of supercooled large drop (SLD) and mixed phase/glaciated conditions on commercial transport power plants (Ref. 1). The EHWG found that most weather-related engine power-loss events on commercial aircraft had occurred in or near deep convective storms. Mason, Strapp, and Chow (Ref. 2) evaluated 46 such power-loss or engine core damage events, and concluded that these events were caused by ingestion of high mass concentrations of ice crystals into the engine core flow path. It was argued that the ingested ice crystals could change phase, refreeze, and block airflow through the engine or shed into the compressor causing damage. Mason, Strapp, and Chow also found that the power-loss events were usually occurring in regions with no significant flight radar echoes (only black or green on pilots radar display) at flight altitude. The lack of radar reflectivity factor (RRF) at flight level was attributed to clouds consisting of small ice crystals, which are inefficient at scattering radar.

The EHWG developed a Mixed-Phase/Glaciated Icing Technology Plan (Ref. 3) that formed the basis for much of the ice crystal icing research and development that followed. Task 2 of this plan was to "conduct flight test research to characterize the high ice water content environments." In 2006, this task initiated the High Ice Water Content (HIWC) Study, which was an international collaboration between

NASA, FAA, Environment Canada, National Research Council Canada (NRC), Australian Bureau of Meteorology, National Center for Atmospheric Research (NCAR), and the Boeing Company. The HIWC Science Plan (Ref. 4) was written to define the aviation and atmospheric science objectives for a flight test campaign to collect cloud in situ data for Task 2. One objective was to investigate the use of onboard weather radar to detect HIWC conditions so that pilots could make tactical decisions to avoid the HIWC environment.

In 2012, the European High Altitude Ice Crystals (HAIC) and HIWC projects initiated collaborations to conduct the flight research defined in the HIWC Science Plan and in the HAIC subproject 2 (SP2) description of work (Ref. 5). Two HAIC–HIWC flight campaigns were conducted using the Service des Avions Français Instrumentés pour la Recherche en Environnement (SAFIRE) Falcon 20 equipped with in situ icing cloud microphysical and icing instruments, the Radar System Airborne (RASTA) 95-GHz research radar, and a Honeywell Primus 660 pilot weather radar. The first HAIC–HIWC campaign was conducted from Darwin, Australia, in January to March 2014. The second HAIC–HIWC campaign was conducted from Cayenne, French Guiana, in May 2015. Thirty-four Falcon 20 research flights were accomplished, which led to a substantial and unique compilation of cloud in situ microphysics data and remote-sensing data from the RASTA radar in HIWC conditions (Refs. 6 to 8). However, the Primus 660 radar on the Falcon 20 only supported noncoherent signal processing and had no means to record the fundamental radar measurements. As a result, only display radar imagery was acquired. Leroy et al. (Ref. 7) commented that the Falcon–20 pilot radar indicated relatively low reflectivity (no echoes or green echoes, i.e., RRF less than 32 dBZ) at flight level during the 2014 HAIC–HIWC flight campaign. Analysis of the Primus 660 radar display bus recordings and ice water content (IWC) measured by a Science Engineering Associates Inc. (SEA) Isokinetic Probe (IKP2) was performed to derive histograms of the reflectivities for three ranges of total water content (TWC). Approximately 94 percent of RRFs observed in HIWC conditions during the 2014 HAIC–HIWC flight campaign were displayed as black (dBZ < 22) and green (22 < dBZ < 32) (Figure 1). These results were consistent with commercial pilot reports (Ref. 2) and confirmed the observations in Leroy et al. (Ref. 7).

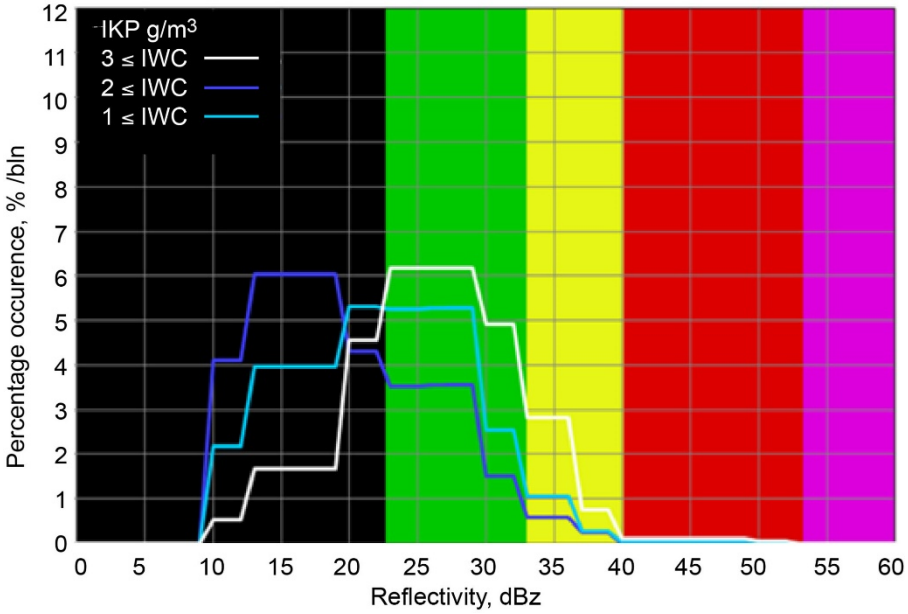

Figure 1.—Percentage of occurrence per bin of radar reflectivity from the 2014 HAIC–HIWC flight (Darwin, Australia). Radar display data courtesy of Service des Avions Français Instrumentés pour la Recherche en Environnement (SAFIRE).

After the 2014 HAIC–HIWC flight campaign, NASA and the FAA initiated plans to conduct the HIWC RADAR flight campaign with the primary objective to quantify onboard weather radar measurements with in situ measurements of high concentrations of ice crystals found in deep convective storms. The effort resulted in two HIWC RADAR flight campaigns. The purpose of this report is to summarize how these campaigns were conducted and highlight key results.

HIWC RADAR I Flight Campaign (2015)

The primary goal of this flight campaign was to collect unprocessed radar return signals (i.e., in-phase and quadrature (I&Q) sample data) and cloud microphysics data in HIWC conditions in order to subsequently develop correlations between the radar data and the levels of IWC. A secondary goal was to collect additional cloud microphysical data at the –50 °C flight level in order to augment the characterization data collected through the HAIC–HIWC flight campaigns.

NASA DC–8 With High Ice Water Content Instrumentation

The NASA DC–8 (NASA 817) is an Airborne Research Laboratory used for Earth, atmospheric, and space science missions. The DC–8 is a four-engine, jet aircraft with a range of 5,400 nmi (10,000 km), a ceiling of 41,000 ft (12,500 m), and a maximum flight duration of 12 hr. The aircraft has been highly modified to accommodate a wide variety of flight research experiments. These modifications include special power systems, viewports, wing pylons, window blanks, and fuselage panels to mount instruments and probe heads to measure in situ and remote conditions. These capabilities met or exceeded the HIWC RADAR flight campaign requirements.

Prior to the 2015 flight campaign, the DC–8 was configured with the Honeywell RDR–4000 radar and cloud microphysical in situ instrumentation. Identification and location of these sensors are shown in Figure 2.

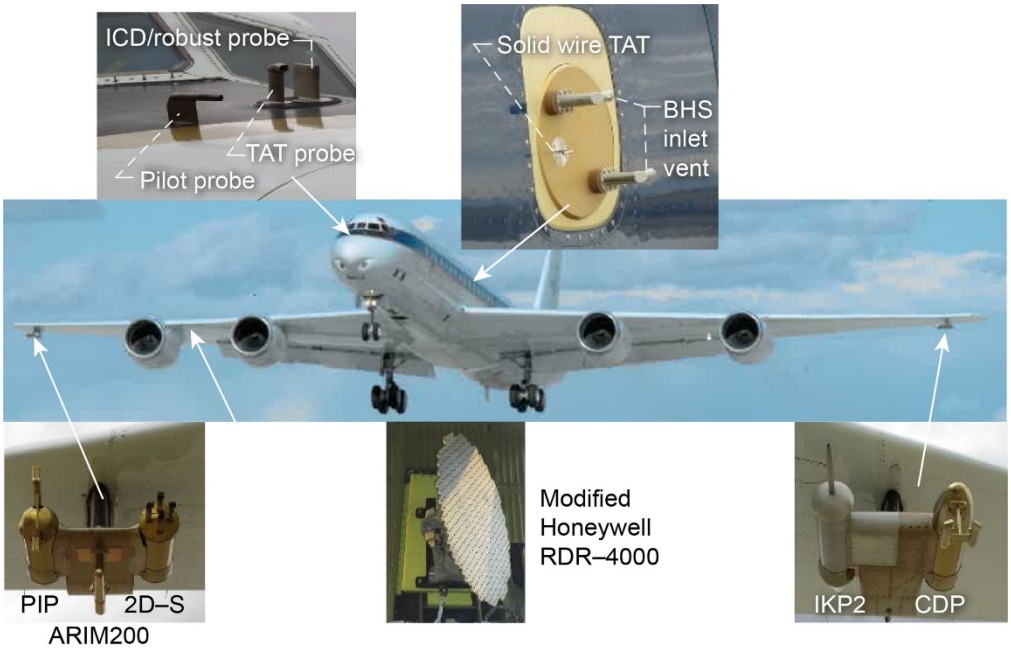

Figure 2.—General layout of DC–8 with high ice water content (HIWC) radar instrumentation. 2D–S is two-dimensional stereo (SPEC). BHS is background humidity system. CDP is Cloud Droplet Probe (Droplet Measurement Technologies (DMT)). IKP2 is Isokinetic probe two (Science Engineering Associates, Inc.). PIP is Precipitation Imaging Probe (DMT). TAT is total air temperature.

The Honeywell RDR–4000 was a commercial-off-the-shelf X-band weather radar with a 24-in. antenna, pedestal, and radar processor that interfaced to a DC–8 multifunction display unit. A Honeywell CertPort Recorder was interfaced with the radar processor to record the unprocessed radar I&Q data. NASA data systems processed the I&Q data and provided customized displays of the radar data to the NASA radar researchers and DC–8 crewmembers (Figure 3). Radar data was displayed at four horizontal levels: 2,500 ft above flight level, at flight level, and 5,000 and 10,000 ft below flight level.

The primary ice cloud parameters of interest for the radar correlations were the bulk IWC and the ice-cloud particle size distribution (PSD). To that end, the icing instruments used on the DC–8 were the same as those used on the SAFIRE Falcon 20 during the HAIC–HIWC flight campaigns. Bulk IWC was measured with the IKP2, a TWC[1] evaporator probe (Refs. 9 and 10). The IKP2 was mounted on the left wing pylon at the inboard position. To support the IKP2 TWC calculations, a background humidity system (BHS) using a LI-COR® LI–840A was mounted in the cabin, but sampled the ambient air through an inlet on a left side window blank near station 530. The PSD was measured using the following three instruments:

- DMT[2] Cloud Droplet Probe (CDP–2) (2 to 50 μm)
- SPEC[3] 2D–S imaging probe (10 to 1,280 μm)
- DMT Precipitation Imaging Probe (PIP) (100 to 6,200 μm)

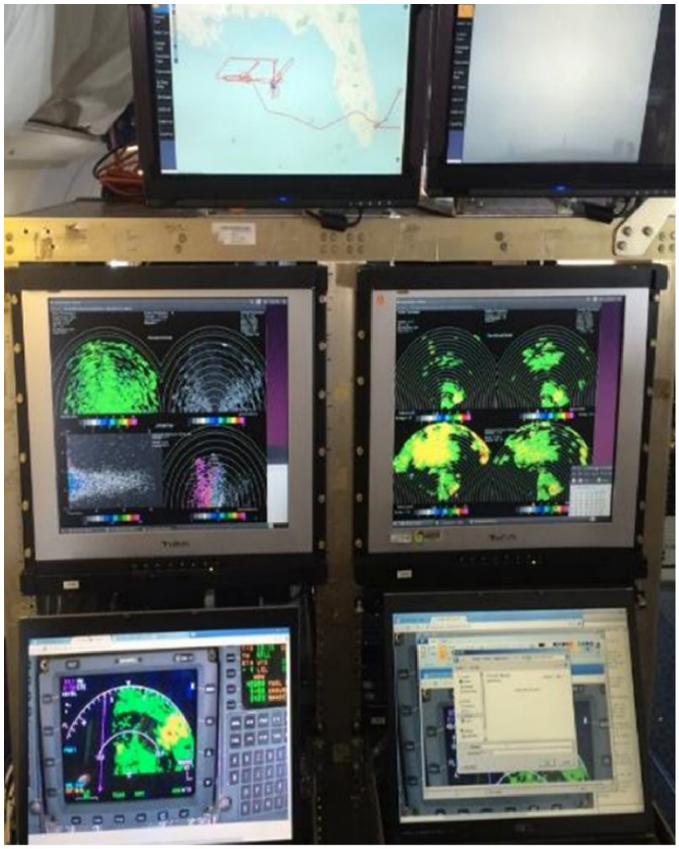

Figure 3.—High ice water content (HIWC) radar displays.

[1]TWC is the total condensed water content, equal to the sum of the cloud liquid water and IWC.
[2]Droplet Measurement Technologies.
[3]Stratton Park Engineering Company.

The CDP–2 was mounted on the left wing pylon, outboard position, on a canister nosecone. The two-dimensional stereo (2D–S) was mounted on the right wing pylon, inboard position, and the PIP was mounted on the right wing pylon, outboard position. All particle probes used antishattering tips to reduce measurements of shattered ice artifacts (Refs. 11 and 12).

Additional measurements were made to support the primary and ancillary analyses. For example, airspeed, air temperature (total and static), pressure altitude, Global Positioning System (GPS) location, etc., were all provided by DC–8 standard systems. A research total air temperature (TAT) probe and a SEA TWC hot-wire probe were also mounted on the fuselage nose in order to investigate localized ice concentration factors and potential for TAT and pitot probe anomalies. Likewise, a solid-wire TAT probe with no deice heating was mounted to the same window blank as the BHS to provide a baseline TAT that would not be subject to TAT anomalies. An L3 Technologies Stormscope WX–1000E was also integrated on the DC–8 to provide lightning detection information to the flight crew and research team.

2015 Campaign Planning and Operations

After the decision was made to use the NASA DC–8 for the 2015 flight campaign, coordination meetings with NASA's Armstrong Flight Research Center, Langley Research Center, and Glenn Research Center, as well as the FAA were held to discuss instrumentation requirements, base of operations and operating area, flight sampling strategies, concepts of operations, and mission rules and flight procedures. The following sections provide the details on these topics.

Base of Operations and Operating Area

Potential basing options were considered with respect to the NASA DC–8 availability and funding levels. Climatology studies of the Caribbean, Gulf of Mexico, and eastern Pacific were conducted. With these constraints, it was determined that a 3-week, 80-flight-hr campaign could be conducted in August 2015 within the United States and its territories. The original plan was to conduct the campaign from Aguadilla, Puerto Rico. However, due to persisting drought conditions in the Caribbean during July 2015, the base of operations was reset to Fort Lauderdale-Hollywood International Airport (KFLL) in Ft. Lauderdale, Florida, just weeks prior to the start of the deployment.

The operating area (Figure 4) was defined to coordinate with air traffic control (ATC) flight information regions (FIR) and to establish diplomatic clearances to transit airspace not controlled by U.S. Government. The range and endurance of the DC–8 enabled the boundaries of the operating area to be quite extensive. Research operations were limited to convective systems that developed over water.

Sampling Strategies

The HIWC RADAR flight sampling strategies were similar to the HAIC–HIWC flight campaigns as outlined in Strapp et al. (Ref. 4). Generally, flights would be in large convective storms, ideally in mesoscale convective systems (MCSs) that developed over the ocean, with cloud tops reaching the tropopause and cloud diameters larger than about 100 nmi. In comparison to deep continental convection, oceanic systems are known to have lower likelihood of hail and lightning, and weaker updraft velocities. The longer lifetimes and larger cloud extent of MCS compared to isolated convection provide more persistent targets and longer cloud traverse lengths that are useful for the cloud characterization effort. To be consistent with the sampling strategy recommended by the EHWG as outlined in the HIWC Science and Technical Plan and the HAIC–HIWC sampling, data were collected in level transects at altitudes associated with the following atmospheric temperature intervals: –50±5, –40±5, –30±5, and –10±5 °C (Figure 5).

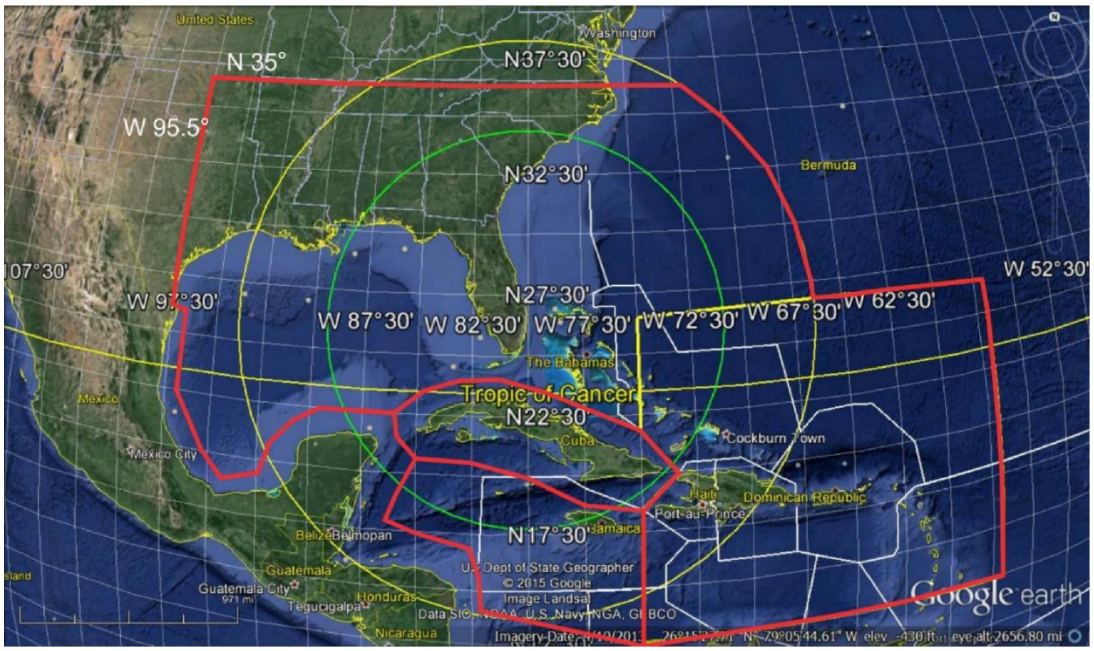

Figure 4.—Operating area for high ice water content (HIWC) campaign HIWC RADAR I (red outline) flight information regions (FIR) indicated by white lines. Ring radii: green 500 nmi, yellow 750 nmi. Map data ©2015 Google, U.S. Dept. of State Geographer, Image Landsat, Data: SIO, NOAA, U.S. Navy, NGA, GEBCO.

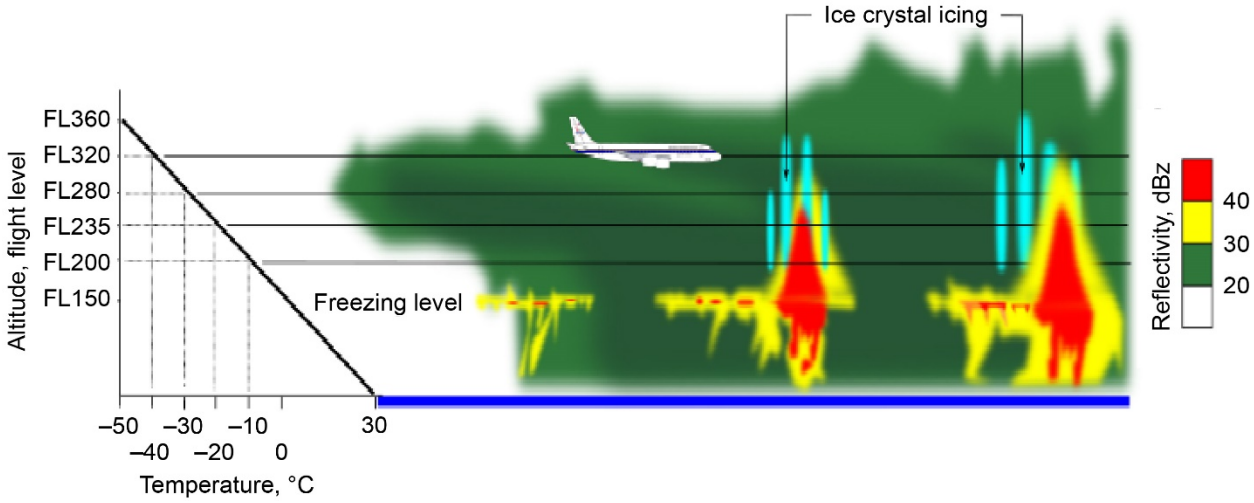

Figure 5.—Vertical cross-sectional schematic of radar reflectivity factor (RRF) with high ice water content (HIWC) RADAR sampling altitudes superimposed.

Concept of Operations

Based on the HAIC–HIWC flight campaign experience and climatological studies of the southeast Florida operating area, the science team anticipated convective system life cycles as short as 1 to 2 hr. To increase readiness, several teams were formed to perform specific functions. These teams included a forecast team, ground guidance team, flight team, instrumentation team, and science team. Although there were no time of day limitations for performing research flights on the DC–8, a 20-yr climatology of satellite-based anvil detections (Ref. 13) determined that deep convection maximized over the Gulf of Mexico near noon local time. As a result, only daytime operations were anticipated and executed. Table I shows the typical daily schedule for a flight duration of 5 hr.

As can be seen from Table I, the forecast team started early in the daily cycle to review weather models and current satellite and radar data and prepare the weather brief for the science team and a DC–8 navigator. Concurrently, the DC–8 ground crew and instrumentation team performed preflight checks. If convective systems were favorable and the aircraft and instruments were "Go," the flight plan commenced as shown in Table I. If the weather systems were not developing, the flight was put on "Hold" and the forecast and ground guidance teams continued to monitor the weather for other opportunities.

During flight operations, the ground guidance team monitored current conditions (Figure 6) and recommended waypoints for the DC–8 to traverse across areas of deep convection (Figure 7), while avoiding areas of intense lightning. The pilots would typically fly along the recommended traverse, but adjusted the course based on radar separation rules (see Mission Rules and Flight Procedures). The flight team reported via a "chat" communication channel to the ground guidance team the variations in IWC during the traverse. Subsequent waypoints and flight levels were identified and discussed via chat.

To facilitate the forecast and ground guidance teams, the NASA Langley satellite group developed products specific for the HIWC RADAR campaign (Ref. 14). These products utilized Geostationary Operational Environmental Satellites (GOES) with GOES–13 data updated every 15 min. The products were used for preflight briefings and uploaded to the DC–8 for onboard decision-making.

After a flight was completed, the whole team debriefed the results of the flight. The forecast team provided an outlook for the next day. The operations plan for the next day was then disseminated to the team.

TABLE I.—NOMINAL FLIGHT DAY SCHEDULE

Planned takeoff		8:00
Planned flight time, hr		5
Start	End	Times are local eastern daylight time (EDT) (UTC–4)
4:00	5:00	Forecasting/nowcasting team preparations
5:00	6:00	Launch ground crew and science team show time Weather team brief navigator
5:45		Go/delay decision announced
6:00	6:00	Flight plan filed
6:30	7:00	Crew brief
7:30	7:30	Flight team onboard; doors closed
8:00		Taxi/takeoff
8:00	13:00	Ground team provide updates to DC–8
13:00		Landing
13:30	14:30	Postflight operations debrief
15:00	17:00	Postflight review of data and Instrument postflight checks
16:00	17:00	Weather forecast for next day
17:00	17:00	Announcement of start time of next day operations

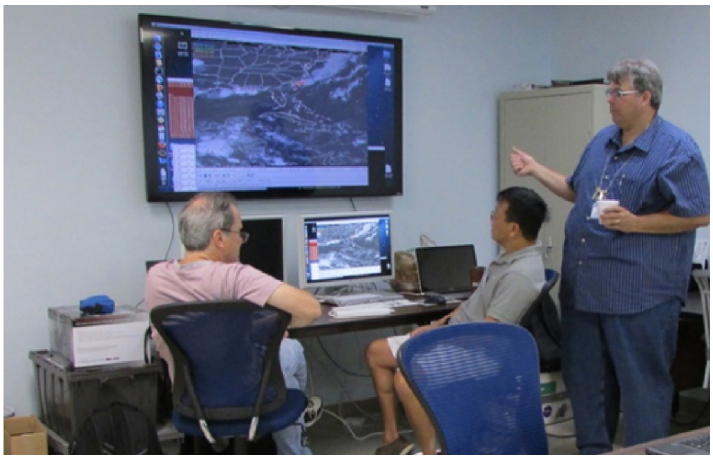

Figure 6.—Ground guidance and briefing room at Fort Lauderdale-Hollywood International Airport (KFLL).

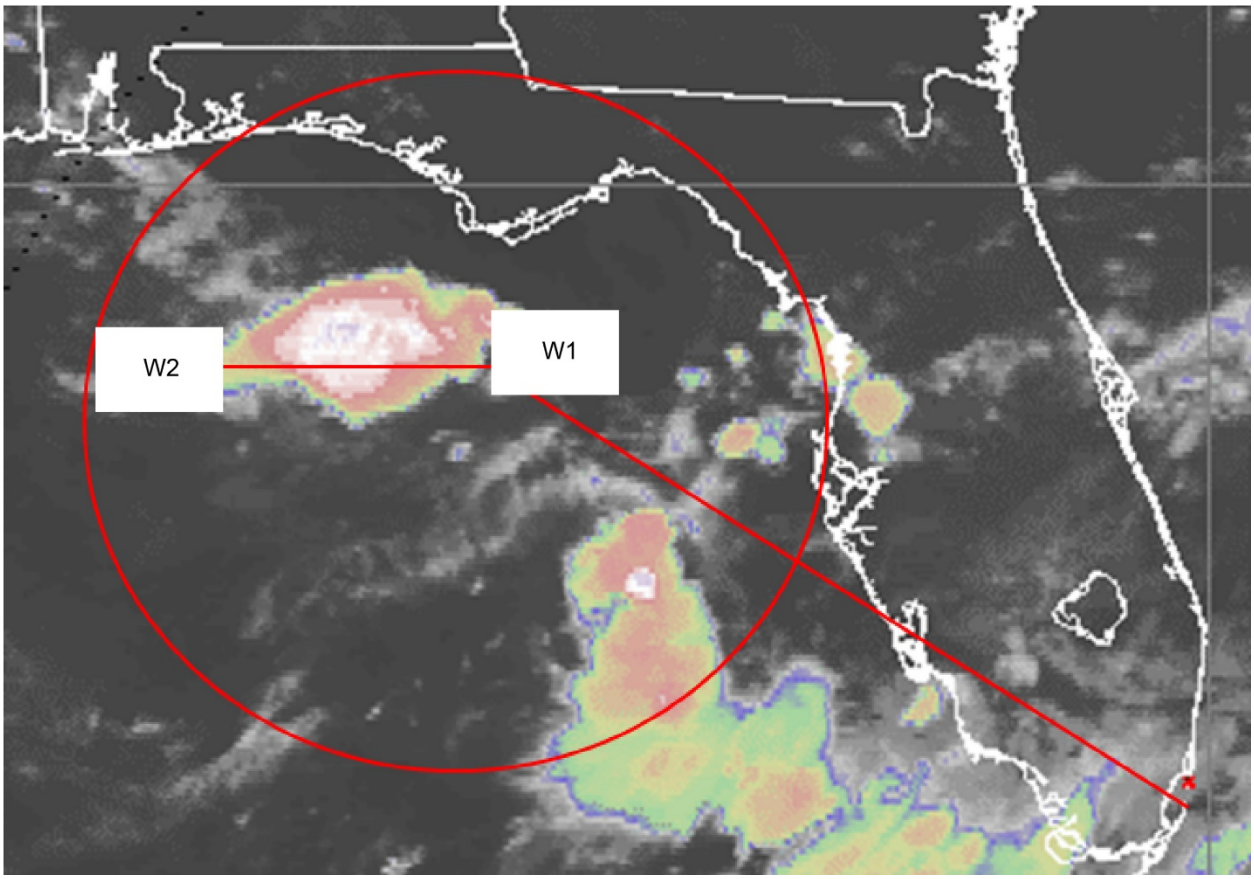

Figure 7.—Region of interest from infrared (IR) satellite image with waypoints for first traverse. White areas represent deepest convection with cloud tops near tropopause.

Mission Rules and Flight Procedures

As part of the campaign planning, NASA Armstrong developed mission rules and procedures to mitigate hazards of flying in and around convective systems. The mission rules included

- A 20-nmi lateral separation from red radar returns (>40 dBZ) at flight level as indicated on the pilots weather radar display. This could be reduced to 10 nmi if the potential for hail was unlikely.
- No flights over red radar returns with less than 5,000 ft of vertical separation.
- A 10-nmi lateral separation from yellow radar returns (30 to 40 dBZ) at flight level as indicated on the pilots weather radar display. This could be reduced provided (1) no potential for hail, (2) turbulence was less than continuous moderate, and (3) lightning was not a hazard.
- Aircraft commander had the final authority to judge acceptability of the weather conditions.
- Engine igniters were on during icing operations.
- Engine throttles were staggered, and every 5 min, the engine powers were cycled to vary engine fan speeds (N1) by 5 to 10 percent for 20 to 30 s to shed small amounts of ice that may have built up within the engines.
- If either of the aircraft indicated airspeed (IAS) readings were unreliable due to pitot icing, the cloud traverse could be continued at the discretion of the aircraft commander.
- If all IAS readings were unreliable, ground speed was monitored. Based on the aircraft commander discretion, the cloud traverse could be continued up to 10 min and then conditions exited as soon as practicable.

"Go/No-Go" criteria included the aircraft minimum equipment list and research instrumentation such as the Honeywell RDR–4000 CertPort and data systems, and the IKP2 and PSD probes. The mission rules and Go/No-Go criteria were reviewed prior to each flight.

Summary of HIWC RADAR I Flights

The NASA DC–8 and test team were on site at KFLL from August 10 to 30, 2015. In that time, ten research flights were conducted into a variety of deep convective storms over the Atlantic Ocean, Gulf of Mexico, and the Caribbean Sea. Table II provides a synopsis of the ten flights including dates, times, locations, types of storms, and notable events. Figure 8 shows the flight tracks for all of the flights. Flight tracks and time histories of altitude, temperature, and TWC for the research flights made in the 2015 deployment are provide in the Appendix A. Time histories are limited to the periods in the clouds of interest. The infrared (IR) satellite image in these figures is for a nominal time during the in-cloud operation and does not show the progression and decay of the storm during the flight. The storm cloud movement and evolution can be viewed at the Langley satellite website (Ref. 14). Note the color scheme in the IR satellite images was adjusted for each flight so that the white-to-pink transition indicated the tropopause temperature for that day. This temperature is indicated on the IR images as "TROPT/PINK = XX" on the image. The deepest convection will have cloud top temperatures colder than at the tropopause as indicated by the white and purple color levels.

TABLE II.—HIGH ICE WATER CONTENT (HIWC) RADAR I FLIGHT SUMMARY

HIWC flight no.	Flight date	Time, UTC	Storm location	Type of storm[a]	Notable events[b]
1	8/12/2015	14:28–19:46	Atlantic seaboard	Oceanic MCS	Initial HIWC buildup
2	8/13/2015	14:52–19:31	Bahamas	Oceanic MCS	First TAT anomaly
3	8/14/2015	13:01–18:40	Bahamas and Gulf of Mexico	Oceanic MCS	TAT anomaly
4	8/16/2015	13:15–20:28	Gulf of Mexico	Oceanic MCS	First pitot anomaly
5	8/19/2015	12:06–19:27	Louisiana coast	Coastal MCS	Pitot anomaly
6	8/21/2015	13:56–21:04	Texas and Louisiana coast	Coastal MCS	No pitot or TAT anomalies
7	8/23/2015	11:20–19:41	Eastern Caribbean	Tropical Storm Danny	Multiple pitot failures
8	8/26/2015	11:06–20:55	Eastern Caribbean	Tropical Storm Erika	Multiple pitot failures
9	8/27/2015	12:03–22:01	Eastern Caribbean	Tropical Storm Erika	Multiple pitot failures
10	8/28/2015	13:20–21:07	South of Dominican Republic	Tropical Storm Erika	Multiple pitot failures

[a]MCS is mesoscale convective system.
[b]TAT is total air temperature.

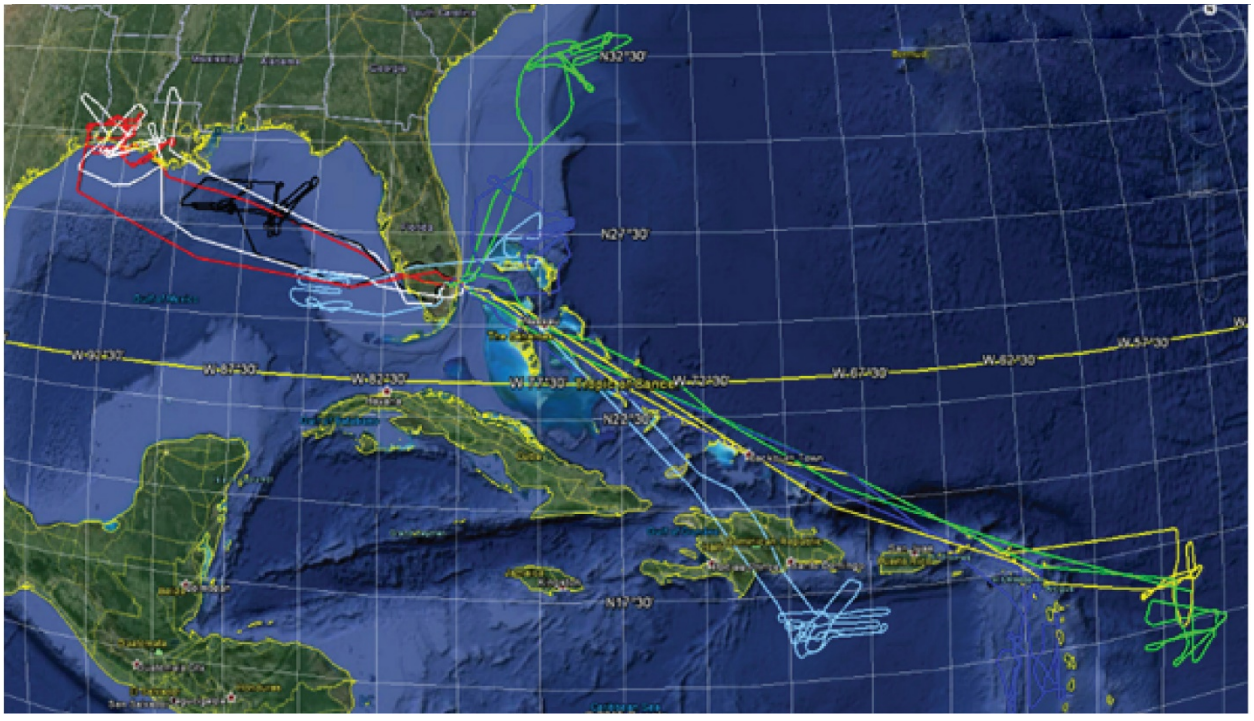

Figure 8.—Flight tracks from the 2015 high ice water content (HIWC) flight campaign HIWC RADAR I. Map data ©2015 Google and INEGI, U.S. Dept. of State Geographer, Data: SIO, NOAA, U.S. Navy, NGA, GEBCO.

Flights 1 to 6: Mesoscale Convective System (MCS) Examples

The HIWC Flight 1 was a "buildup" flight since this was the first intentional flight with the DC–8 into HIWC conditions. This entailed limiting the exposure time to HIWC to confirm acceptable engine performance was met. Flight sampling was conducted at an altitude of 37,000 ft (–50 °C) where IWC was less than 0.1 g/m^3 and at 29,000 ft (–30 °C) where IWC ranged from 0.25 to 1.5 g/m^3 with periods less than 2 min where IWC increased up to 2.0 g/m^3. The radar and icing instruments performed normally and no engine performance issues were observed.

The HIWC Flights 1 to 6 were in MCSs that developed over the Atlantic Ocean and the Gulf of Mexico. These storm systems tended to have smaller areas of deep convection, more lightning, and were in areas of increased air traffic (particularly Flights 5 and 6), all of which adversely affected the data sampling by limiting the traverses that could be taken. The flight and ground guidance teams worked diligently to identify waypoints for datalines that would traverse through areas of deep convection, but provide safe distances from lightning and other hazards. The ground guidance team had the benefit of rapid satellite updates, while the flight team had the benefit of the onboard radar and the Stormscope (which provided real-time lightning information). In this way, the flight sampling tracks were adjusted based on the current conditions.

To exemplify some challenges from the first six flights, Figure 9 shows a portion of the Flight 5 flight track overlaid on IR satellite imagery. The white and purple areas indicate the coldest tops and deepest convection where the potential for higher concentrations of ice crystals was expected, and generally experienced, in the HAIC–HIWC flight campaigns. After the first track on the east side of the storm, the team decided it was better to work on the west side to avoid higher concentrations of lightning and any potential for hail. The ATC was unable to approve a route around the northern edge due to other air traffic. Consequently, the DC–8 flight track skirted around the southern edge of the storm.

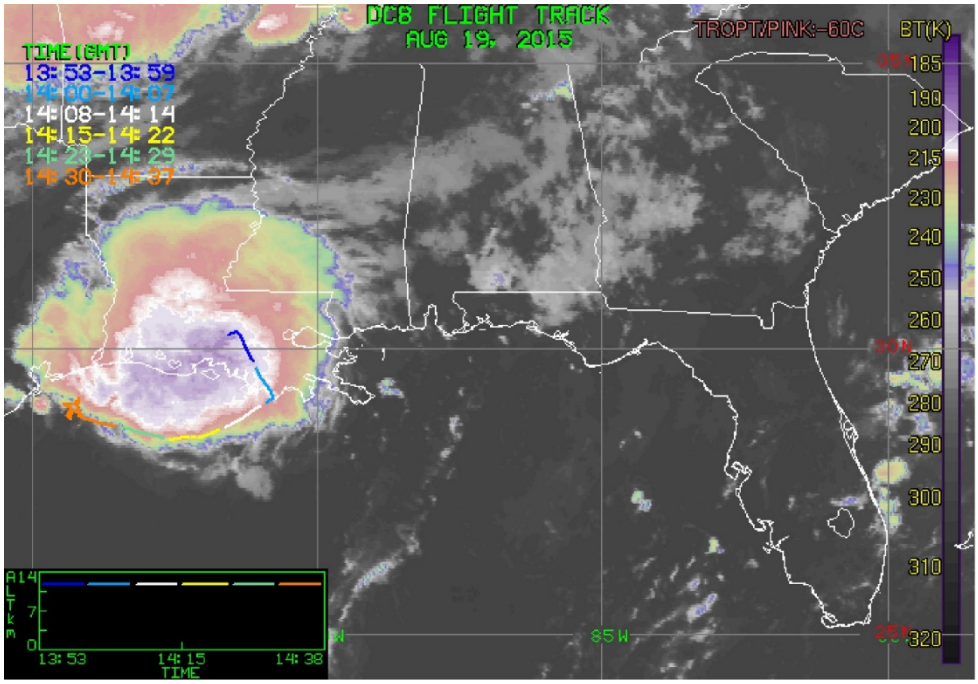

Figure 9.—Flight track from Flight 5 with infrared (IR) satellite. Purple area indicates cold tops and deepest areas of convection. TROPT/PINK = tropopause temperature.

Subsequent flight tracks were altered either due to ATC direction or due to the potential for hail inferred from the National Oceanic and Atmospheric Administration (NOAA) Next Generation Weather Radar (NEXRAD). Figure 10 illustrates an extended flight track to the north away from the area of interest due to instructions from ATC to allow other traffic to pass through the area. This figure also illustrates the decaying nature of the storm 3 hr after the data in Figure 9 was taken.

Another notable characteristic of the storms sampled in these first six flights was the relatively short extent of HIWC regions. Figure 11 illustrates the repeatability of TWC during the course of four parallel tracks at the same altitude during Flight 4 (August 16, 2015). As can be seen in Figure 11 as well as in the Appendix A, the duration between the rise and fall of TWC is typically less than 6 min, which equates to about 40 nmi in length scale.

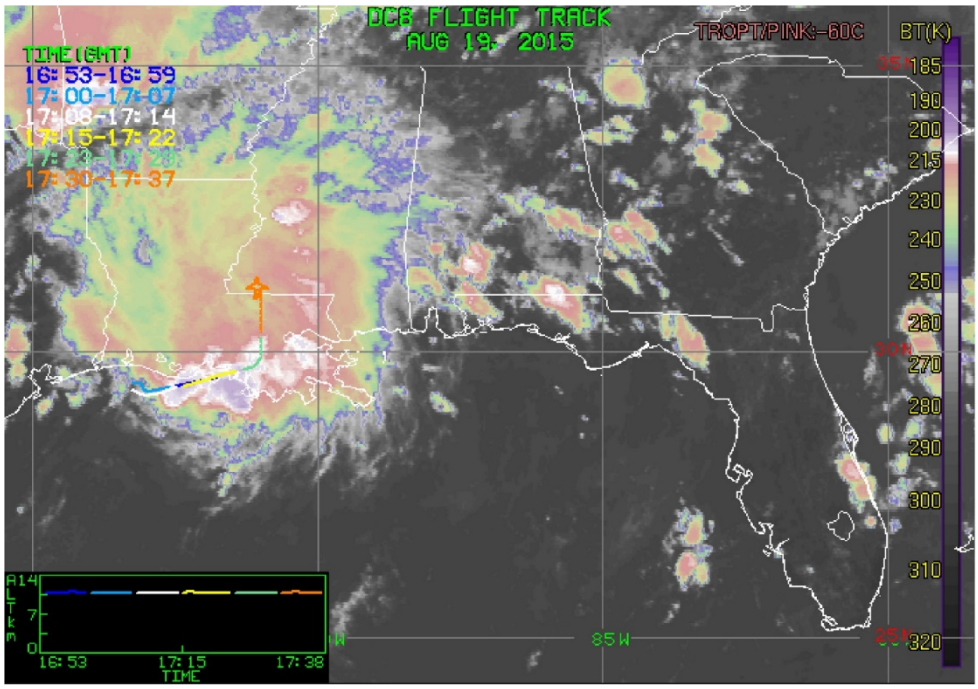

Figure 10.—Flight track from Flight 5 with infrared (IR) satellite. Northerly track extended due to the air traffic control (ATC). TROPT/PINK = tropopause temperature.

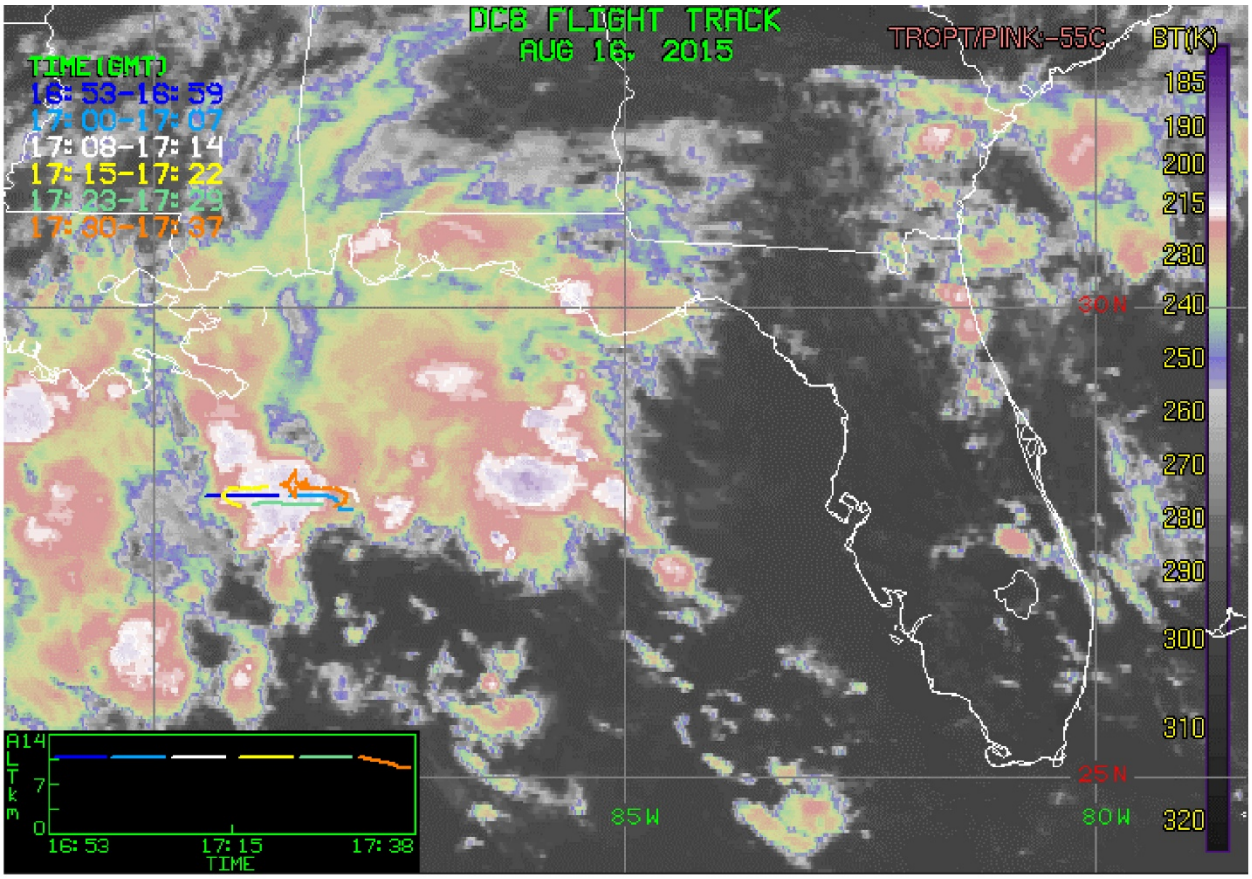

(a)

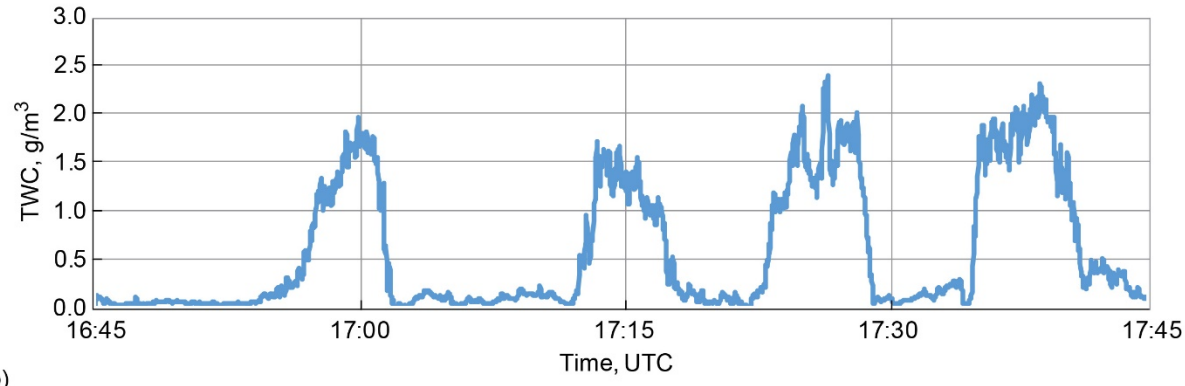

(b)

Figure 11.—Four parallel repeat flight tracks from August 16, 2015. (a) Flight track. TROPT/PINK = tropopause temperature. (b) Isokinetic Probe (IKP2) total water content (TWC) time history.

Flights 7 to 10: Tropical Storm Examples

During the latter part of the 2015 deployment, tropical systems began to develop off the west coast of Africa, and were monitored by the forecast team as they moved westward. Although these tropical systems were over 2,500 nmi to the southeast of KFLL, it was anticipated that they would provide long fetches of HIWC at the desired higher flight altitudes (e.g., –50 °C). They also were anticipated to have a lower likelihood of lightning than in some of the previous flights, as well as less ATC restrictions due to being over the ocean. Therefore, after Flight 6 near the Louisiana coast was completed, the team decided to focus on these tropical systems as they tracked westward toward the Caribbean.

The HIWC Flights 7 to 10 (see Appendix A) were conducted in Tropical Storms Danny and Erika. As anticipated, these storms provided good HIWC data collection without the need for course deviations due to lightning and/or conflicting air traffic. However, in-cloud course deviations were still often necessary to maintain lateral separation from higher RRF at flight level and to allow iced pitot probes to recover.

As an example of the flights into tropical storms, Figure 12 shows the Flight 10 track overlaid on the IR satellite imagery. The initial waypoint was at the northwest part of the storm and the first data track (shown in light blue) was across the northern side of the storm to an eastern point. The second data track (also shown in light blue) was a back track from east to west with a 10-nmi offset distance to the south of the Track 1. As the aircraft approached the western side of the storm during Track 2, the pilots deviated to the north to avoid higher reflectivity associated with a significant cell embedded in the tropical storm.

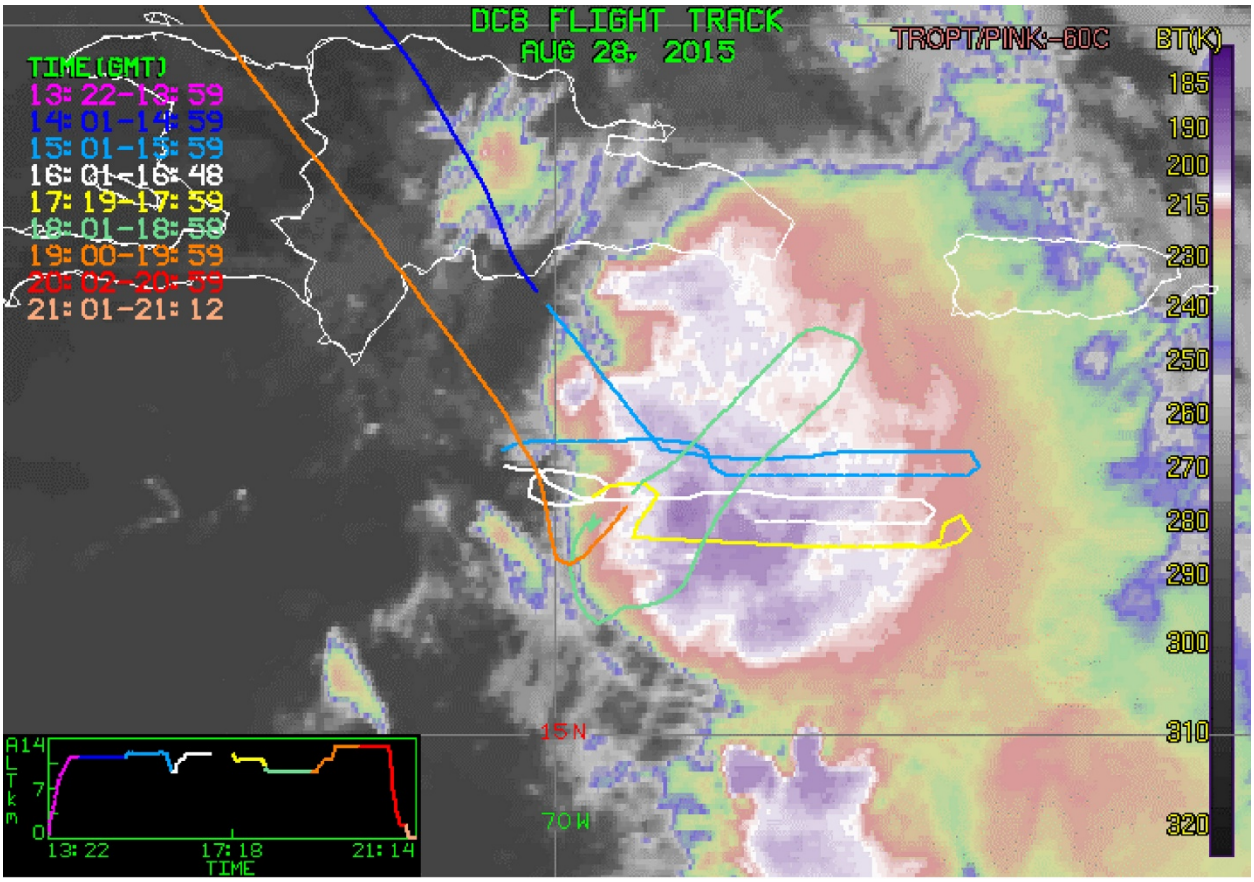

Figure 12.—Flight track from Flight 10 with infrared (IR) satellite (Tropical Storm Erika). White and purple areas indicate cold tops and deepest areas of convection. TROPT/PINK = tropopause temperature.

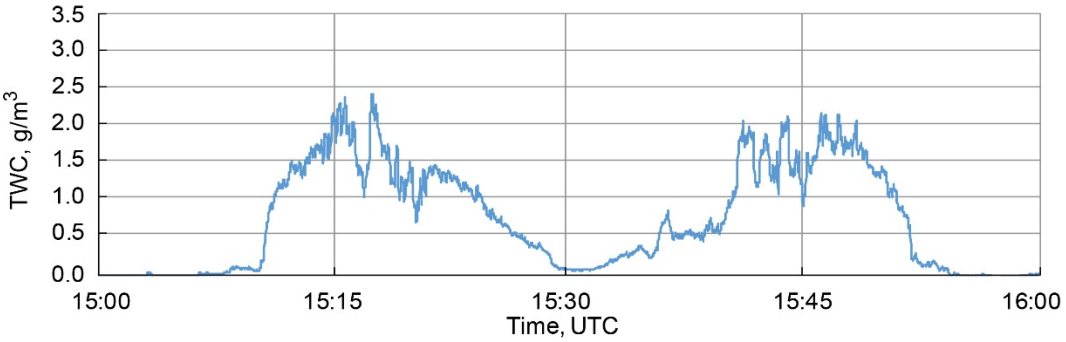

Figure 13.—Isokinetic Probe (IKP2) total water content (TWC) time history during two parallel repeat flight tracks from August 28, 2015.

As anticipated, the tropical storms provided longer exposures to HIWC conditions and the clouds were generally deeper than storms sampled earlier in the campaign, enabling more sampling at higher (colder) altitudes. Figure 13 shows the TWC from Tracks 1 and 2 through the northern side of the tropical storm. Note the sharper rise and fall in TWC on the western side (15:10 to 15:15 and 15:47 to 15:52 UTC) and more gradual rise and fall of TWC on the eastern side (15:20 to 15:30 and 15:30 to 15:40 UTC). The storm was tracking westward, so the outflow was generally toward the east. The variation and magnitude of the TWC was remarkably repeatable in these two flight segments. The duration of the TWC "bubble" was about 20 min, which equates to about 130 nmi in length scale. The higher TWC during these passes corresponded to the closer proximity of the DC–8 to the higher reflectivity areas displayed on the pilot's weather radar.

Pitot Probe Icing

One type of in-service event that has occurred during flights in HIWC conditions is pitot probe icing (Ref. 15). During the HIWC RADAR I campaign, pitot icing occurred in 6 of 10 flights. The DC–8 has two pitot probes, one for each air data computer (ADC) to provide airspeed indications to the pilot and copilot. The ADC airspeed was also provided to the research data systems to calculate TWC, static temperature, PSD, etc. Consequently, airspeed errors needed to be minimized during the flights and then corrected in postflight data processing. When pitot anomalies occurred, the flight crew followed the mission rules and monitored alternate sources of airspeed and ground speed, or departed the cloud and descended to clear the pitot probes of icing and restore the airspeed measurements. Figure 14 shows a 15-min departure to the outside of the western side of cloud and descent to clear the pitot probe icing.

Two types of airspeed errors were found. In some cases, the pitot probe icing caused abrupt changes to the airspeed. In other cases, the airspeed changed slowly, which was more difficult to detect. Both types were experienced during the first two tracks of Flight 10 as illustrated in Figure 15. At 15:15 UTC, the airspeed dropped precipitously from 200 to about 80 m/s for a minute, recovered briefly, dropped again for another minute, and then recovered again. At about 15:31 UTC, the IAS slowly increased, but not so much as to attract attention. Only after the quick drop at about 15:53 UTC was it clear that the airspeed was still unreliable and a descent was initiated to clear the ice blockage from the pitot probes. Postflight analyses using ground speed, track, and prevailing winds were used to correct the time periods when the IAS was unreliable.

Figure 16 shows ice that formed on the backside of one of the DC–8 pitot probes after encountering HIWC conditions. This ice formed by ice crystals impinging and melting on the warm pitot probe. This liquid water flowed along the pitot to the colder surface and refroze. Although the ice shown in this figure does not cause the pitot anomaly, it illustrates the melting and refreezing process that is thought to be occurring inside the pitot probe inlet.

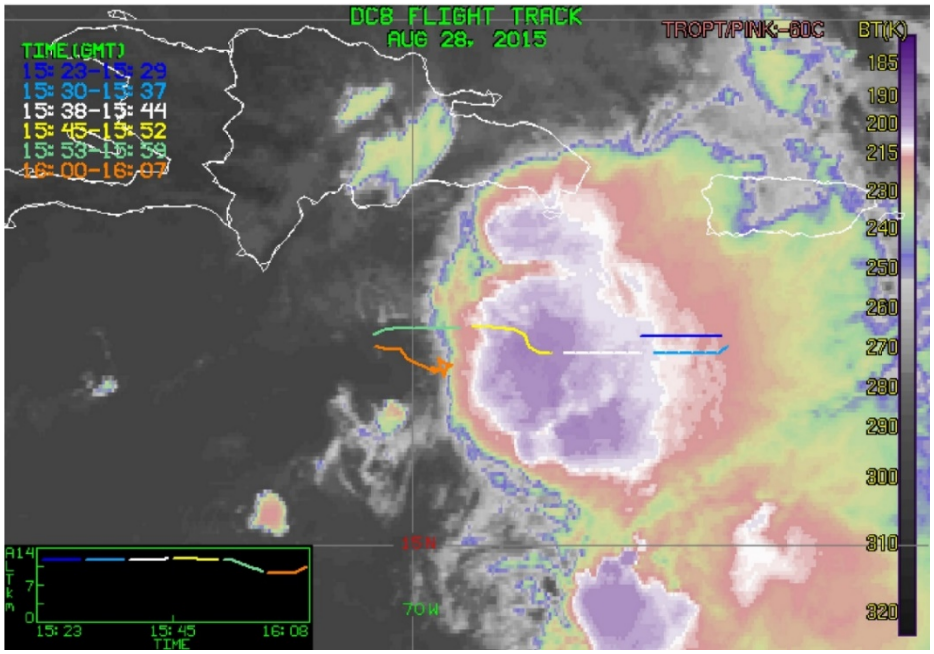

Figure 14.—Flight track showing departure from cloud and descent to clear pitot probe icing. Green and orange segments corresponded to flight in clear sky conditions required to clear pitot probe icing. TROPT/PINK = tropopause temperature.

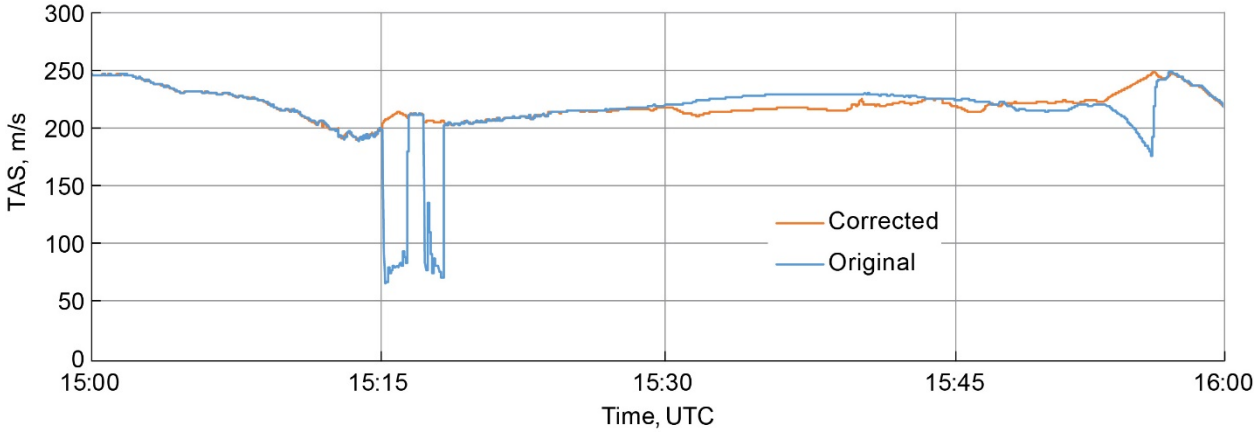

Figure 15.—Airspeed anomalies caused by pitot probe icing (August 28, 2015). Original and corrected true airspeed (TAS).

Figure 16.—Ice on backside of DC–8 pitot probe after flight in high ice water content (HIWC).

Total Air Temperature Probe Icing

Anomalies of the TAT probe have also occurred during in-service engine power-loss events (Refs. 2 and 16). Similar to the pitot probe icing, TAT anomalies are thought to result from high concentrations of ice crystals melting and refreezing in the probe inlet, redirecting ice into the sensor cavity, where it accumulates and partially melts near the temperature sensor. This ice-water bath causes the temperature probe to sense a near 0 °C reading instead of the actual TAT. During this flight campaign, a research TAT probe model known to experience TAT anomalies while in service was installed on the DC–8 nose ahead of the windscreen and next to an SEA TWC hot-wire probe measuring the local ice concentrations. Figure 17 shows the ice that formed on the backside of the research TAT probe after flight through HIWC conditions. Figure 18 illustrates the differences in TAT measurements between the research TAT probe and the DC–8 TAT probe. Note how the research TAT probe readings rose to near 0 °C during the anomalies. The DC–8 TAT probe did not appear to exhibit TAT anomalies during the flight campaign. It was a different model and design from the research TAT probe, and was mounted further forward and on the bottom of the DC–8 nose.

Figure 17.—Ice on backside of total air temperature (TAT) probe after flight in high ice water content (HIWC).

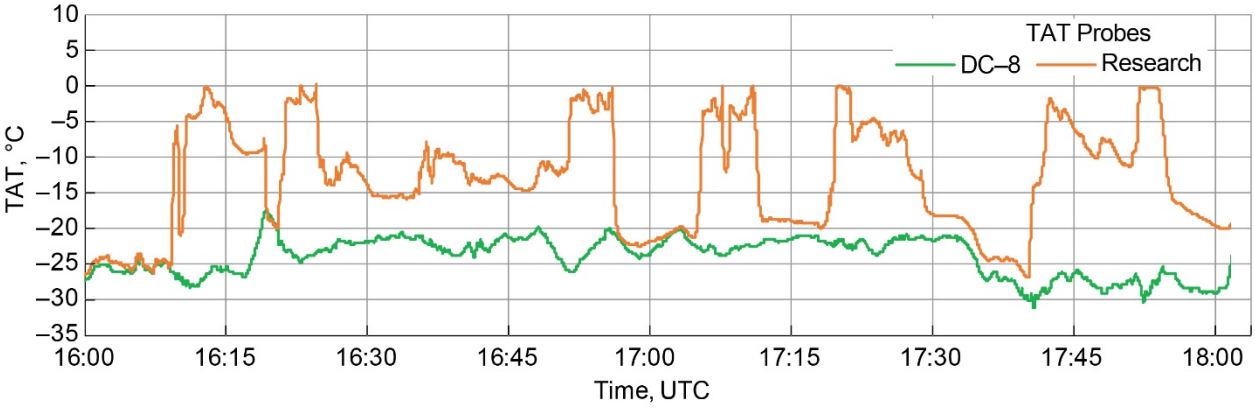

Figure 18.—Total air temperature (TAT) anomalies from research TAT probe (August 14, 2015).

Key Findings and Lessons Learned From HIWC RADAR I Flights

Post campaign, the meteorological and radar data sets were processed into quality-controlled data sets of TWC, PSDs, RRF, and other supporting parameters. The processing methods for the TWC have been described in Strapp et al. (Ref. 9) and Davison et al. (Ref. 10). The PSD processing has been described in Leroy et al. (Ref. 6). The radar I&Q data processing is described in Harrah et al. (Ref. 17). These data sets were archived by NCAR (Refs. 18 and 19), and made available to the science team for further analyses.

A primary result of HIWC RADAR I was the correlation of RRF to IWC. Figure 19 presents the X-band RRF measured at the nearest practical range ahead of the airplane versus the IWC measured by the IKP2 for all flights made in the 2015 campaign for static air temperature (SAT) < –15 °C. The broad scatter and near vertical segments in the IWC to RRF relationship suggest that RRF alone is not sufficient to estimate IWC levels since a wide range of IWC are related to a narrow range of RRF. Harrah et al. (Ref. 17) parsed this data into temperature bins to see if that improved the correlations, but concluded it did not alter the finding significantly, even for radar measurements at close range. Moreover, longer-range radar measurements caused larger standard deviations in the correlations, rendering the correlations impractical for operational purposes.

This RRF to IWC correlation data was essential for recommendations made by the European Organization for Civil Aviation Equipment (EUROCAE) working group (WG) 95 Long-Range Awareness Subgroup and Radio Technical Communications for Aeronautics (RTCA) subcommittee (SC) 230 WG–8 in their report entitled, “Feasibility Study: Weather Radar for Ice Crystal Detection” (Ref. 20). The group concluded that current airborne weather radar systems do not have sufficient performance to meet the operational targets defined by the aircraft manufacturers. This conclusion was based on the RRF and temperature data available to current airborne weather radar systems. This finding compelled NASA radar researchers to look for other methods to identify HIWC at long ranges, and led to the HIWC RADAR II flight campaign.

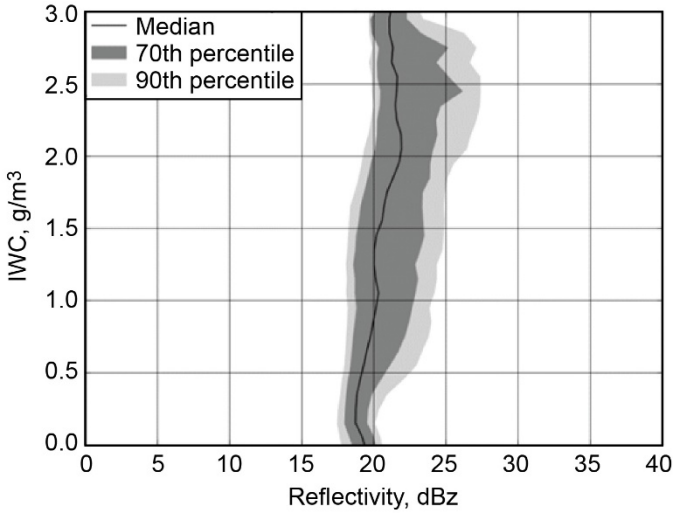

Figure 19.—Correlation of radar reflectivity factor (RRF) to ice water content (IWC) from Isokinetic Probe (IKP2) for all 2015 flights and static air temperature (SAT) < –15 °C (Ref. 17).

Another key result was the contribution of TWC and particle size data, particularly at the –50 °C flight level, for an ongoing assessment of the Title 14 Code of Federal Regulations (CFR) Part 33 Appendix D and corresponding European Aviation Safety Agency (EASA) certification specification (CS) 25 Appendix P. The results of the assessment are summarized in Strapp et al. (Ref. 21), an FAA Technical Report to be published in 2020. The IKP2 TWC data from deep convective clouds sampled in the 2014 and 2015 HAIC–HIWC and the first HIWC RADAR flight campaigns were combined to provide maximum and 99th percentile TWC values as a function of distance scale. Additionally, particle size data from the three flight campaigns were combined to provide PSD and mass size distributions (MSDs), and median mass diameters in HIWC conditions, using techniques described in Leroy et al. (Ref. 6). The first HIWC RADAR campaign provided the majority of the data at –50 °C, which was considered the highest priority temperature interval for the assessment.

Numerical weather modeling of several of the 2015 data sets was also conducted. Numerical modeling is useful for (1) model validation, (2) providing detail and understanding to the characterization of HIWC events, and (3) providing high-resolution data sets containing wind fields, RRF, and temperature, as well as cloud, precipitation, and ice fields that can be used to refine HIWC detection and warning systems.

Results from modeling the MCS encountered in Flight 5 were presented by Proctor et al. (Ref. 22). The numerical simulation showed that large volumes of ice crystals can be percolated into the uppertroposphere by regenerating convective plumes associated with a long-lasting MCS. Cloud material carried by the upper-level outflow from these plumes merge to form a large overhanging canopy that contain large areas of HIWC. Large concentrations of ice crystals accumulate over time due to the duration of the system and the presence of weak environmental wind shear. The HIWC conditions developed in spite of the updrafts being unsteady, nonadiabatic, and transitory. The model simulations also confirmed that HIWC can occur with low values of RRF due to the large number of small ice particles. The highest concentrations of ice water were located between 20,000 to 35,000 ft, within and downshear of updraft plumes.

Many of the pilot observations from in-service events (Ref. 2) and research flights (Ref. 23) were also confirmed during this campaign. Specifically, there were a number of encounters when IWC exceeded 1 g/m^3 with RRF less than 30 dBZ (black or green displayed on the pilot radar). The DC–8 pilots observed “streaming water” on the windscreen under certain HIWC conditions. Moreover, as previously indicated, both TAT and pitot anomalies were experienced when the probes were subjected to specific IWC and temperature conditions. More detailed studies on these events are needed to understand threshold conditions that trigger the anomalies, and the localized flow-field and particle concentration effects.

This flight campaign provided lessons learned, which were implemented in the follow-on campaign. As previously discussed, the occurrence of pitot probe icing can cause operational and research data issues that require exiting the icing cloud to restore the measurement and the need for substantial postflight airspeed corrections. This led to a requirement for an “auxiliary” pitot probe with higher deicing heat to be installed prior to a second campaign. Other icing instrumentation issues found during the campaign included significant lags in the BHS, occasional fogging of the PIP and CDP–2 optical windows, stuck diodes, and at times, frequent image buffer decompression issues on the PIP. Most of these were managed in postprocessing, but the corrections were labor and time intensive. The takeaway was to add further instrumentation and procedures to mitigate these issues in the second campaign.

Lastly, the operational lessons learned included the value of tropical storms in providing persistent sources of HIWC, and the importance of the DC–8’s range in reaching such storms at significant distances from a base of operation. Tropical Storms Danny and Erika provided data at longer distance

scales and colder temperatures than any of the MCSs that were flown in the first campaign. The tropical storms also had less lightning and hail threats, and less air traffic, which enabled fewer diversions from planned flight tracks. Another valuable lesson was that the DC–8 engines were able to safely operate in the HIWC conditions encountered when using the mission rules and mitigation procedures.

HIWC RADAR II Flight Campaign (2018)

As stated in the previous section, radar and cloud in situ data from HIWC RADAR I (2015) campaign were analyzed to determine that RRF alone was insufficient to identify regions of HIWC ahead of the aircraft. However, as a result of the analysis, several radar techniques were considered to be promising candidates for further research. These techniques included multifrequency radar, dual-polarimetric (dual-pol) radar, and a new NASA-developed process called Swerling that related the index of dispersion (I_D) in X-band RRF to IWC (Ref. 17). As discussed in Reference 17, the name "Swerling" is attributed to Peter Swerling, a radar theoretician from the 1950s who developed statistically "fluctuating target" scattering models, but the HIWC discrimination process is very different from his statistical target detection models. The Swerling process was a leading candidate based on test cases from the HIWC RADAR I campaign and was recognized as an easier retrofit to the current transport aircraft fleet.

A second flight campaign was planned to evaluate the HIWC detection performance of dual-pol radar, the Swerling process, and other radar processes as a means for tactical avoidance and decision-making. However, due to hardware delivery issues, the dual-pol capability was not available by the start of the flight campaign. Although this resulted in a shortfall in objectives, the FAA and NASA team decided to continue the flight campaign in order to evaluate the new Swerling process in HIWC conditions. A secondary goal of the campaign was to collect additional cloud in situ measurements in HIWC conditions to compare to data collected in previous flight campaigns.

NASA DC–8 With High Ice Water Content Improved Instrumentation

The NASA DC–8 was used again for this campaign and was similarly instrumented as in the HIWC RADAR I campaign (see NASA DC–8 With High Ice Water Content Instrumentation section). However, based on the lessons learned in the previous campaign, improvements were made to mitigate pitot anomalies, lags in background humidity, and fogging of particle probe optics. Additional instruments were added to obtain wind and turbulence measurements, and localized TWC measurements at the wing pylon and off-fuselage stations. Each of these is described briefly in the following subsections.

Auxiliary Pitot-Static Probe

A Rosemount 856DE–6 pitot-static probe with approximately 450 W of anti-icing heat was mounted to the right side fuselage at station 100 (Figure 20). This pitot-static probe was previously tested at NRC M–7 Test Cell 5 in IWC up to 9 g/m^3 at –17 °C and 150 m/s with no pitot anomaly. The standard DC–8 pitot probes have approximately 250 W of anti-icing heat, so the extra 200 W of heat was expected to keep this auxiliary pitot probe from failing in HIWC conditions. The pitot inlet was 5 in. off the fuselage surface. Data from the auxiliary pitot-static probe was compared to those from the DC–8 ship pitot-static systems during the instrument checkout flight to develop an airspeed correlation for the former. Unfortunately, during flight in HIWC conditions, the auxiliary pitot probe accumulated melted water, which subsequently froze and caused pitot anomalies. Once this was recognized, the data from this probe was not used as a backup to the DC–8 pitot system.

Figure 20.—Auxiliary pitot probe installed on DC–8. Inset shows closeup.

Background Humidity Measurement

Since the IKP2 measures water vapor from the ambient air plus the water vapor from evaporated cloud particles, an accurate and responsive measurement of the background humidity is needed to calculate the TWC contained in the evaporated particles. In 2018, several improvements were made to the BHS used in 2015, and additional BHS components were installed. First, the flow path of the BHS used in 2015 was updated to reduce time lags, and a SpectraSensors Water Vapor Sensing System (WVSS–II) was added in 2018 as a supplementary sensor inline with the Licor LI–840A. Several inlet options for this BHS were mounted on the left side window blank at station 530 (Figure 21). During initial flights in 2018, the BHS was connected to each of these inlets, and after examining these data sets, the aft-facing inlet made from 0.5-in.-outer-diameter tubing with a flare at the end (about 10 o'clock position on Figure 21) was determined to be the best option and used thereafter. Unfortunately, even with these improved inlets, the background humidity values appeared to be elevated during HIWC encounters. This indicated ice crystals were ingested into the aft-facing tubes, as previously reported by Strapp et al. (Ref. 9) for similar HAIC–HIWC Falcon 20 humidity observations.

A second BHS was added to the IKP2 probe itself in 2018. This enabled the background humidity to be measured at the same location as the IKP2 TWC measurement to minimize TWC calculation errors and noise caused by phase lag and spatial differences of the IKP2 water vapor and background water vapor measurements (Ref. 9). In order to make two water vapor measurements within the IKP2, a customized dual LI-COR® LI–850 system was developed by SEA to replace the single LI–840A that had been used in the IKP2 previously. One of the LI–850 units measured the water vapor within the IKP2 flow path (cloud TWC plus background humidity), while the second LI–850 unit measured the background humidity through a small aft-facing inlet on the side of the IKP2 canister (Figure 22). Review of the background humidity data from this source found it also had periods of elevated humidity during HIWC encounters, indicating ice crystals contaminated the inlet.

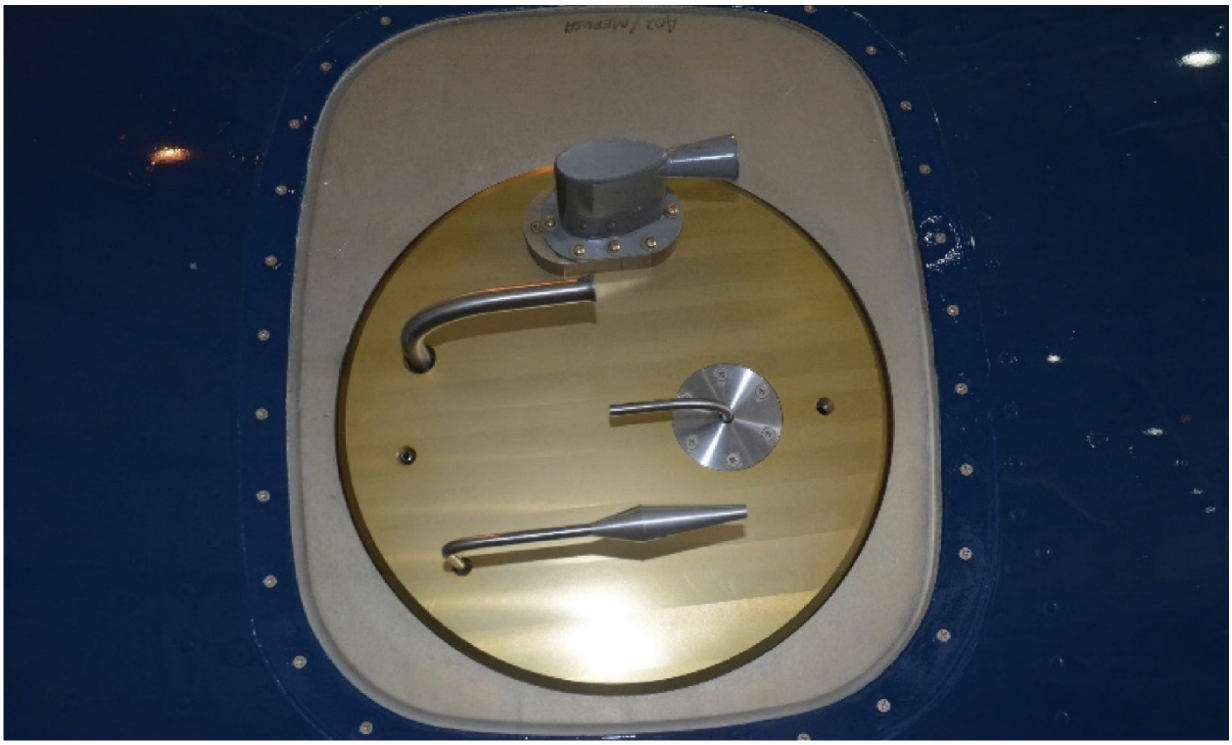

Figure 21.—Background humidity system (BHS) inlets and solid wire total air temperature (TAT) probe on window blank (station 530).

Figure 22.—Isokinetic Probe (IKP2) canister with inlet for background humidity circled in red.

Lastly, the Langley diode laser hygrometer (DLH) (Refs. 24 and 25) was installed on the DC–8 to measure background humidity. The DLH utilizes an open-path, double-pass configuration, where the path is defined on one end by a laser transceiver mounted in the cabin on a modified window blank, and on the other end by a panel of retroreflecting material mounted on the DC–8's outboard engine nacelle. The DLH is thus not subject to inlet contamination by ice crystals as previously described. The DLH proved to be an excellent addition to the HIWC RADAR II instrument suite, and the best source of background humidity for the IKP2 TWC calculations.

Nitrogen Purge System

A purge system using ultra-high-purity gaseous nitrogen (N_2) was used for preventing fogging in the particle probe optics and for providing purge and zero calibration values for the BHS. The N_2 tanks were installed in the DC–8 cabin and connected to the purge lines that run through the wings to each wingtip pylon. After the completion of a flight, a set of tubing was connected to the wing pylon purge-line so that dry N_2 would flow through the PIP and 2D–S probes on the right wing (Figure 23) and to the CDP–2 probe head/canister and the IKP2 flow path and background humidity inlet on the left wing (Figure 24).

Figure 23.—Precipitation Imaging Probe (PIP) and SPEC 2D–S probe with purge lines installed on tail cones.

Figure 24.—Isokinetic Probe (IKP2) and Cloud Droplet Probe (CDP–2) with purge lines installed.

During preflight checks, the purge lines were removed and the canisters quickly sealed. This procedure was effective at preventing moist air from entering the canister and then condensing inside the canister and optic windows during the flight in subfreezing temperatures. The N_2 tanks were also connected to the rack mounted BHS in order to periodically provide zero humidity air for water vapor instrument calibrations and to purge the inlet lines to keep them dry, for example, during descent from high altitude when condensation on cold-soaked inlet lines might be expected.

Meteorological Measurement System for Winds and Turbulence

The meteorological measurement system (MMS) (Refs. 26 and 27) was installed on the NASA DC–8 to provide high resolution and accurate meteorological parameters (pressure, temperature, turbulence index, and the three-dimensional (3D) wind vector). The MMS consists of three major systems: (1) an air motion sensing system to measure the air velocity with respect to the aircraft, (2) an aircraft motion sensing system to measure the aircraft velocity with respect to the Earth, and (3) a data acquisition system to sample, process, and record the measured quantities. The MMS has supported many DC–8 missions during the past 20 years and was a very valuable addition to the HIWC RADAR II measurements. It not only provided 3D winds as originally intended, but it also provided the best source of airspeed and static temperature that was used in subsequent data analyses. The MMS pitot probe is uniquely integrated into a TAT probe that was mounted on the lower nose of the DC–8 for this mission (Figure 25). Although the DC–8 pitot probes and the auxiliary pitot-static probe suffered numerous pitot anomalies during the 2018 campaign, the MMS airspeed was not significantly affected by the HIWC conditions encountered.

Figure 25.—Meteorological Measurement System (MMS) pitot (left) and total air temperature (TAT) probe (right).

Total Water Content Measurements at Off-Fuselage Locations

As part of an effort to understand concentration effects of TWC at various locations, another two SEA hot-wire TWC probes were added to the instrument suite. One was located on the CDP–2 canister on the left wing pylon (Figure 26) and considered to be close to a free-stream location, while a second was mounted on a window blank pylon at station 330 on the left side of the fuselage (Figure 27). Both locations accommodated either a SEA Robust probe (Refs. 23 and 28) or an ice crystal detector probe (Ref. 29). Analysis of these measurements, along with the SEA TWC probe on the fuselage nose, will facilitate a better understanding of the ice concentration variation due to localized effects.

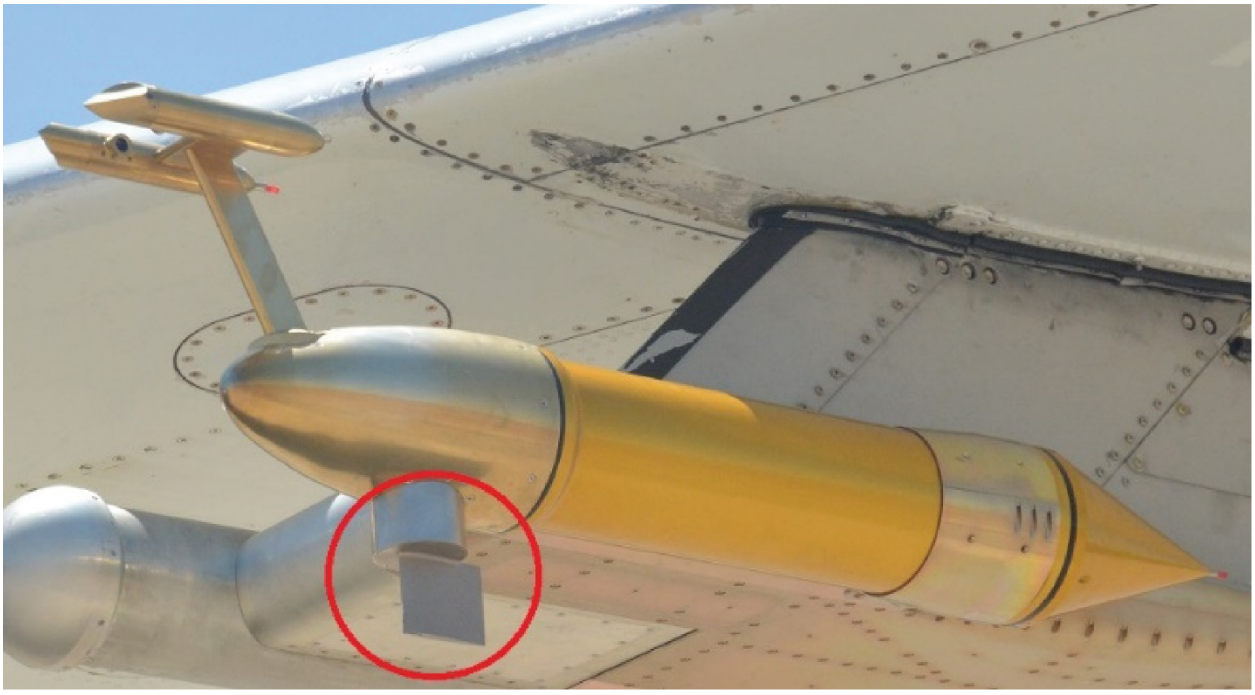

Figure 26.—Droplet Measurement Technologies (DMT) Cloud Droplet Probe (CDP–2) canister with Science Engineering Associates, Inc. (SEA) ice crystal detector circled in red.

Figure 27.—Science Engineering Associates, Inc. (SEA) ice crystal detector on window-mounted pylon (station 330).

Optical Ice Detector

The Collins Aerospace Optical Ice Detector (OID), a compact, short-range cloud Light Detection and Ranging (LIDAR) system (Refs. 30 and 31), was installed on the DC–8 Airborne Science Laboratory to supply additional cloud water content measurements. The OID transmitted and received light through an optical viewport installed in a left side window blank at station 290, and sampled the airstream up to 10 m outside the aircraft. The use of circularly-polarized pulses of laser light allows the OID to determine cloud density and cloud phase, providing estimates of liquid water content (LWC), IWC, and TWC.

2018 Campaign Planning and Operations

The campaign plans were nearly identical to the 2015 campaign. The base of operation was Ft. Lauderdale, Florida. The campaign duration was 21 days in August 2018 with 50 flight hours for research. The operating area was the same as 2015 as shown in Figure 4. The concept of operations and the mission rules were also the same as 2015.

Sampling Strategies

The sampling strategy was consistent with 2015 in terms of the sampling altitudes (–50±5, –40±5 –30±5, and –10±5 °C), but with an added interest to fly also at –25±5 °C levels when mission rules allowed. Based on adiabatic estimates of maximum condensed water that are the basis of the TWC envelope (Ref. 1, Appendix D), and numerical simulation results by Proctor et al. (Ref. 22), there was reason to believe that TWC values might maximize in the –20 to –30 °C temperature interval. This flight level was not identified as a priority by the EHWG, and was not a focus for the HAIC–HIWC and first HIWC RADAR campaigns.

As in 2015, the regions of interest were identified by the forecast team for preflight planning and then adjusted per ground guidance team using the products developed by the Langley satellite group (Ref. 32). For the 2018 campaign, these products used GOES–16, which had a 2- to 3-km resolution and was normally updated every 15 min, and on special request to NOAA, was updated every 1 or 5 min. The increased temporal sampling and reduced time latency of the GOES–16 satellite imagery increased situational awareness to optimize the in-cloud sampling.

Additionally, as the flight team gained experience with the radar identified IWC (R–IWC) levels defined by the Swerling process, the sampling strategy transitioned from point-to-point level transects to tracks that were modified in realtime to intercept areas of HIWC that were detected ahead by the radar.

Summary of HIWC RADAR II Flights

The instrument upload took place at NASA Armstrong's Palmdale, California, facility in July 2018 and instrument test flights were conducted from there as well. The DC–8 and research teams arrived at KFLL on July 30. The operations base was set up and the forecast team monitored conditions.

Table III provides a synopsis of the 10 flights including dates, times, locations, types of storms, and notable events. Appendix A provides time histories of key parameters for the seven 2018 research flights, including flight track and time histories of altitude, temperature, updraft velocity, and TWC. Time histories are limited to the periods in the clouds of interest. As with the 2015 figures, the IR satellite imagery in these figures is for a nominal time during in-cloud operation, so it does not show the progression and decay of the storm during the flight.

TABLE III.—HIGH ICE WATER CONTENT (HIWC) RADAR II FLIGHT SUMMARY

HIWC flight no.	Flight date	Time, UTC	Storm location	Type of storm[a]	Notable events[b]
1	7/27/2018	20:05–23:10	NA	----------	Instrument check flight
2	7/30/2018	16:04–20:525	NA	----------	Ferry to KFLL
3	8/2/2018	14:07–19:02	Gulf of Mexico	Oceanic MCS	TAT anomaly
4	8/6/2018	11:13–16:36	Gulf of Mexico	Oceanic MCS	TAT and auxiliary pitot anomalies
5	8/8/2018	14:25–18:52	NA	----------	Ferry to KPMD; #4 engine oil leak
6	8/15/2018	15:19–01:23*	Eastern Pacific	Tropical Depression 14–E	TAT, ADC, and pitot anomalies
7	8/16/2018	16:22–02:30*	Eastern Pacific	Tropical Storm Lane	TAT and auxiliary pitot anomalies
8	8/18/2018	14:57–22:41	Eastern Pacific	Hurricane Lane	TAT and auxiliary pitot anomalies
9	8/19/2018	17:20–00:13*	Eastern Pacific	Hurricane Lane	TAT and auxiliary pitot anomalies
10	8/20/2018	17:57–03:09*	Eastern Pacific	Hurricane Lane	TAT and auxiliary pitot anomalies

*Denotes next day.
[a]MCS is mesoscale convective system.
[b]KFLL is the Fort Lauderdale-Hollywood International Airport. TAT is total air temperature. KPMD is the Palmdale Regional Airport. ADC is air data computer.

Plans Versus Actual

Two research flights were made into MCS within the Gulf of Mexico on August 2 and 6, 2018 (Figure 28). These storms tended to be shallower, smaller scale, and shorter lived than anticipated for typical HIWC systems. The forecast team noted that dry air and dust coming from Africa and cooler ocean temperatures in the Caribbean were suppressing the development of deep convection systems. Meanwhile, multiple MCS, tropical storms, and hurricanes were developing in the eastern Pacific off the Mexican coast.

After completing the August 6 flight, the team decided to move the base of operations back to Armstrong's Palmdale facility to fly into the convective systems occurring in the eastern Pacific. During the ferry flight back to Palmdale, a significant engine oil leak developed, requiring replacement of the number 4 engine. The Armstrong crew worked quickly to remove and replace the engine, perform ground checks, and then replace another component within 5 working days.

When continuation of flight operations was approved, five flights were made over the eastern Pacific to acquire data in Tropical Depression 14–E, and subsequently as it developed into Tropical Storm and Hurricane Lane (Figure 29). As the hurricane moved westward, it was determined that more time could be spent in the storm system if the base of operations was moved to Kona, Hawaii. Consequently, the last three flights had Kona as an arrival and/or departure location.

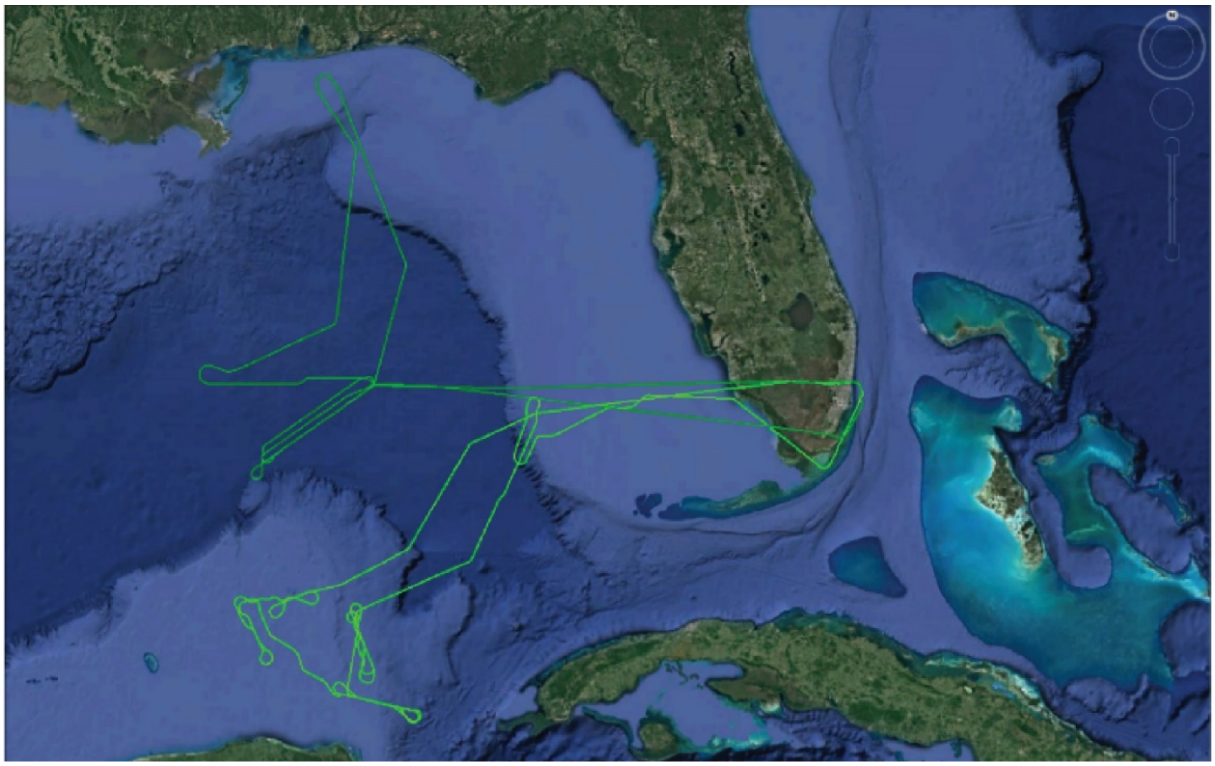

Figure 28.—Flight tracks for Flight 3 (central Gulf of Mexico) and Flight 4 (near Yucatan Peninsula). Map data Google earth, Image Landsat and Copernicus, Data: SIO, NOAA, U.S. Navy, NGA, GEBCO.

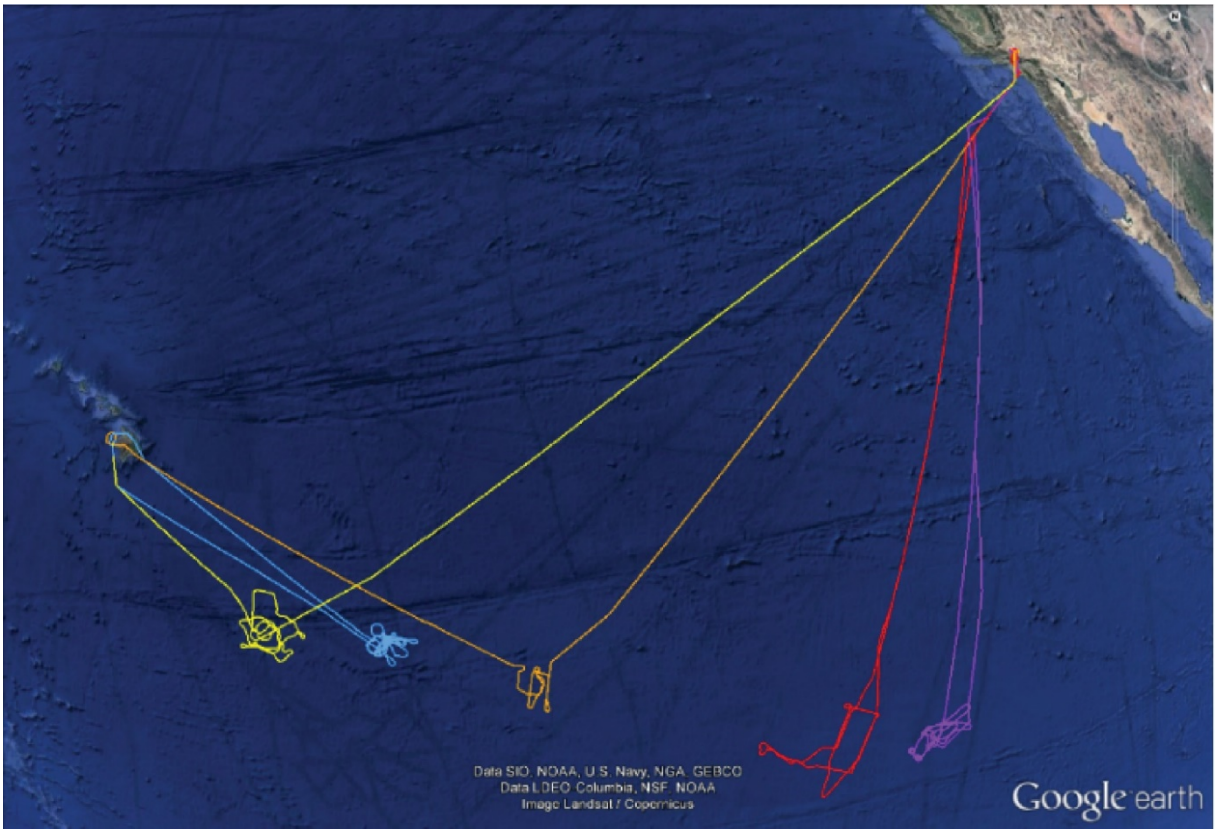

Figure 29.—Flight tracks for Flights 6 to 10. Map data Google earth, Image Landsat and Copernicus, Data: SIO, NOAA, U.S. Navy, NGA, GEBCO, LDEO (Columbia), NSF.

A Closer Look at Flight 7: Tropical Storm Lane

After a successful, but long 10.1-hr flight on August 15 into Tropical Depression 14–E, the forecast team continued to watch the system as it moved westward. The August 16 14:00 UTC weather brief indicated that Tropical Depression 14–E had intensified into Tropical Storm Lane and was the best target for HIWC research that day. The storm was approximately 300 nmi in diameter and had large regions of deep cloud embedded within the storm system (Figure 30).

The DC–8 took off at 16:22 UTC and arrived at the outer bands on the northeast edge of Tropical Storm Lane at 19:16 UTC. During the transit, some of the deeper clouds in the outer bands decayed, but the central deep cloud remained, and new deep convective cells were forming into distinct bands. The first transect was made at an altitude of 34,000 ft and SAT of –39 °C through the deep clouds as shown in Figure 31. The magnitude of IWC during this track was relatively moderate with peaks up to about 1.5 g/m^3. These deeper cloud regions were in a decaying phase.

The next track turned north to return to the larger deep region nearly 200 nmi away at the north side of the storm. On the way, the radar flight team requested a slight left turn to intercept a cloud region that the Swerling process' R–IWC indicated was approximately 2.5 g/m^3. Figure 32 shows the DC–8 left deviation to intercept the eastern edge of a developing deep band (black circled region). At 20:28 UTC, a peak TWC of nearly 2 g/m^3 was measured by the IKP2 during this intercept. This level of agreement between the R–IWC and IKP2 TWC was also observed in previous flights, and this event further increased the team confidence in the R–IWC product.

As the storm transitioned and the areas of deep convection changed rapidly, the remaining flight tracks were guided by the radar flight team using the onboard R–IWC product and the HIWC potential satellite product (Refs. 33 and 34). These products were displayed in the cockpit, which enabled the pilots to quickly make course changes to intercept the shrinking HIWC regions.

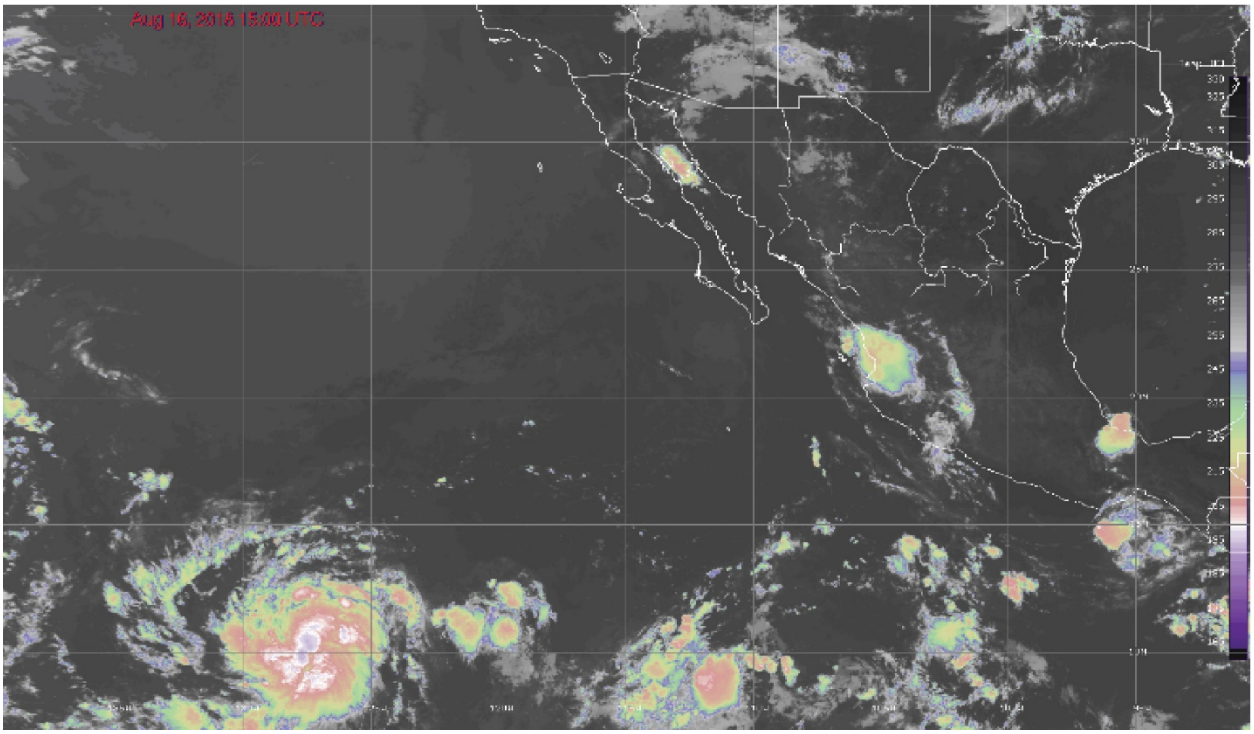

Figure 30.—Infrared (IR) satellite image at 15:00 UTC on August 16, 2018 (1 hr before takeoff).

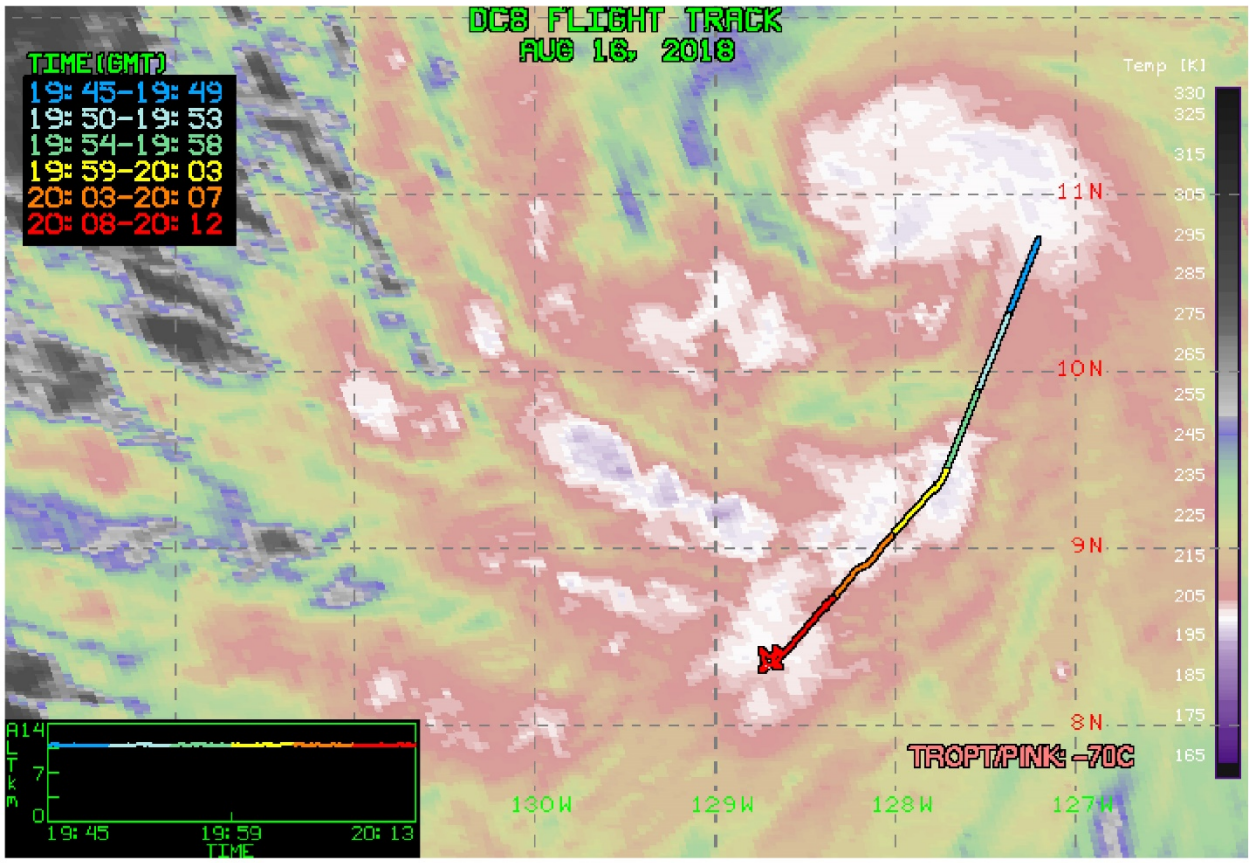

(a)

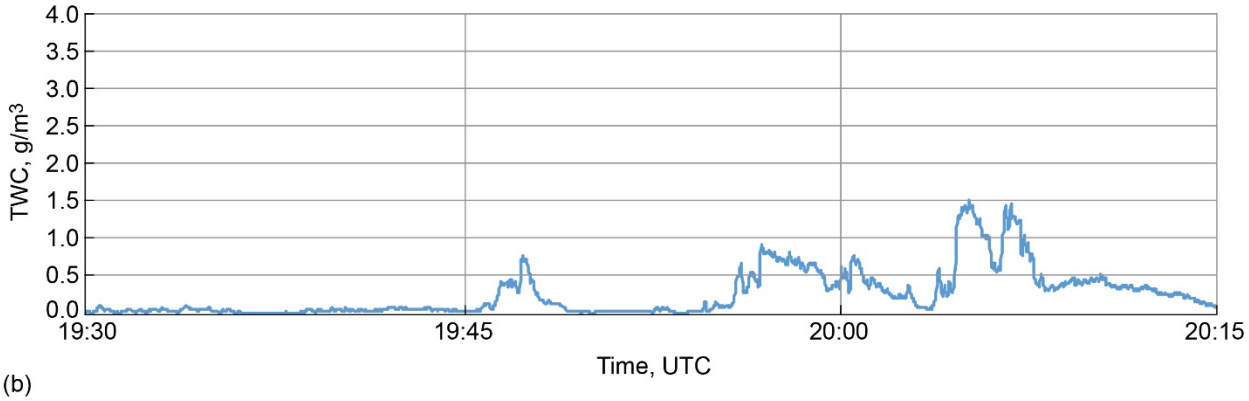

(b)

Figure 31.—Flight on August 16, 2018. (a) Flight track on infrared (IR) satellite image from 20:00 UTC. TROPT/PINK = tropopause temperature. (b) Isokinetic Probe (IKP2) total water content (TWC) time history.

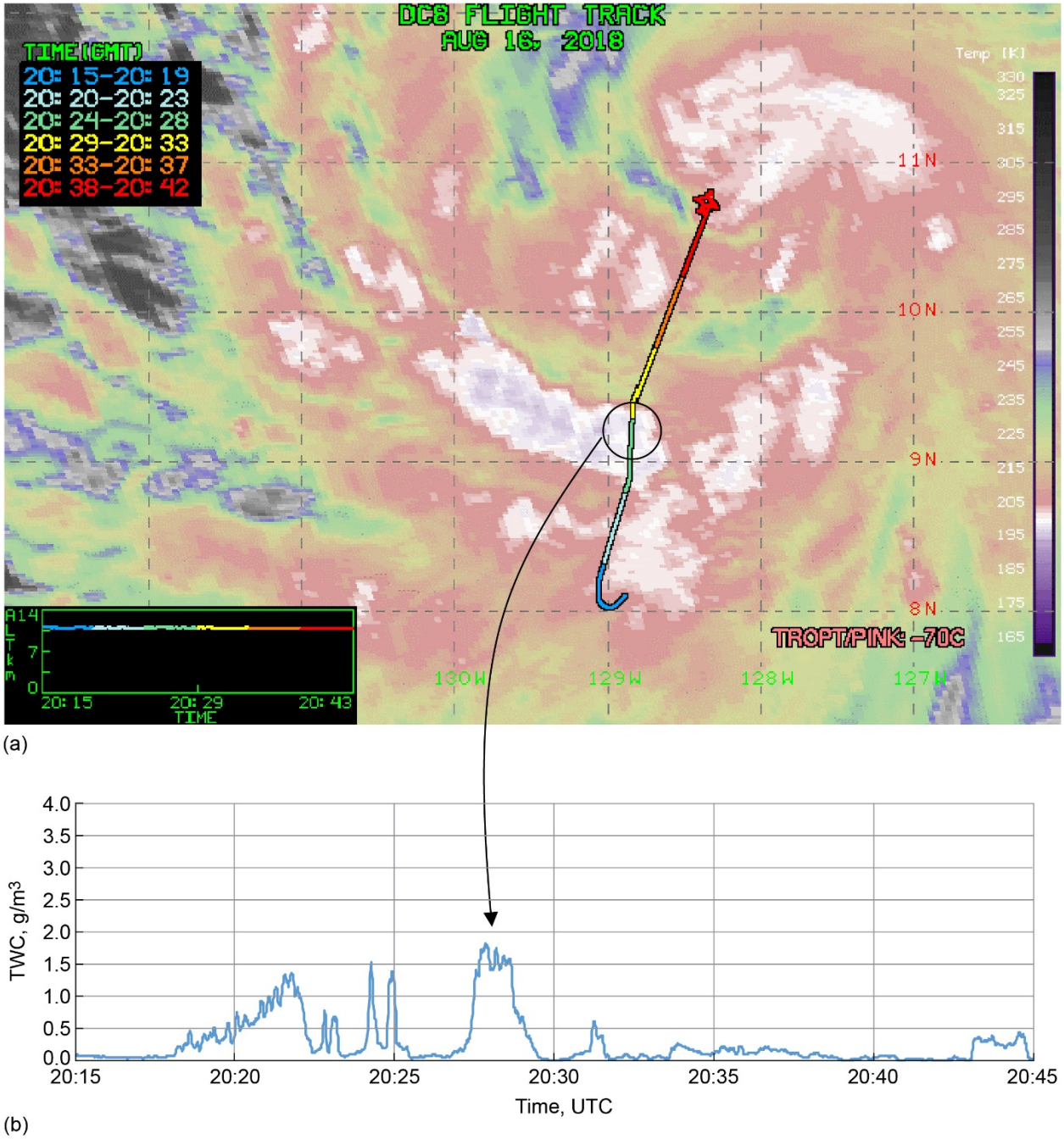

Figure 32.—Flight August 16, 2018. (a) Flight track on infrared (IR) satellite image from 20:30 UTC. TROPT/PINK = tropopause temperature. (b) Isokinetic Probe (IKP2) total water content (TWC) time history.

Figure 33 provides an example of flight track deviations made to intercept areas identified by the R–IWC display. This figure also shows a plan position indicator (PPI) display of R–IWC out to 60 nmi ahead of the DC–8 with the flight track colorcoded based on the IKP2 binned TWC values. A similar PPI display of R–IWC was presented to the radar flight team during the flights. The TWC time history in this figure also has the R–IWC values coplotted with the IKP2 values. The DC–8 position on the PPI is indicated on the TWC time history with a yellow star. As shown on the PPI at 21:37 UTC, there was a region with 2 g/m^3 < R–IWC < 3 g/m^3 about 50 nmi ahead and to the left of track. Through discussion onboard and chat, the team decided to make a left deviation to intercept that region.

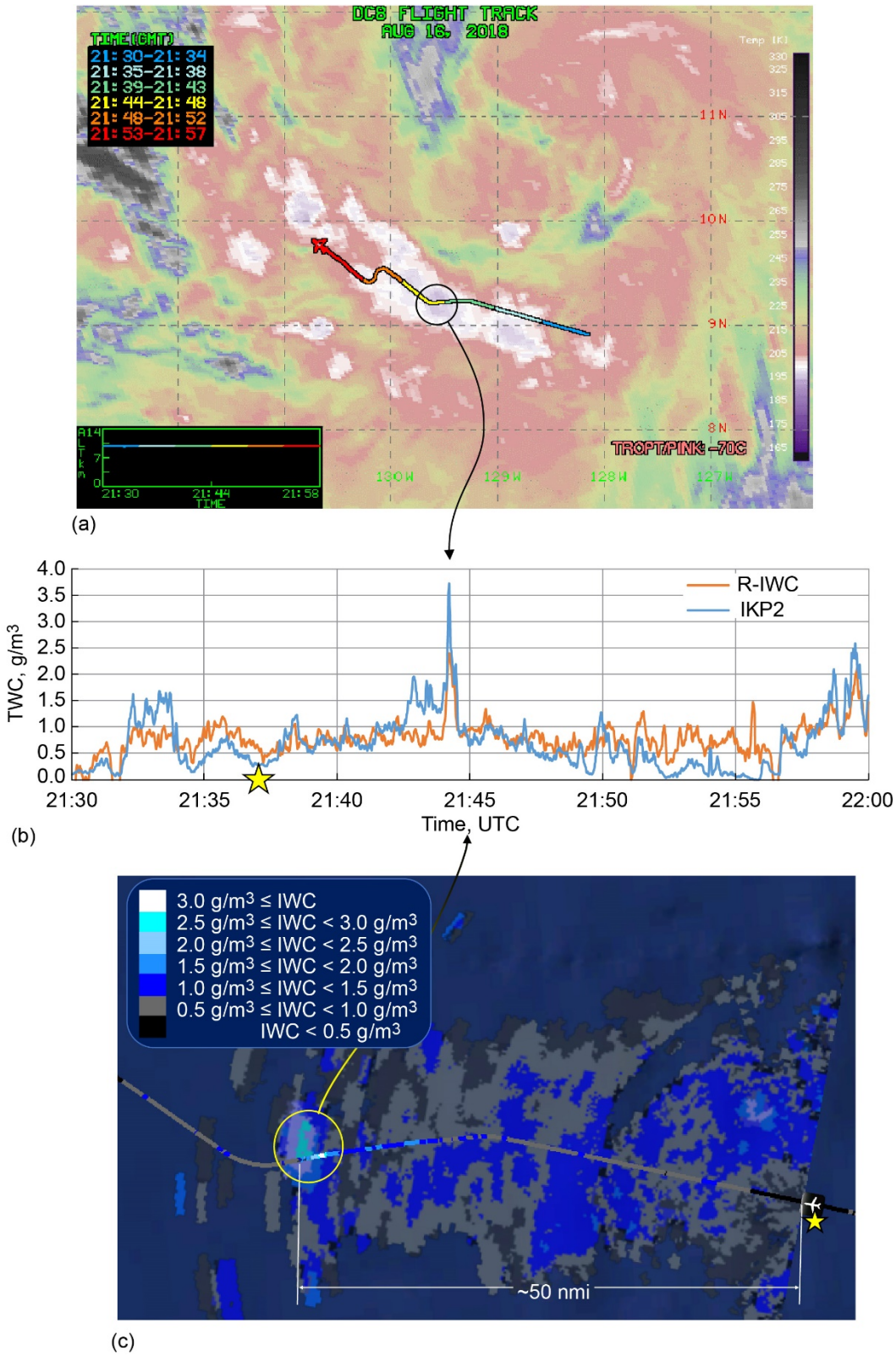

Figure 33.—Flight on August 6, 2018. (a) Flight track on infrared (IR) satellite image from 21:45 UTC. TROPT/PINK = tropopause temperature. (b) Time history of Isokinetic Probe (IKP2) and radar-identified ice water content (R–IWC) total water content (TWC). (c) Plan position indicator (PPI) of R–IWC display.

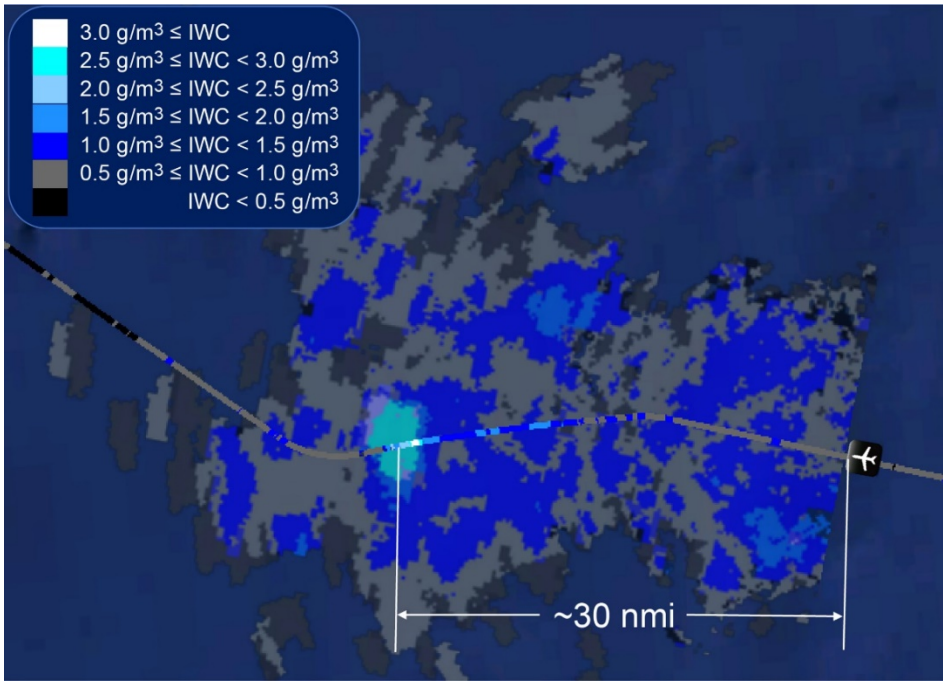

Figure 34.—Plan position indicator of radar-identified ice water content (R–IWC) and DC–8 flight track with Isokinetic Probe (IKP2) binned values from August 16, 2018.

Figure 34 shows the PPI at 30 nmi from the regions of interest. Note the R–IWC values increased to 2.5 to 3.0 g/m^3 (cyan color), but the general size of the region was consistent with the R–IWC estimate made from a 50-nmi range. Also note, the general agreement in IKP2 to R–IWC values in the flight track.

Flight 7 was a clear transition point when confidence in the Swerling R–IWC product was established, and it was used to guide flight track choices in the remaining flights into Hurricane Lane. The maximum range of the R–IWC Swerling product was approximately 60 nmi as configured for this flight campaign. Harrah et al. (Ref. 17) have concluded that the range can be extended to 80 nmi or more.

Key Findings and Lessons Learned From HIWC RADAR II Flights

Meteorological and radar data sets were processed into quality-controlled data sets, although at the time of this publication, some quality-controlled work was ongoing. The IKP2 TWC utilized background humidity from the DLH and static temperature and true airspeed from the MMS using the process described in Strapp et al. (Ref. 9). The IKP2 data shown in this report for the 2018 flights is version 1.5. The RRF and R–IWC were derived as described in Harrah et al. (Ref. 17). The PSD and MSD are being processed by NCAR using methods similar to Leroy et al. (Ref. 6). These files will be archived by NCAR (Ref. 19), and made available to the science team for reference and further analyses.

The primary objective of the HIWC RADAR II campaign was to acquire data to evaluate and assess the Swerling R–IWC detection method to enable tactical avoidance of regions of potentially hazardous ice crystal icing conditions. Seven flights were made into regions of HIWC conditions that were remotely detected using the R–IWC product, followed by in situ measurements of the ice cloud conditions. Real-time estimates of IWC were made up to 60 nmi ahead of the aircraft and then confirmed with the in situ measurements within ±0.5 g/m^3 in certain cases as previously described. Postflight data from all 2015 and 2018 flights were reprocessed using the same relationship between the I_D to IWC that was used in realtime during the 2018 flights. Analyses are ongoing to identify improvements as described in Harrah, et al. (Ref. 17).

Data from this campaign can also be used to compare to HIWC characterization data from previous flight campaigns, support satellite and weather forecast tool development, examine ice concentration factors in localized areas of an airplane, and much more.

Several diagnostic products were developed by the Langley satellite group and were very useful for providing strategical and tactical guidance during the HIWC deployments. One diagnostic product provided current probability of HIWC with IWC greater than 0.5 g/m^3 (Ref. 33). This product is based on geostationary satellite imagery and was developed from statistical relationships between IWC and satellite-derived parameters. Preliminary assessments produced a 75 percent probability of detection (POD) and 37 percent false alarm rate (FAR). Further evaluation is underway using the HIWC data collected in 2018 (Ref. 34).

Lessons learned in this campaign include the value of the DLH in solving a long-standing problem in measuring background water vapor in HIWC conditions to support IKP2 TWC calculations, and the value of the MMS in providing accurate and dependable true airspeed, temperature, and wind measurements in HIWC conditions. As a result, processing time and confidence in IKP2 TWC measurements were improved. The DLH enabled comparisons to previous and new methods for acquiring background humidity using aft-facing air inlets. The comparisons showed the inlets of various designs continued to have contamination issues when encountering HIWC conditions.

Lastly, an operational lesson learned was the value of using an aircraft with long-range capability for this type of research and having a flight and research team that was willing and persistent to adapt to the weather changes and overcome unpredictable obstacles and events.

Key Results and Outcomes From the HIWC RADAR Campaigns

- Measurements of RRF and PSD confirmed findings and observations by Mason et al. (Ref. 2), Protat et al. (Ref. 8), and Leroy et al. (Ref. 7), that high concentrations of small ice particles can cause HIWC conditions with low RRF.
- Relationships between X-band RRF and IWC were developed for various ranges ahead of the aircraft. Even at the closest range, the degree of variability in the measured reflectivity to IWC relationship prevents the RRF alone from meeting commercial operational goals.
- NASA developed a new radar data processing technique called Swerling using the HIWC RADAR I data that related the I_D in X-band radar reflectivity to IWC. The Swerling technique was tested during HIWC RADAR II, which identified HIWC regions up to 60 nmi ahead of the airplane (Ref. 17).
- Cloud characterization data (TWC, PSD, and MSD) from the HIWC RADAR I campaign supplemented HAIC–HIWC flight campaign data requirements, particularly at the –50 °C flight level.
- Peak IWC values over distances of approximately 1 km ranged between 1.8 to 3.7 g/m^3 during these flights. Encounters with persistent IWC greater than 1 g/m^3 could last 15 min during flight legs in tropical oceanic convective systems. Highest concentrations tended to be near and downstream from active convection with overshooting cloud tops.
- Flight campaign data including onboard weather radar, TWC, PSD, MSD, air data, and flight parameters are currently being archived at NCAR (Refs. 18 and 19). These data are a unique source of validation data for numerical weather models and special forecast and nowcast tools such as the NASA Langley HIWC potential satellite product (Refs. 33 and 34) and NCAR's Algorithm for the Prediction of HIWC Areas (ALPHA) product (Ref. 35).

Concluding Remarks

NASA and the Federal Aviation Administration (FAA) conducted two high ice water content (HIWC) RADAR flight campaigns to understand and improve radar detection of HIWC regions ahead of an airplane, and to develop and test new remote detection algorithms that will enable pilots to tactically avoid hazardous regions with high concentrations of ice crystals. The flight campaigns used NASA's DC–8 Airborne Science Laboratory fitted with a Honeywell RDR–4000 radar and cloud in situ microphysical instruments, specifically modified for HIWC conditions, in order to correlate the radar and HIWC cloud data.

Lessons Learned

- Tropical systems such as tropical depressions and tropical storms can be efficient and reliable sources of HIWC data. These systems are relatively easy to track, persist for days, have less lightning and hail than continental convection, and produce areas of high ice concentrations over long distance scales.
- The DC–8 proved to be an excellent aircraft for HIWC research due to its range and altitude performance. No engine icing issues were experienced, although pitot probe icing did occur in certain HIWC conditions. The long range and endurance capability of the DC–8 was essential for flights into tropical storms and hurricanes.
- The technical capabilities of Geostationary Operational Environmental Satellites–16 (GOES–16) increased temporal sampling and reduced time latency. This advancement, coupled with improved satellite products, led to better identification of storm cell growth and decay that informed flight routing decisions.
- The diode laser hygrometer (DLH) and meteorological measurement system (MMS) proved to be very valuable additions to the instrument suite in 2018 to obtain accurate background humidity, static air temperature, true airspeed, and winds during these flights into HIWC conditions. Other systems previously used to obtain these parameters were compromised to varying degrees due to ice contamination.

Future Work and Issues

- The HIWC RADAR data sets are limited to oceanic, northern hemisphere, low- to mid-latitude storms. Radar-based IWC detection is untested and unknown for other storm types such as continental deep convection, which typically is more vigorous, has higher lightning frequency, and likely contains higher RRF at flight altitude.
- Radio Technical Communications for Aeronautics (RTCA) subcommittee (SC) 230 working group (WG) 10 has initiated development of Minimum Operational Performance Standards (MOPS) for radar detection of HIWC conditions. Data from these campaigns will provide critical information to this group.
- The Aviation Rulemaking Advisory Committee (ARAC) has formed an Ice Crystal Icing Working Group to assess the Title 14 Code of Federal Regulations Part 33 Appendix D mixed-phase and glaciated environmental envelope, using flight in situ data from the 2014 Darwin and 2015 Cayenne High Altitude Ice Crystals (HAIC)–HIWC flight campaigns, and the first HIWC-RADAR flight campaign (Ref. 21). Any gaps in the current data sets identified by this WG may establish the need for additional flight measurements. If so, further testing of onboard pilot radar detection would be beneficial.

Appendix A.—Flight Tracks and Data

Figure 35 to Figure 44 provide the 2015 flight tracks and time histories of altitude, temperature, and TWC. Figure 45 to Figure 51 provide the 2018 flight tracks and time histories of altitude, temperature, updraft velocity, and TWC.

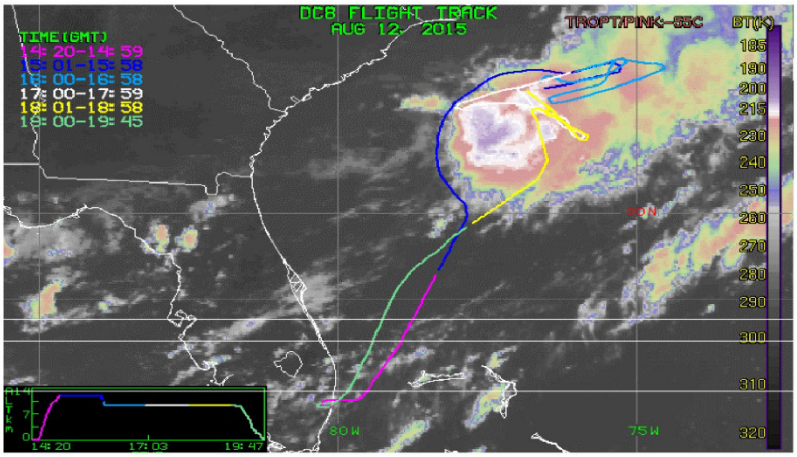

(a)

Flight Date	8/12/2015
Flight Hours	5.6

# Tracks	Alt., kft	SAT, °C
2	37.0	–48.1
10	29.0	–28.3

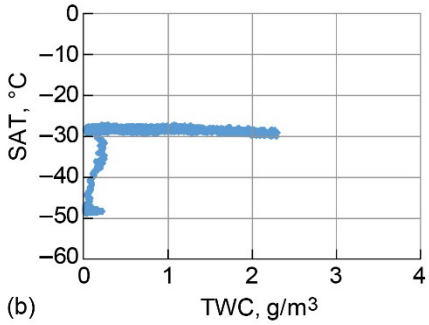

(b)

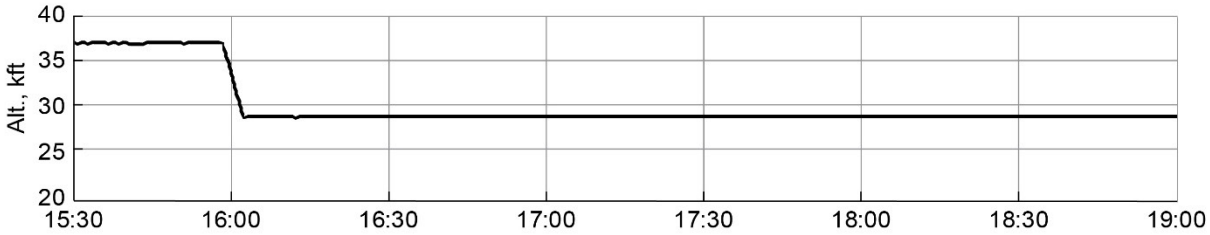

(c)

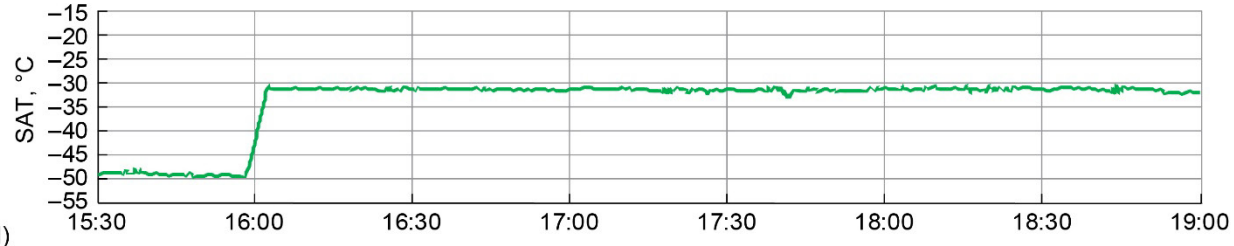

(d)

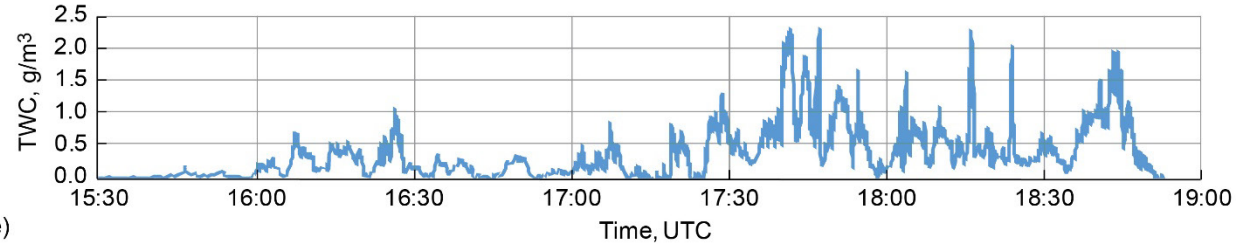

(e)

Figure 35.—August 12, 2015, flight track overlay on infrared (IR) satellite image and select time histories. (a) DC–8 flight track. TROPT/PINK = tropopause temperature. (b) Isokinetic Probe (IKP2) total water content (TWC) 5 s average versus static air temperature (SAT). (c) Pressure altitude (IWG1). (d) SAT (IWG1). (e) IKP2 TWC.

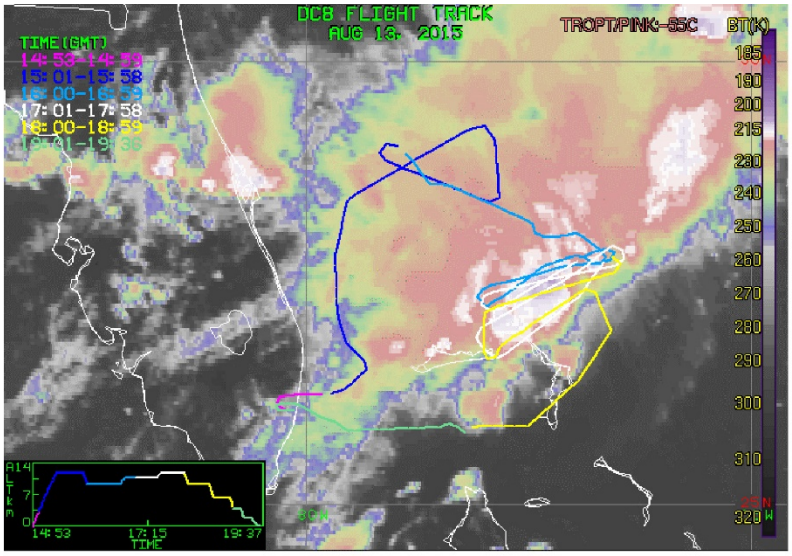

(a)

Flight Date	8/13/2015
Flight Hours	5.0

# Tracks	Alt., kft	SAT, °C
4	37.0	–49.7
2	34.0	–42.0
5	29.0	–29.7

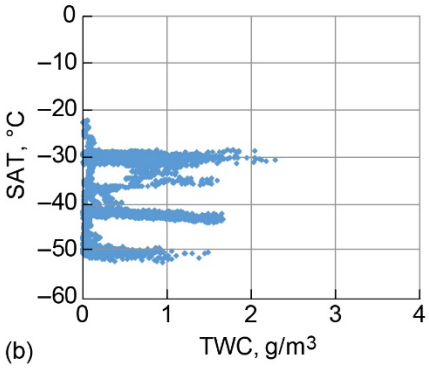

(b)

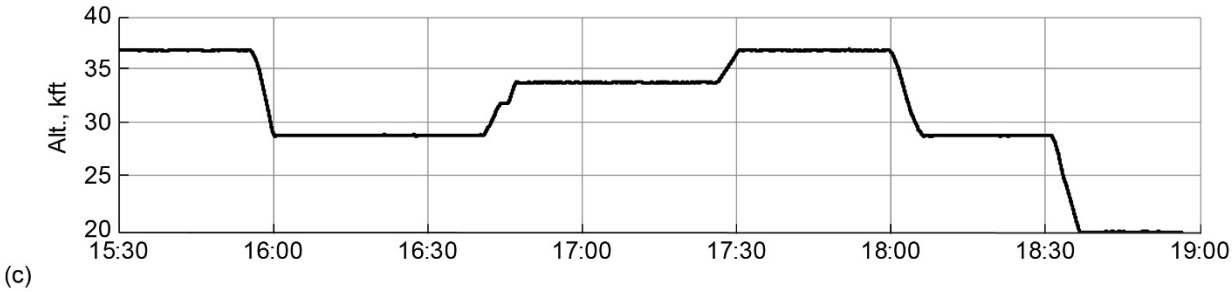

(c)

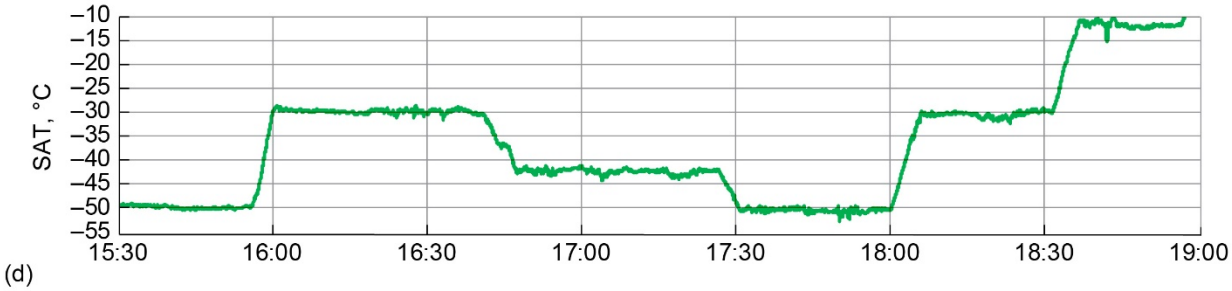

(d)

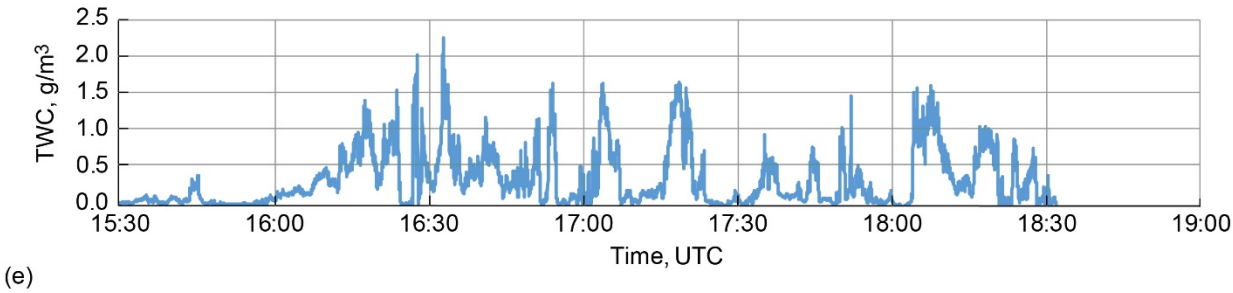

(e)

Figure 36.—August 13, 2015, flight track overlay on infrared (IR) satellite image and select time histories. (a) DC–8 flight track. TROPT/PINK = tropopause temperature. (b) Isokinetic Probe (IKP2) total water content (TWC) 5 s average versus static air temperature (SAT). (c) Pressure altitude (IWG1). (d) SAT (IWG1). (e) IKP2 TWC.

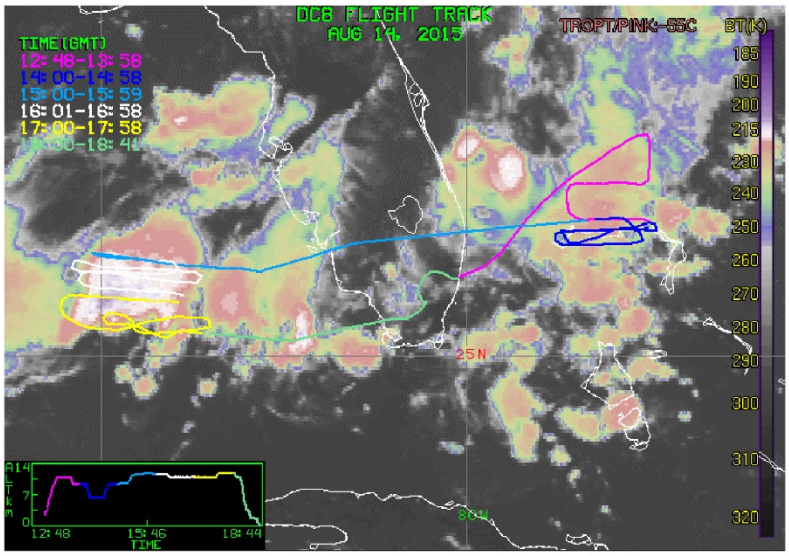

(a)

Flight Date	8/14/2015
Flight Hours	6

# Tracks	Alt., kft	SAT, °C
5	36.6	–48.9
6	34.1	–42.5
4	29.0	–30.2
2	20.0	–11.9

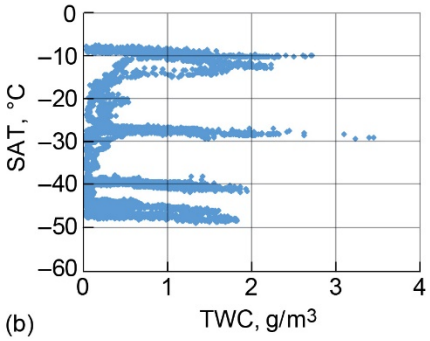

(b)

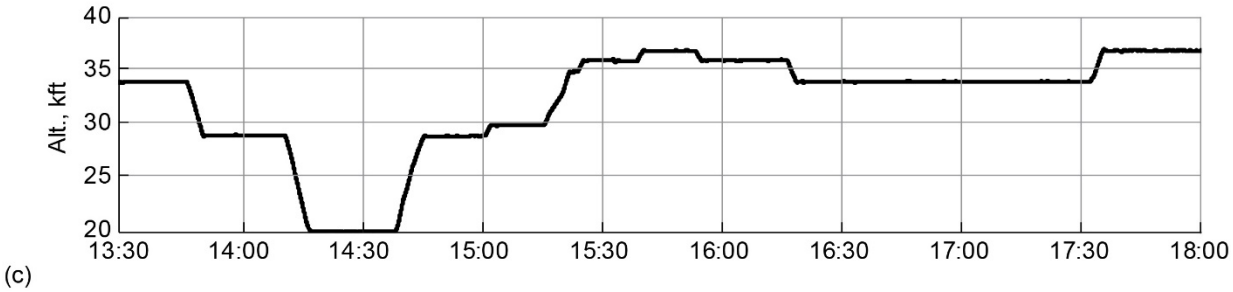

(c)

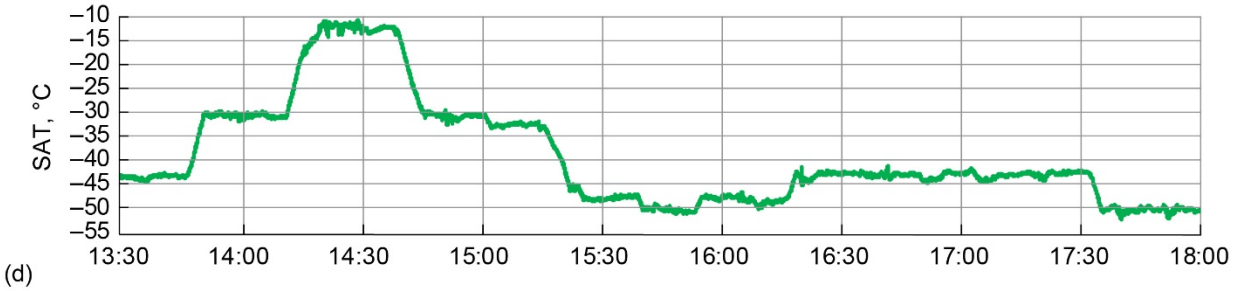

(d)

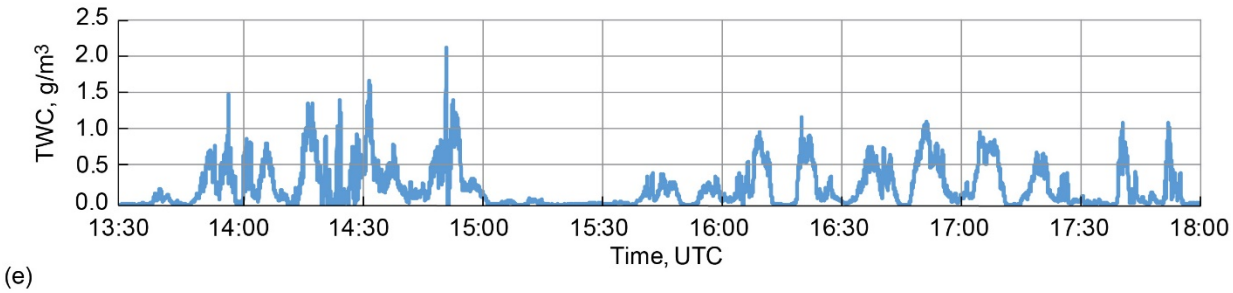

(e)

Figure 37.—August 14, 2015, flight track overlay on infrared (IR) satellite image and select time histories. (a) DC–8 flight track. TROPT/PINK = tropopause temperature. (b) Isokinetic Probe (IKP2) total water content (TWC) 5 s average versus static air temperature (SAT). (c) Pressure altitude (IWG1). (d) SAT (IWG1). (e) IKP2 TWC.

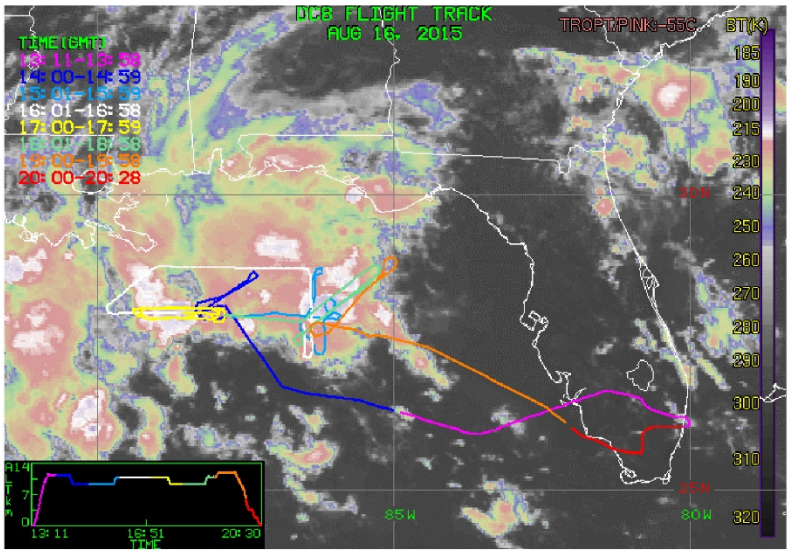

(a)

Flight Date	8/16/2015
Flight Hours	7.5

# Tracks	Alt., kft	SAT, °C
2	37.0	–49.6
8	34.0	–41.5
9	29.0	–29.1

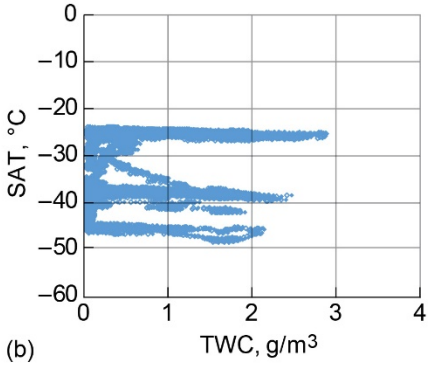

(b)

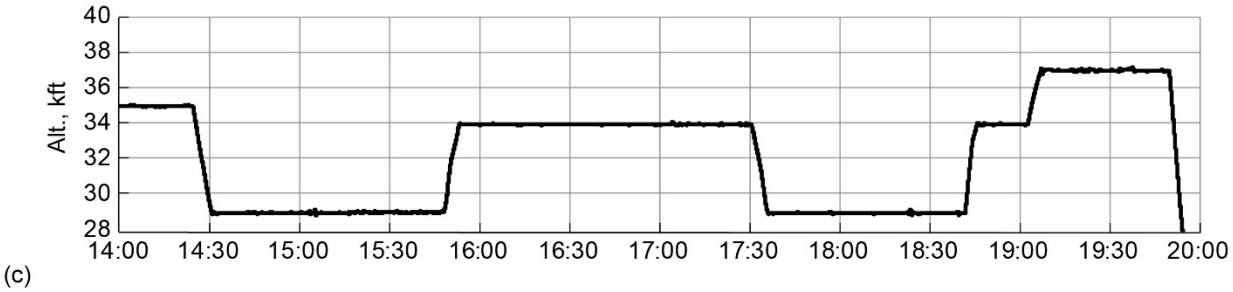

(c)

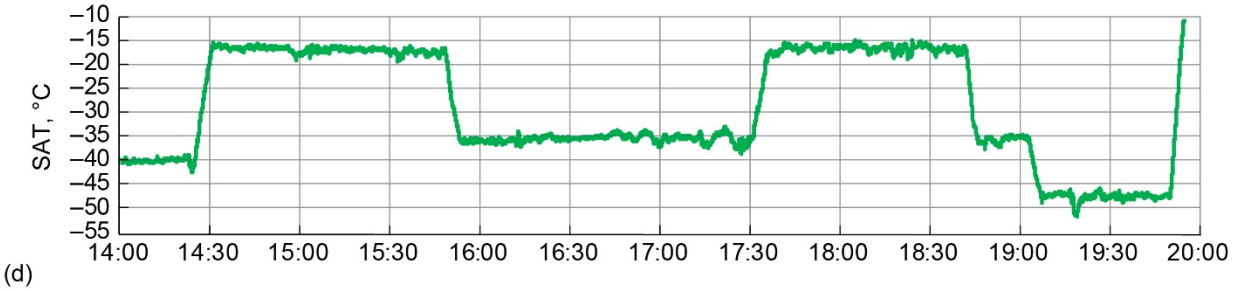

(d)

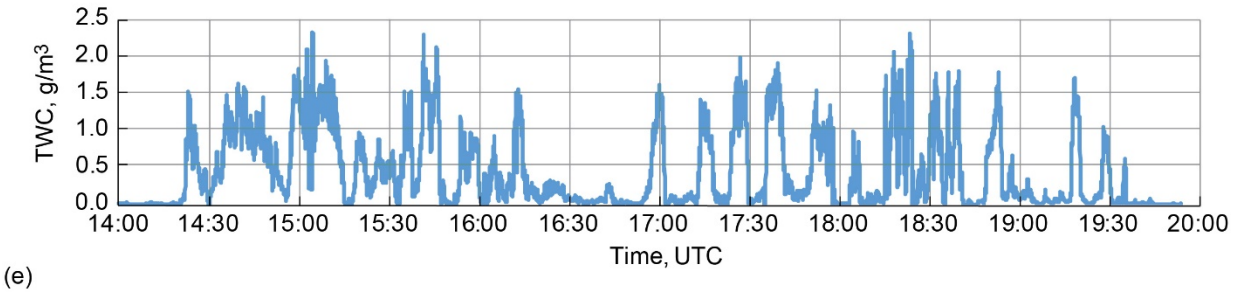

(e)

Figure 38.—August 16, 2015, flight track overlay on infrared (IR) satellite image and select time histories. (a) DC–8 flight track. TROPT/PINK = tropopause temperature. (b) Isokinetic Probe (IKP2) total water content (TWC) 5 s average versus static air temperature (SAT). (c) Pressure altitude (IWG1). (d) SAT (IWG1). (e) IKP2 TWC.

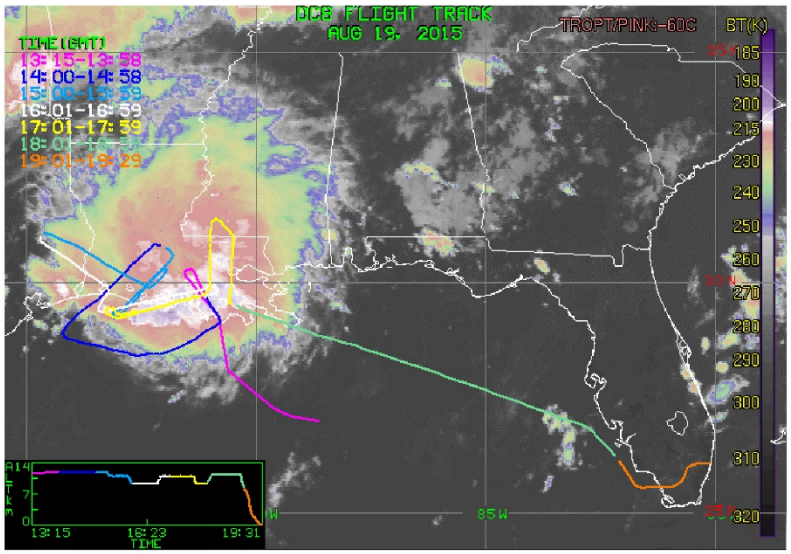

(a)

Flight Date	8/19/2015
Flight Hours	7.7

# Tracks	Alt., kft	SAT, °C
4	37.0	–47.8
5	34.0	–40.1
4	29.1	–28.0

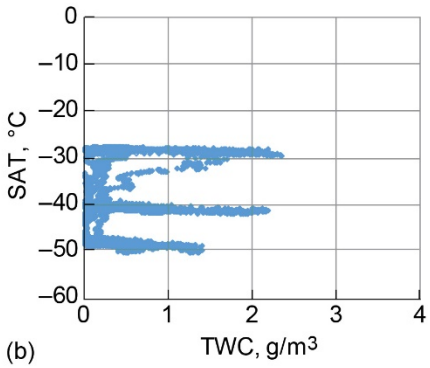

(b)

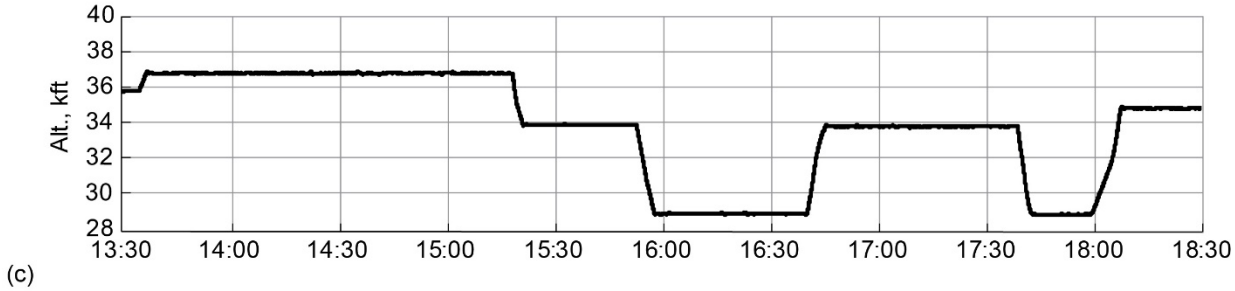

(c)

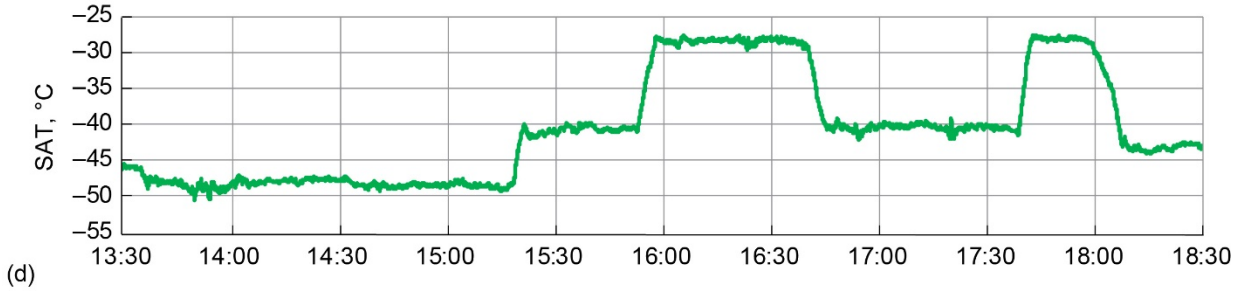

(d)

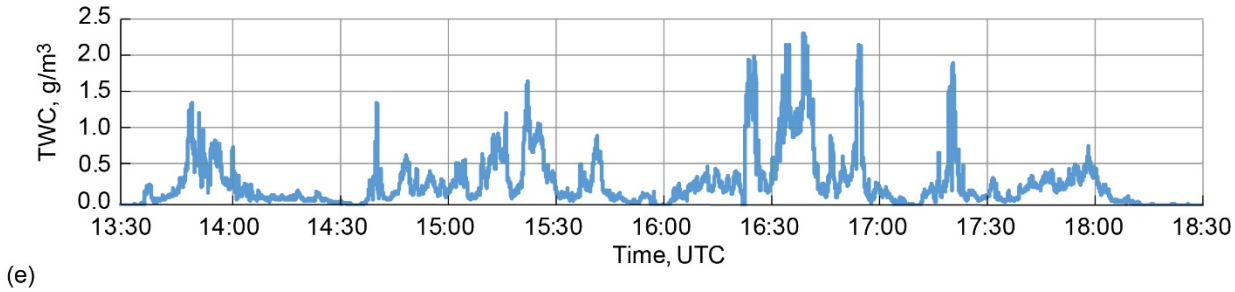

(e)

Figure 39.—August 19, 2015, flight track overlay on infrared (IR) satellite image and select time histories. (a) DC–8 flight track. TROPT/PINK = tropopause temperature. (b) Isokinetic Probe (IKP2) total water content (TWC) 5 s average versus static air temperature (SAT). (c) Pressure altitude (IWG1). (d) SAT (IWG1). (e) IKP2 TWC.

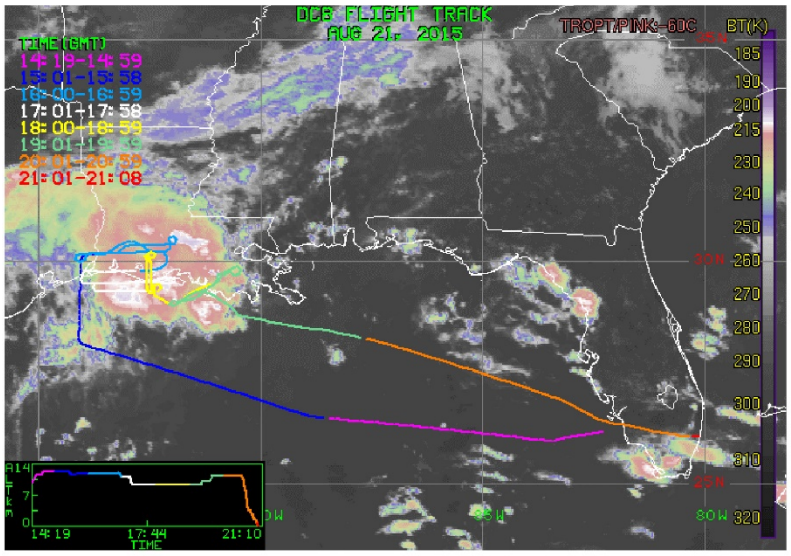

(a)

Flight Date	8/21/2015
Flight Hours	7.4

# Tracks	Alt., kft	SAT, °C
4	37.0	–48.4
1	34.1	–40.3
2	31.0	–33.2
8	29.1	–28.3

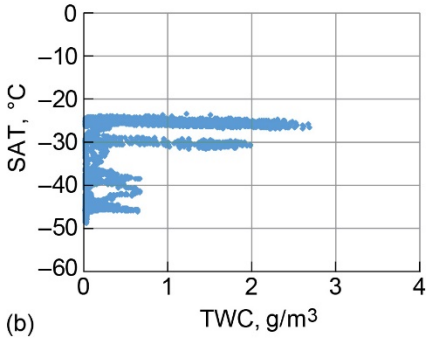

(b)

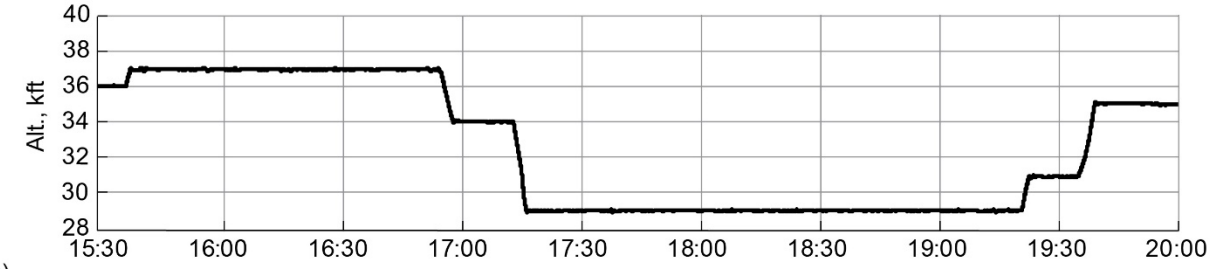

(c)

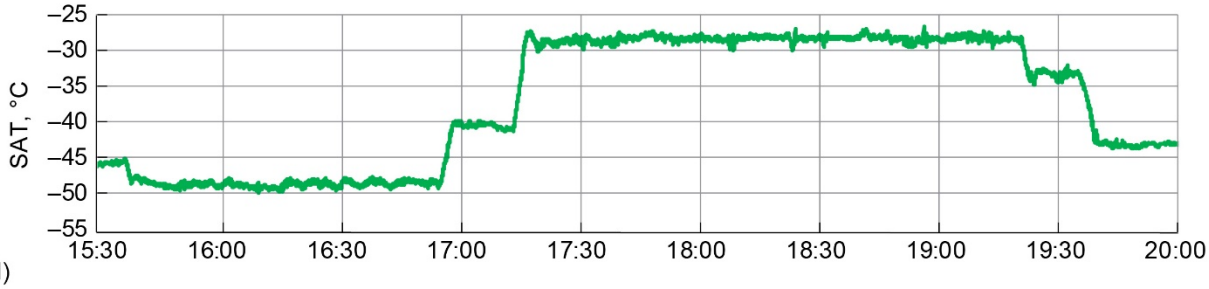

(d)

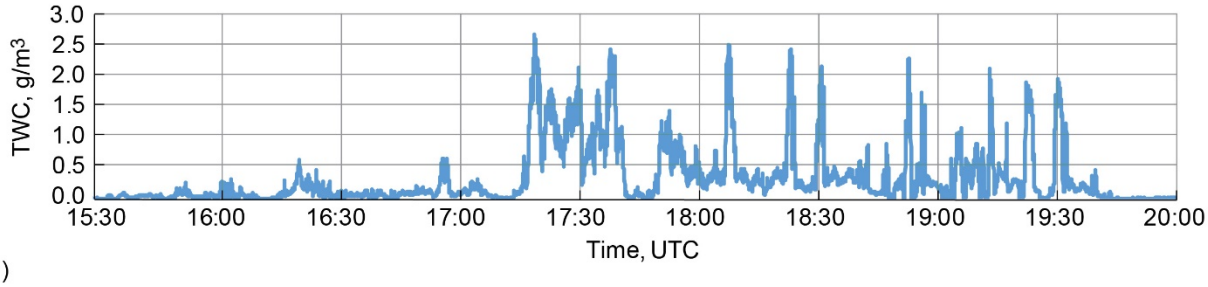

(e)

Figure 40.—August 21, 2015, flight track overlay on infrared (IR) satellite image and select time histories. (a) DC–8 flight track. TROPT/PINK = tropopause temperature. (b) Isokinetic Probe (IKP2) total water content (TWC) 5 s average versus static air temperature (SAT). (c) Pressure altitude (IWG1). (d) SAT (IWG1). (e) IKP2 TWC.

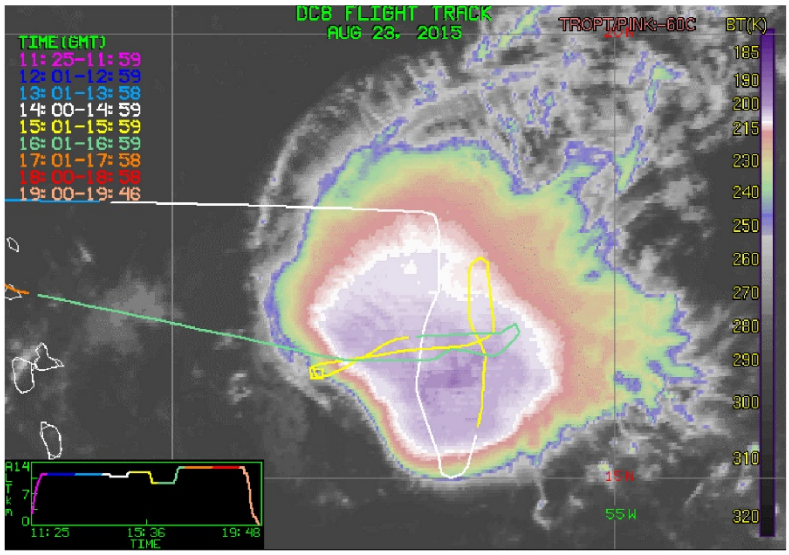

(a)

Flight Date	8/23/2015	
Flight Hours	8.7	
Tropical Storm Danny		
# Tracks	Alt., kft	SAT, °C
2	37.0	–49.1
1	34.0	–40.6
2	29.0	–28.4

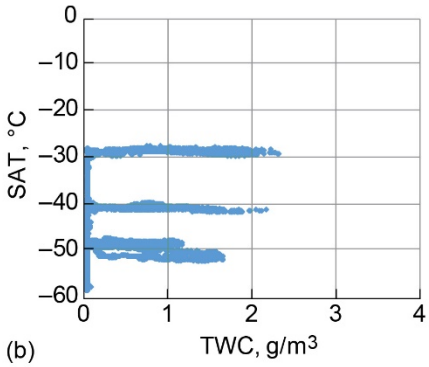

(b)

(c)

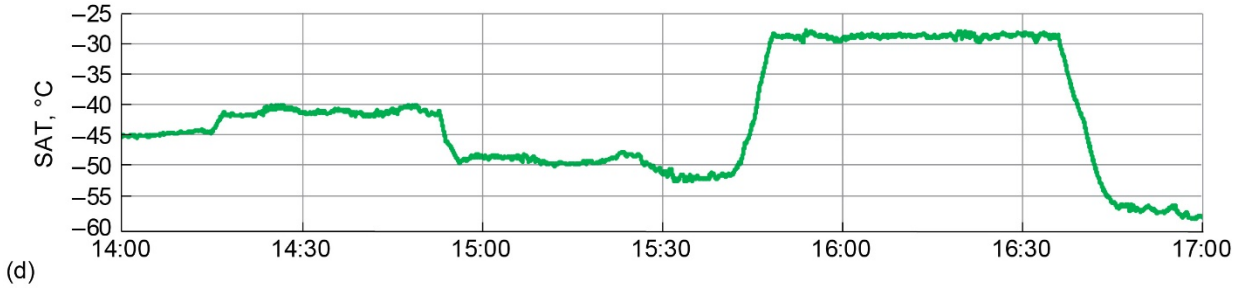

(d)

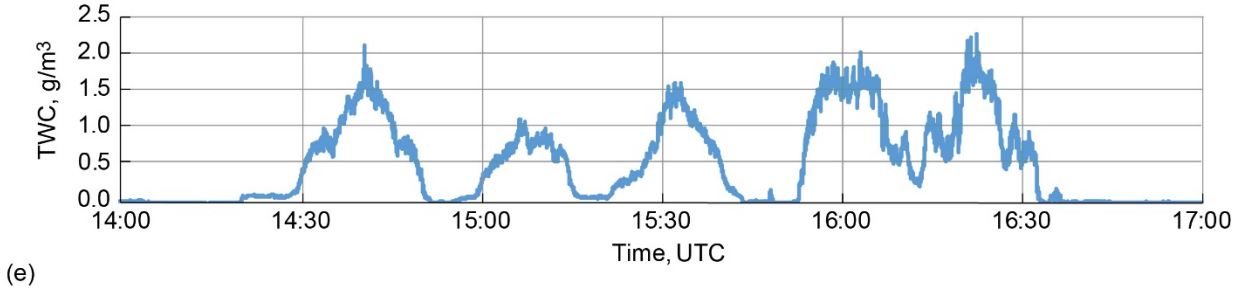

(e)

Figure 41.—August 23, 2015, flight track overlay on infrared (IR) satellite image and select time histories. (a) DC–8 flight track. TROPT/PINK = tropopause temperature. (b) Isokinetic Probe (IKP2) total water content (TWC) 5 s average versus static air temperature (SAT). (c) Pressure altitude (IWG1). (d) SAT (IWG1). (e) IKP2 TWC.

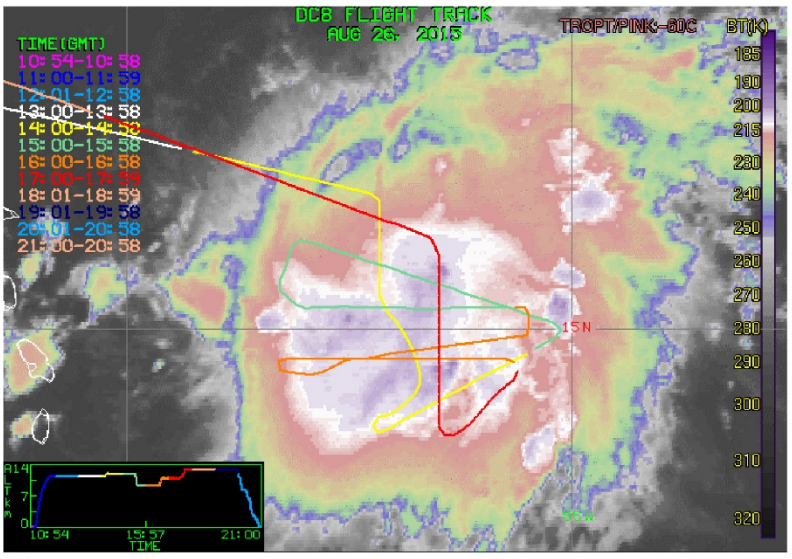

(a)

Flight Date	8/26/2015
Flight Hours	10.1

# Tracks	Alt., kft	SAT, °C
3	37.0	–48.1
3	34.0	–39.6
2	29.1	–27.2

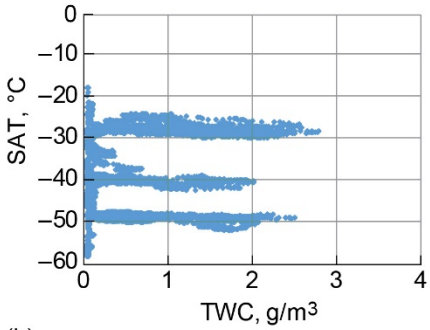

(b)

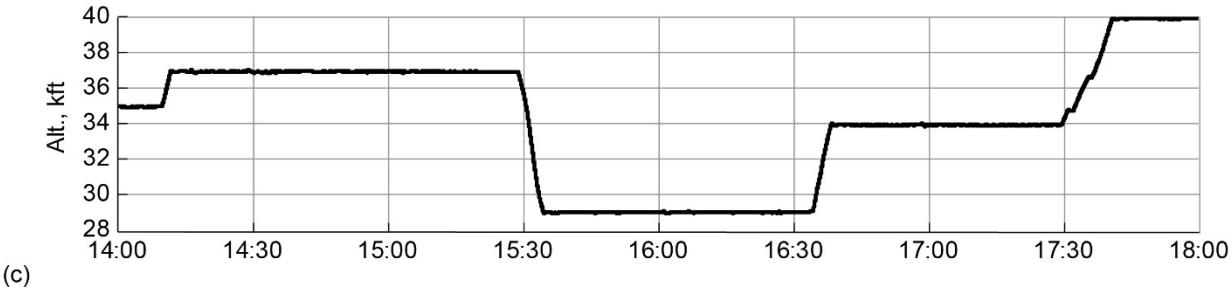

(c)

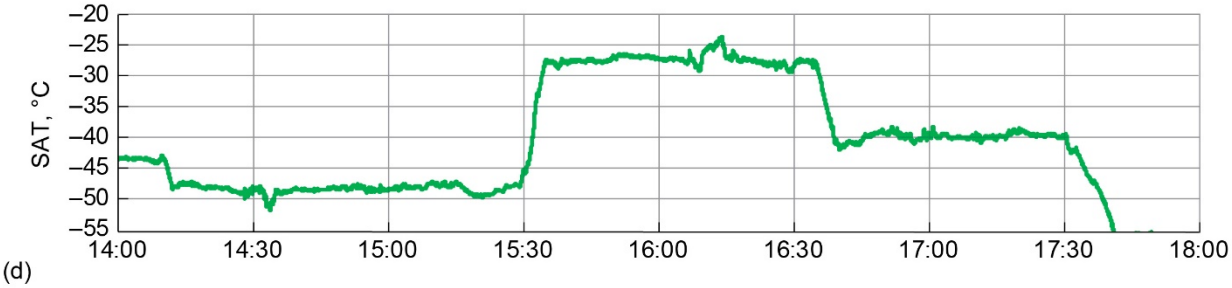

(d)

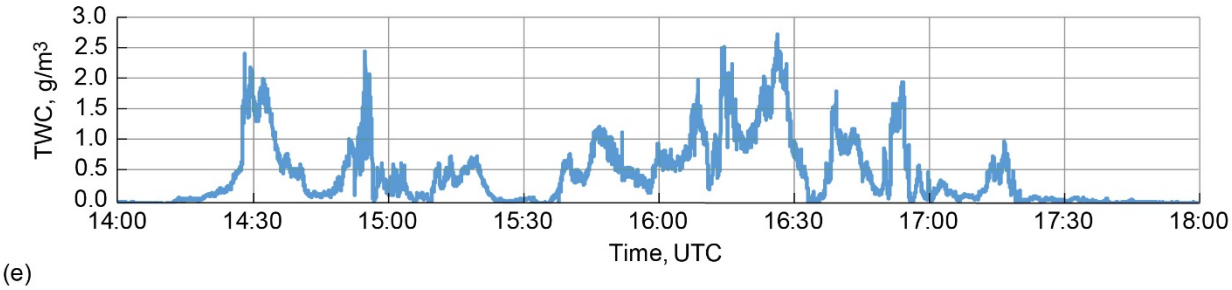

(e)

Figure 42.—August 26, 2015, flight track overlay on infrared (IR) satellite image and select time histories. (a) DC–8 flight track. TROPT/PINK = tropopause temperature. (b) Isokinetic Probe (IKP2) total water content (TWC) 5 s average versus static air temperature (SAT). (c) Pressure altitude (IWG1). (d) SAT (IWG1). (e) IKP2 TWC.

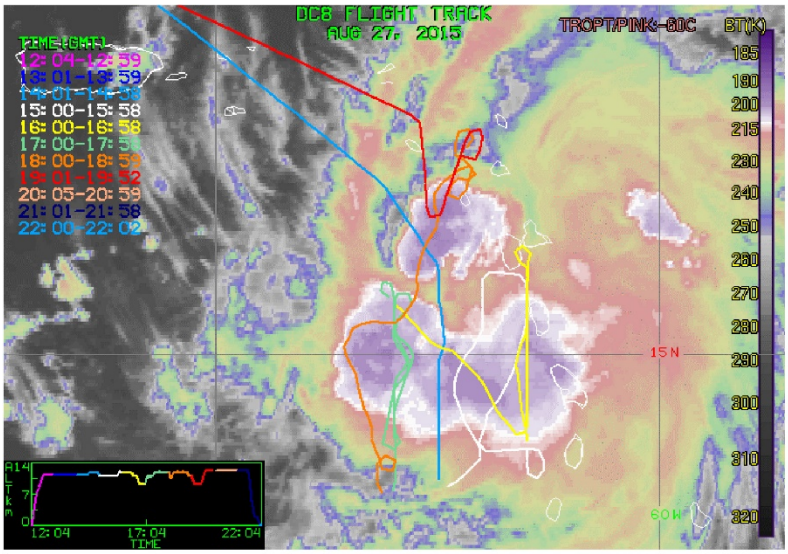

(a)

Flight Date	8/27/2015
Flight Hours	10.3

# Tracks	Alt., kft	SAT, °C
6	37.0	–47.8
4	34.0	–39.9
3	29.0	–27.5

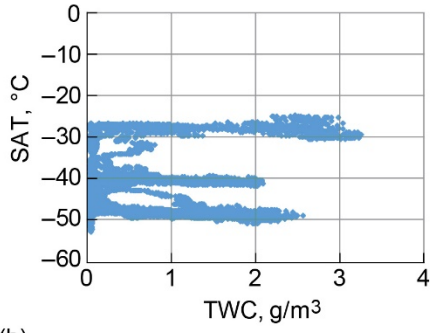

(b)

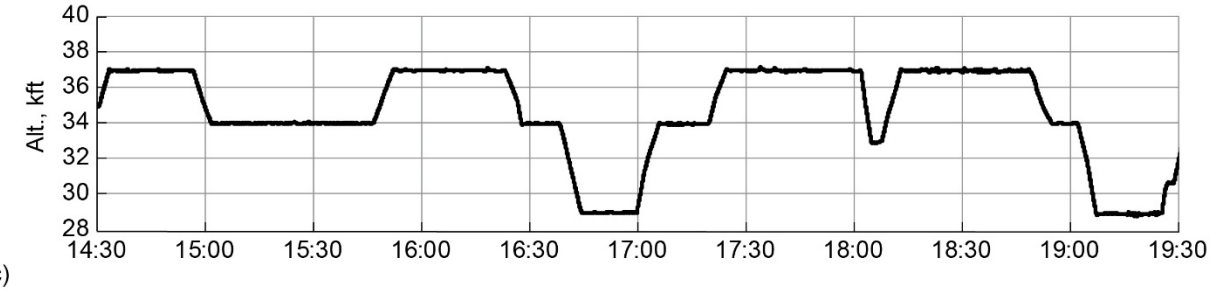

(c)

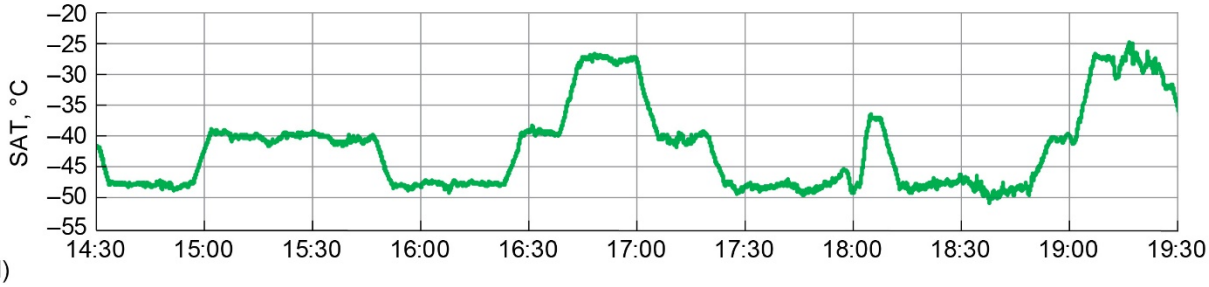

(d)

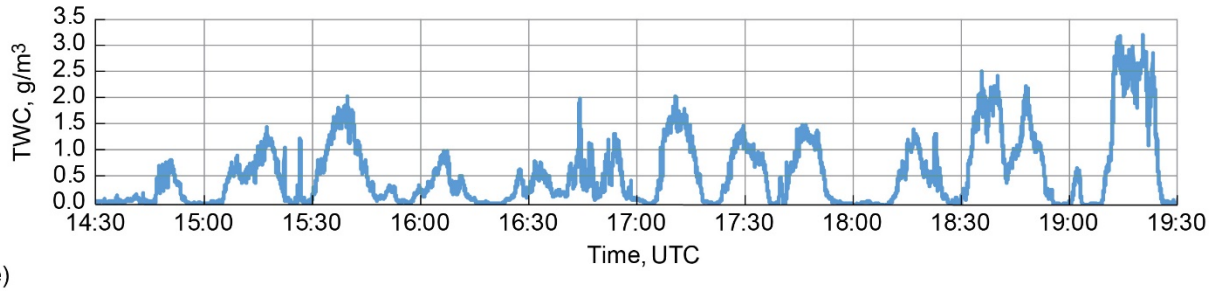

(e)

Figure 43.—August 27, 2015, flight track overlay on infrared (IR) satellite image and select time histories. (a) DC–8 flight track. TROPT/PINK = tropopause temperature. (b) Isokinetic Probe (IKP2) total water content (TWC) 5 s average versus static air temperature (SAT). (c) Pressure altitude (IWG1). (d) SAT (IWG1). (e) IKP2 TWC.

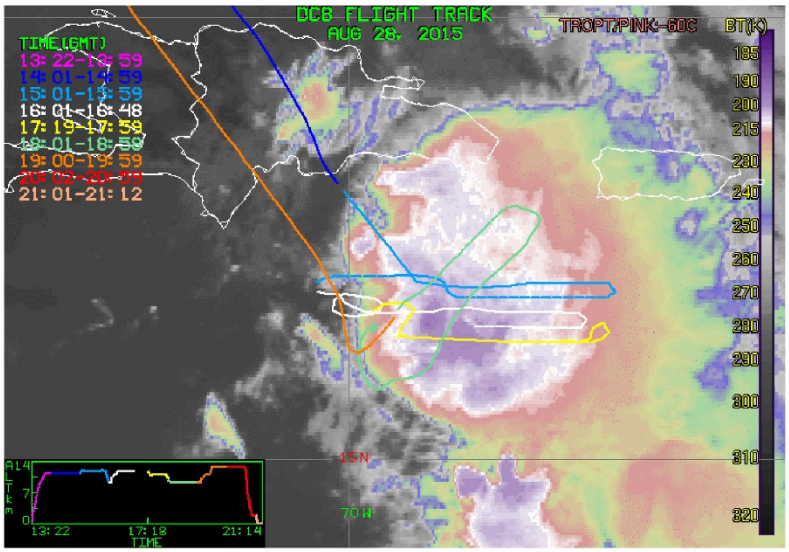

(a)

Flight Date	8/28/2015	
Flight Hours	8.1	
Tropical Storm Erika		
# Tracks	Alt., kft	SAT, °C
5	36.9	–48.0
1	34.0	–39.7
2	29.0	–27.7

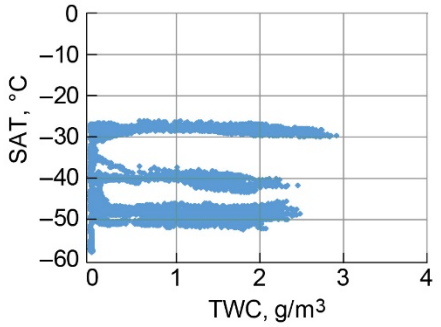

(b)

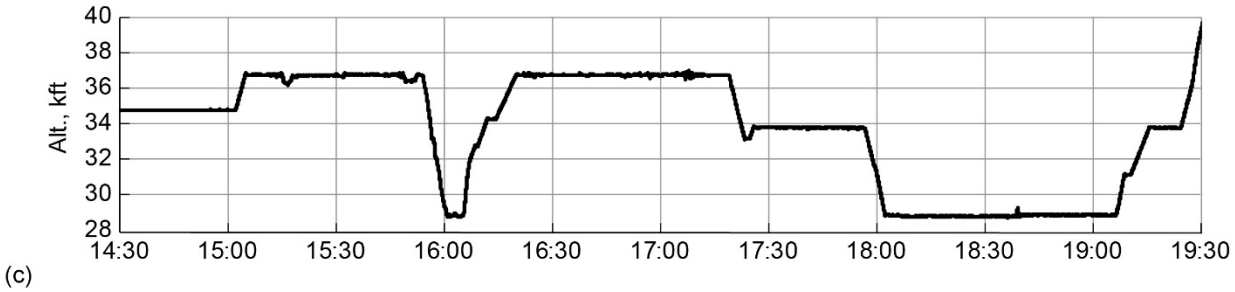

(c)

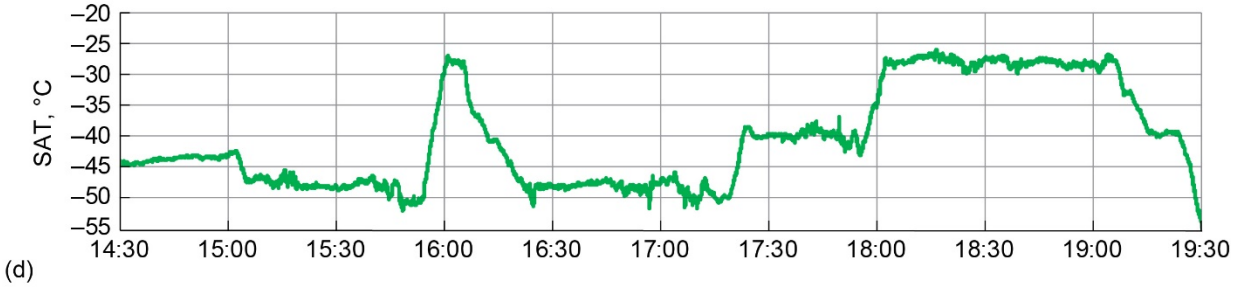

(d)

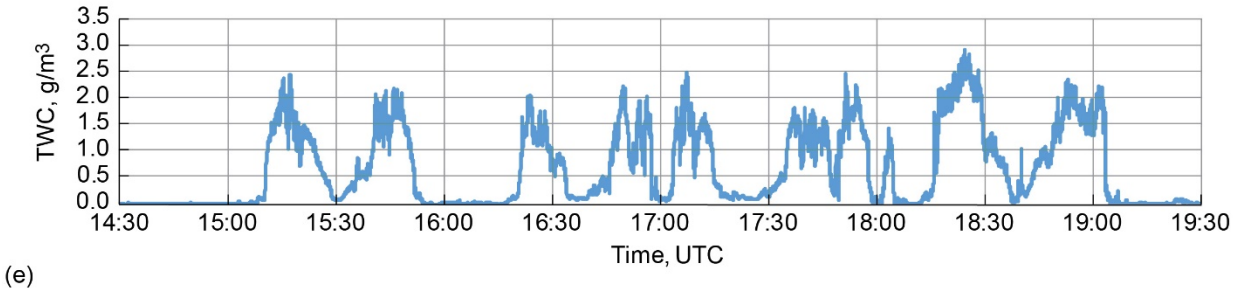

(e)

Figure 44.—August 28, 2015, flight track overlay on infrared (IR) satellite image and select time histories. (a) DC–8 flight track. TROPT/PINK = tropopause temperature. (b) Isokinetic Probe (IKP2) total water content (TWC) 5 s average versus static air temperature (SAT). (c) Pressure altitude (IWG1). (d) SAT (IWG1). (e) IKP2 TWC.

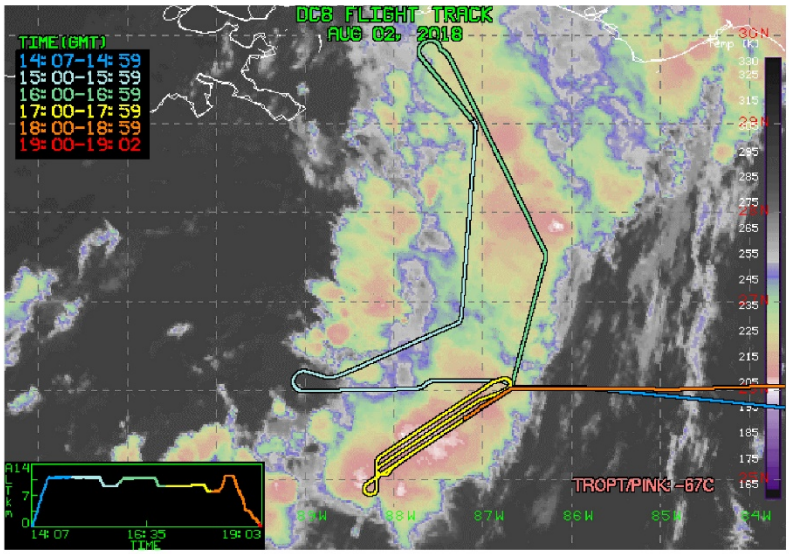

(a)

Flight Date	8/2/2018
Flight Hours	4.9

# Tracks	Alt., kft	SAT, °C
2	34.0	–40.6
2	33.3	–38.7
1	29.0	–27.8
3	28.0	–25.4
1	24.7	–18.0

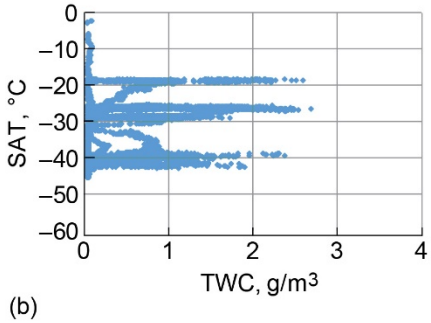

(b)

(c)

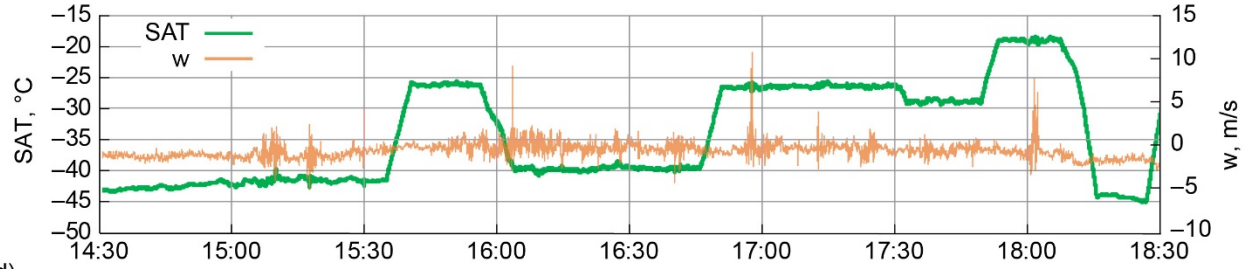

(d)

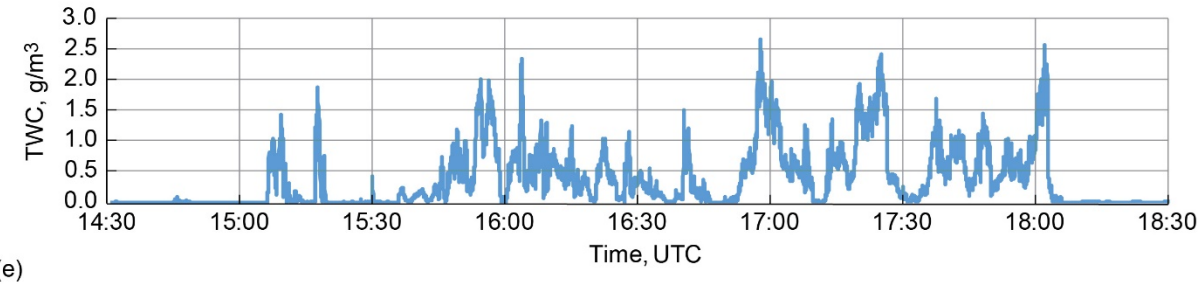

(e)

Figure 45.—August 2, 2018, flight track overlay on infrared (IR) satellite image and select time histories. (a) DC–8 flight track. TROPT/PINK = tropopause temperature. (b) Isokinetic Probe (IKP2) total water content (TWC) 5 s average versus static air temperature (SAT). (c) Pressure altitude using the meteorological measurement system (MMS). (d) SAT and updraft velocity (MMS). (e) IKP2 TWC.

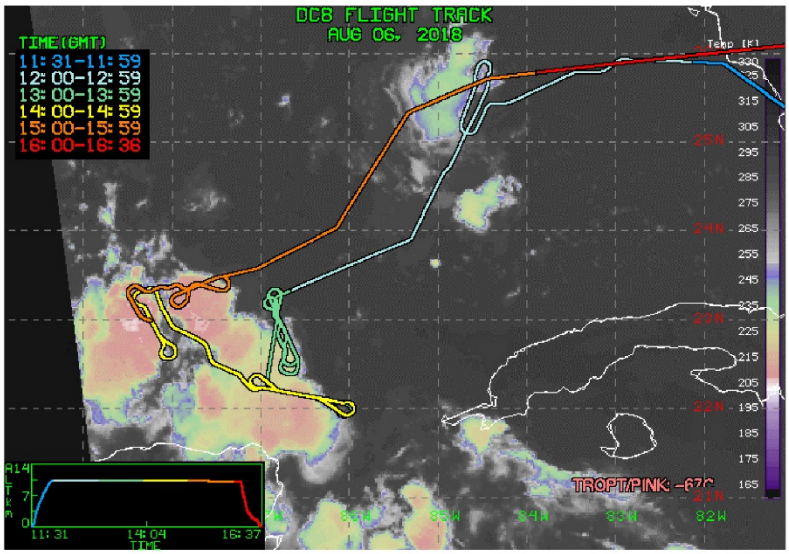

(a)

Flight Date	8/6/2018
Flight Hours	5.1

# Tracks	Alt., kft	SAT, °C
14	31.9	–36.9

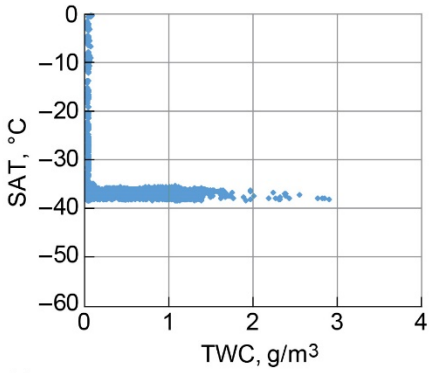

(b)

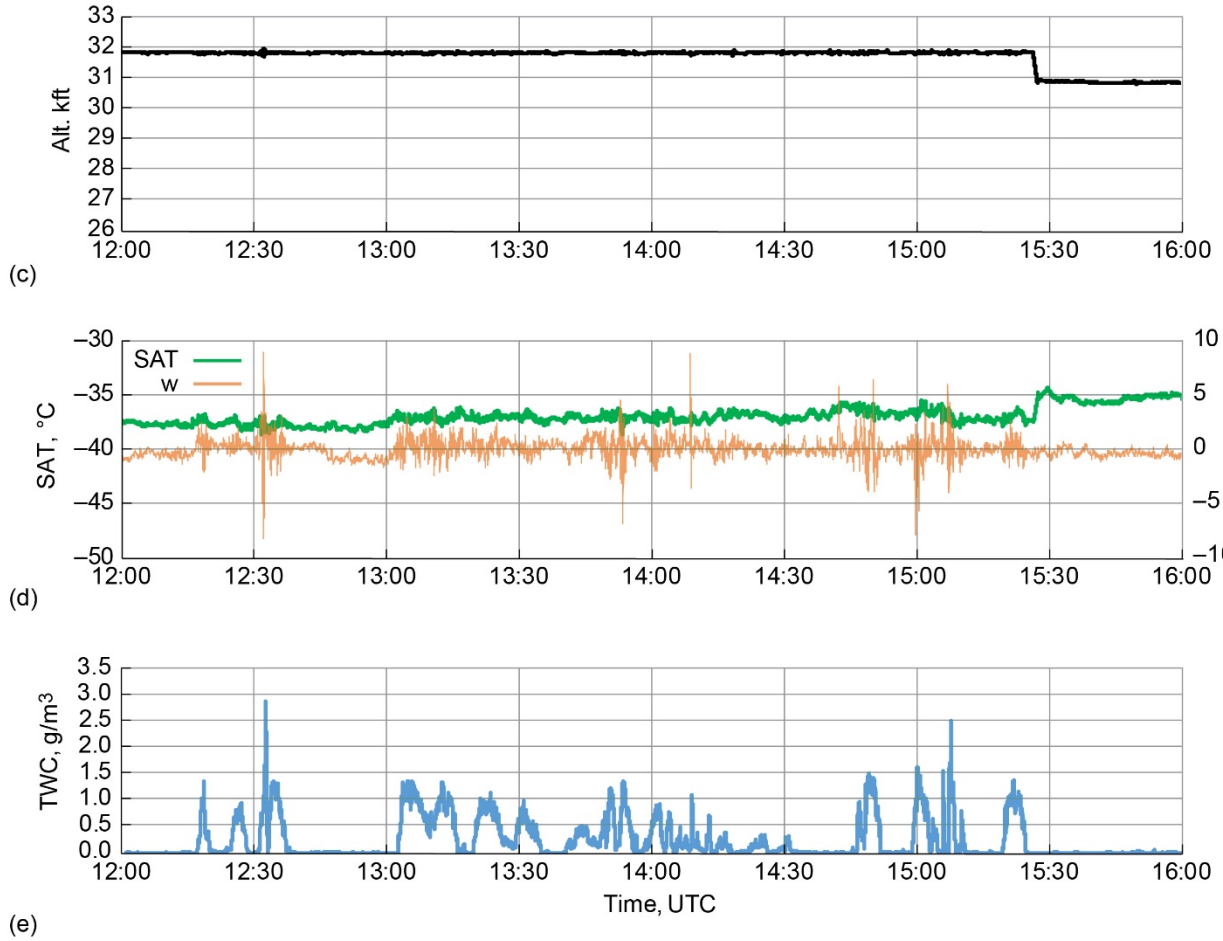

(c)

(d)

(e)

Figure 46.—August 6, 2018, flight track overlay on infrared (IR) satellite image and select time histories. (a) DC–8 flight track. TROPT/PINK = tropopause temperature. (b) Isokinetic Probe (IKP2) total water content (TWC) 5 s average versus static air temperature (SAT). (c) Pressure altitude using the meteorological measurement system (MMS). (d) SAT and updraft velocity (MMS). (e) IKP2 TWC.

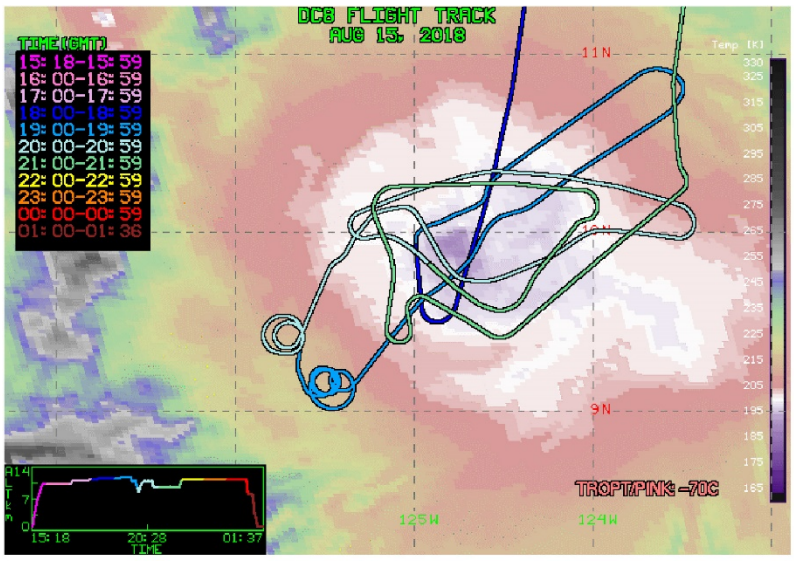

(a)

Flight Date	8/15/2018
Flight Hours	10.1

Tropical Depression 14–E

# Tracks	Alt., kft	SAT, °C
3	36.1	–45.2
2	34.0	–39.0
7	30.1	–28.7

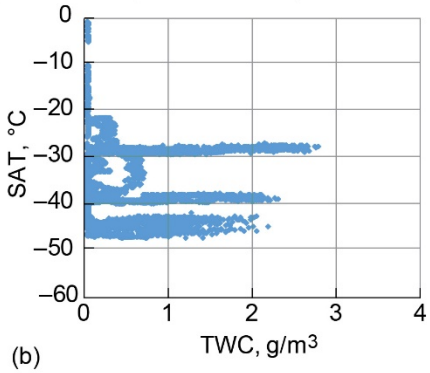

(b)

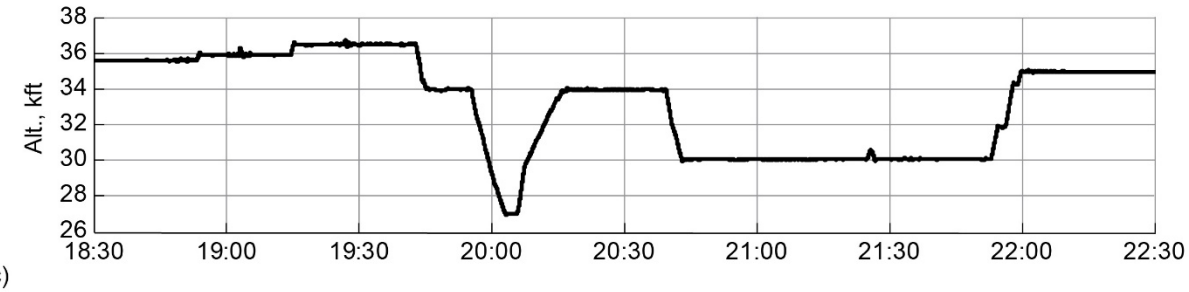

(c)

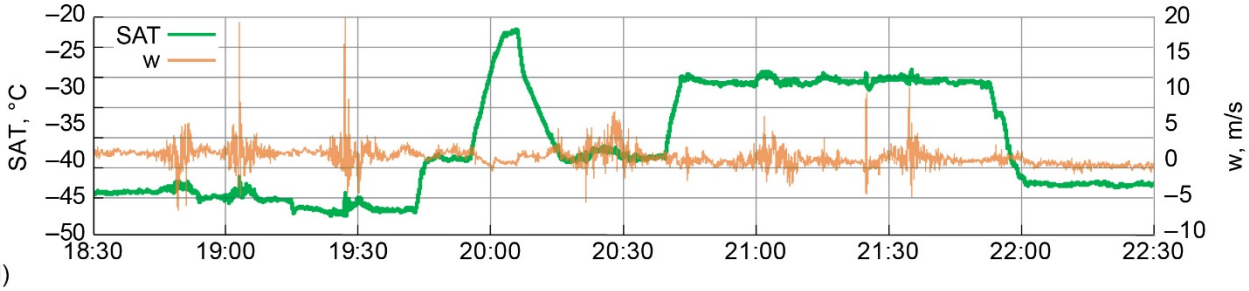

(d)

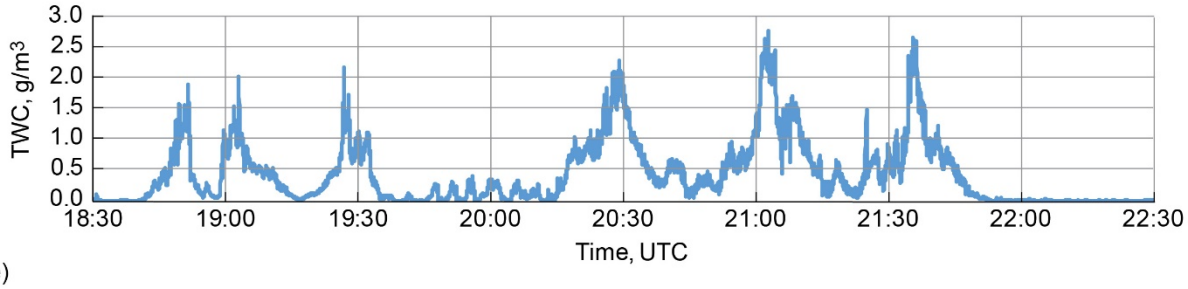

(e)

Figure 47.—August 15, 2018, flight track overlay on infrared (IR) satellite image and select time histories. (a) DC–8 flight track. TROPT/PINK = tropopause temperature. (b) Isokinetic Probe (IKP2) total water content (TWC) 5 s average versus static air temperature (SAT). (c) Pressure altitude using the meteorological measurement system (MMS). (d) SAT and updraft velocity (MMS). (e) IKP2 TWC.

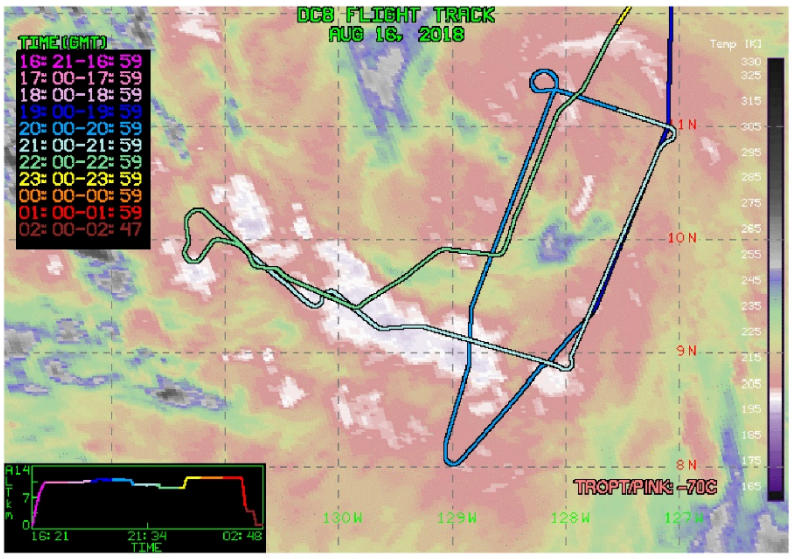

(a)

Flight Date	8/16/2018	
Flight Hours	10.1	
Tropical Storm Lane		
# Tracks	Alt., kft	SAT, °C
2	33.9	–38.8
3	30.3	–29.2
3	28.2	–23.9

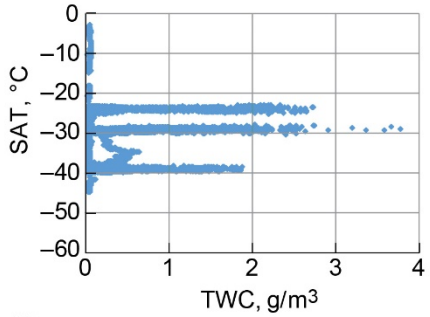

(b)

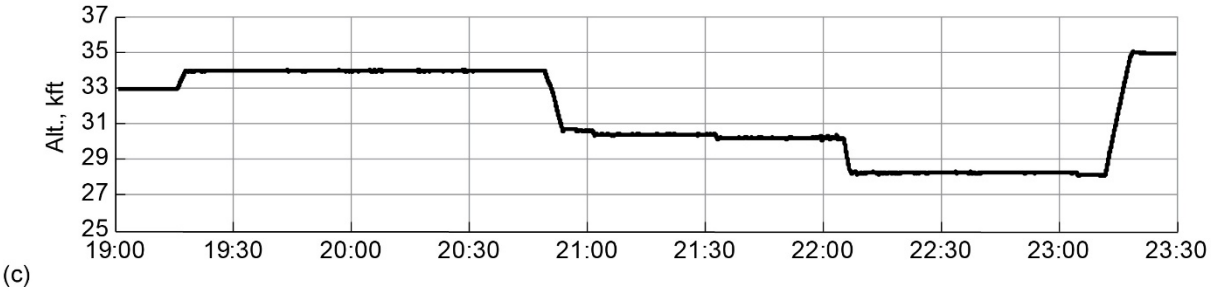

(c)

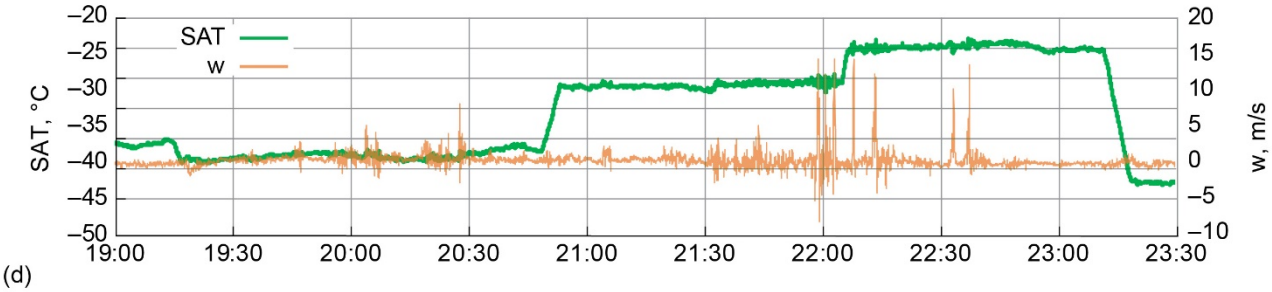

(d)

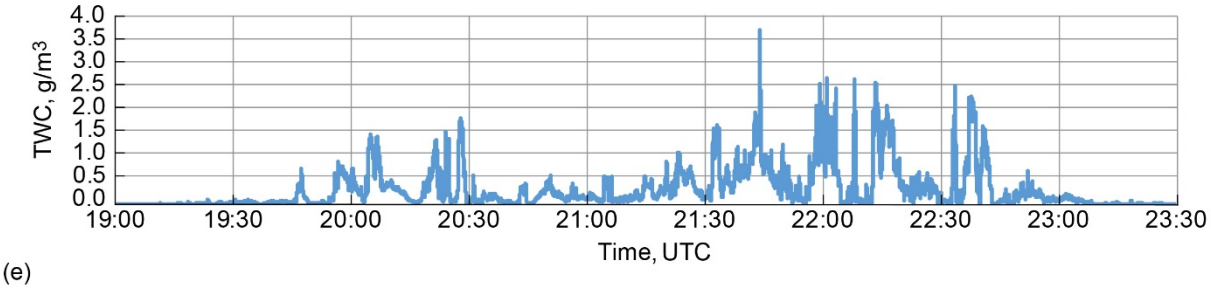

(e)

Figure 48.—August 16, 2018, flight track overlay on infrared (IR) satellite image and select time histories. (a) DC–8 flight track. TROPT/PINK = tropopause temperature. (b) Isokinetic Probe (IKP2) total water content (TWC) 5 s average versus static air temperature (SAT). (c) Pressure altitude using the meteorological measurement system (MMS). (d) SAT and updraft velocity (MMS). (e) IKP2 TWC.

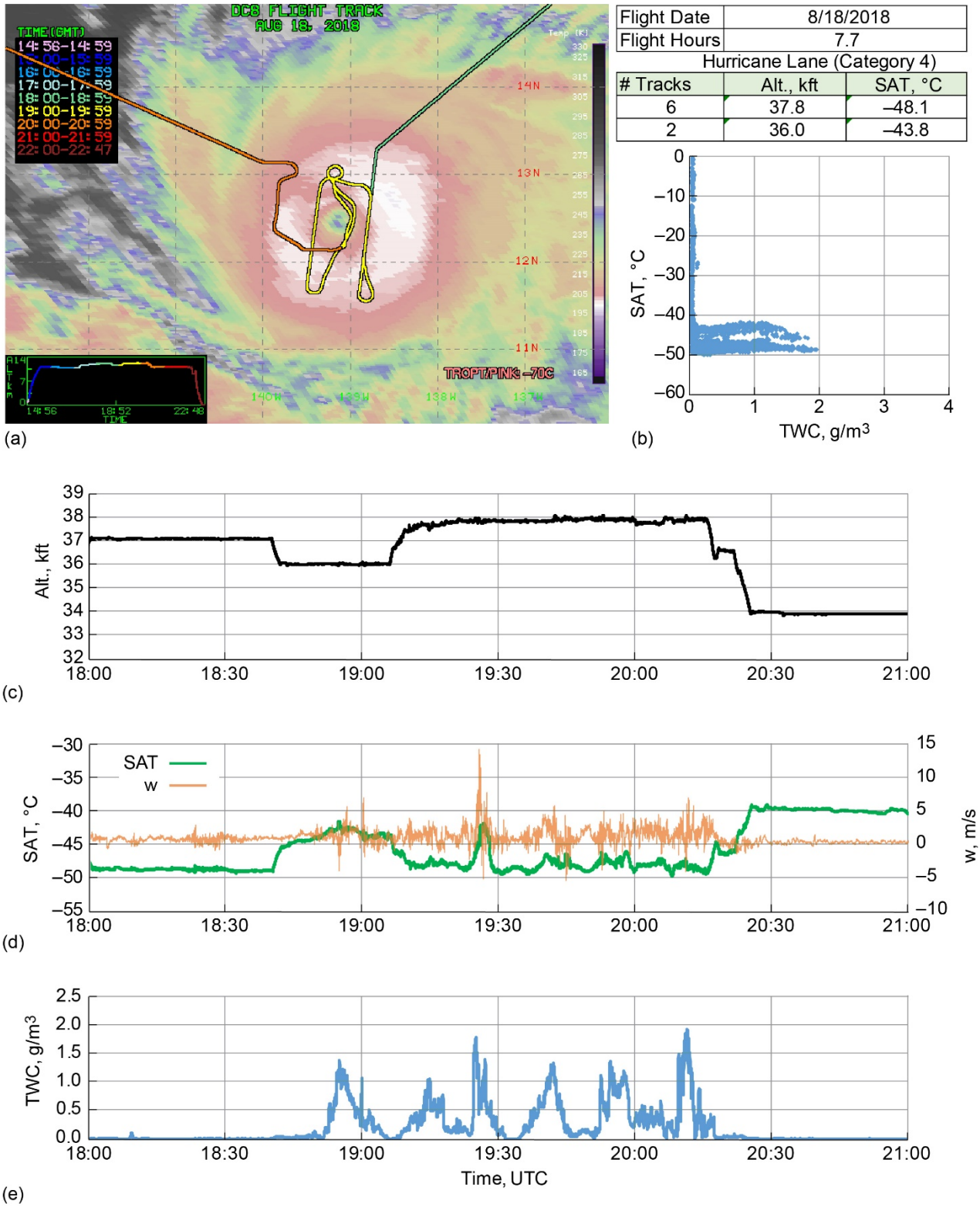

Figure 49.—August 18, 2018, flight track overlay on infrared (IR) satellite image and select time histories. (a) DC–8 flight track. TROPT/PINK = tropopause temperature. (b) Isokinetic Probe (IKP2) total water content (TWC) 5 s average versus static air temperature (SAT). (c) Pressure altitude using the meteorological measurement system (MMS). (d) SAT and updraft velocity (MMS). (e) IKP2 TWC.

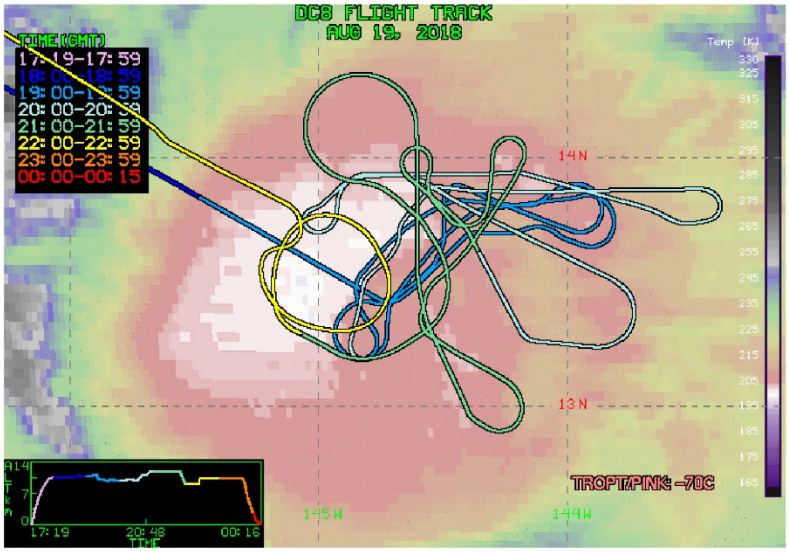

(a)

Flight Date	8/19/2018	
Flight Hours	6.9	
Hurricane Lane (Category 3)		
# Tracks	Alt., kft	SAT, °C
8	36.9	–45
4	34.2	–38
8	31.0	–29
4	28.6	–22

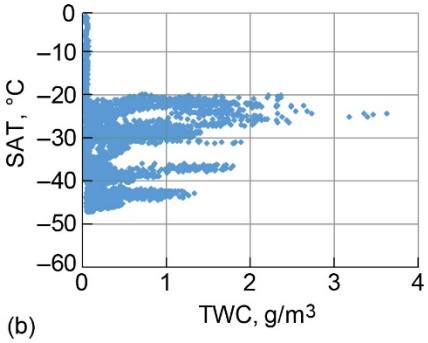

(b)

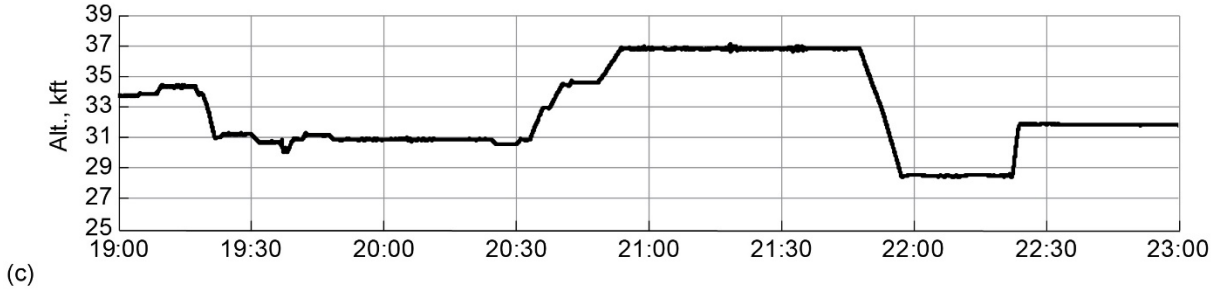

(c)

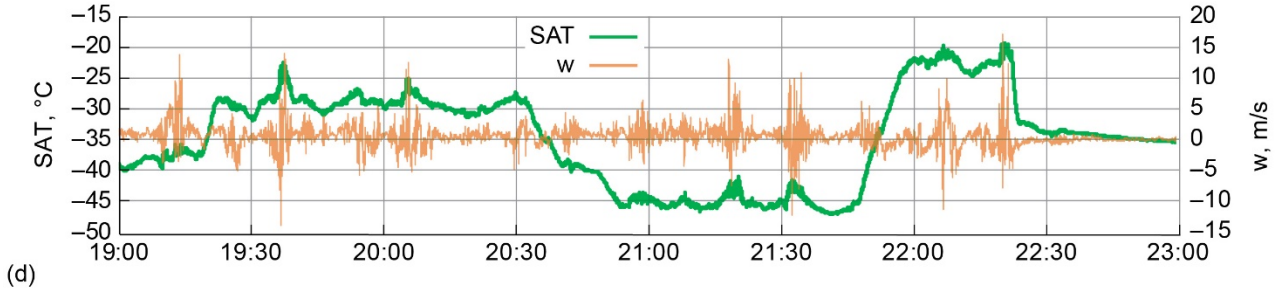

(d)

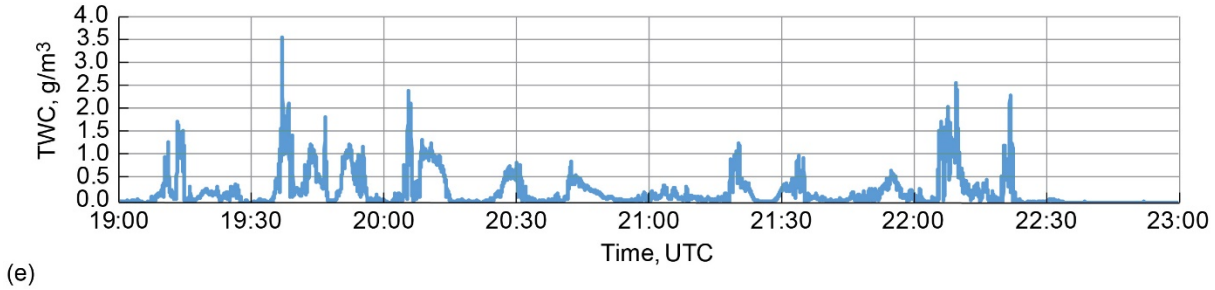

(e)

Figure 50.—August 19, 2018, flight track overlay on infrared (IR) satellite image and select time histories. (a) DC–8 flight track. TROPT/PINK = tropopause temperature. (b) Isokinetic Probe (IKP2) total water content (TWC) 5 s average versus static air temperature (SAT). (c) Pressure altitude using the meteorological measurement system (MMS). (d) SAT and updraft velocity (MMS). (e) IKP2 TWC.

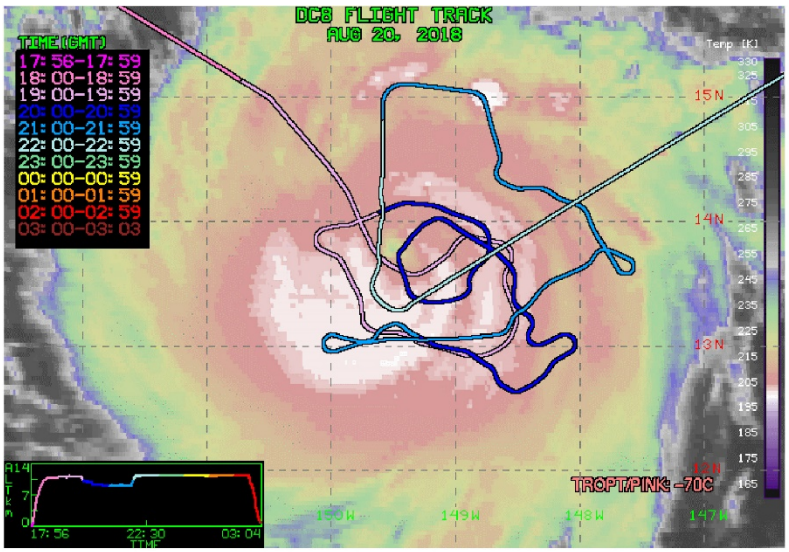

(a)

Flight Date	8/20/2018	
Flight Hours	9.2	
Hurricane Lane (Category 4)		
# Tracks	Alt., kft	SAT, °C
2	34.9	–38.9
3	34.2	–38.1
4	31.0	–28.9
3	29.2	–24.4
8	28.5	–23.6

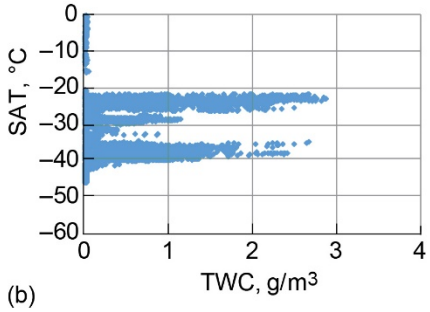

(b)

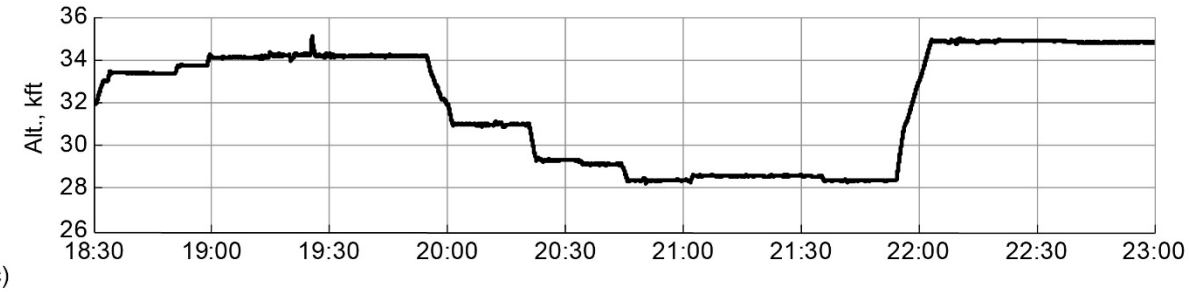

(c)

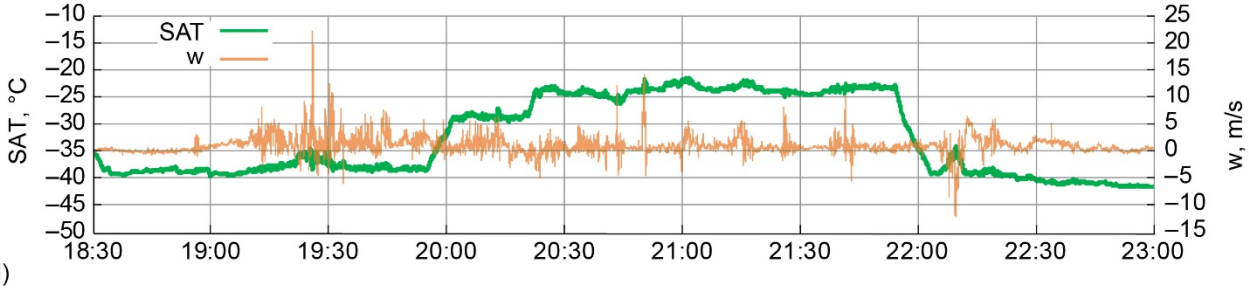

(d)

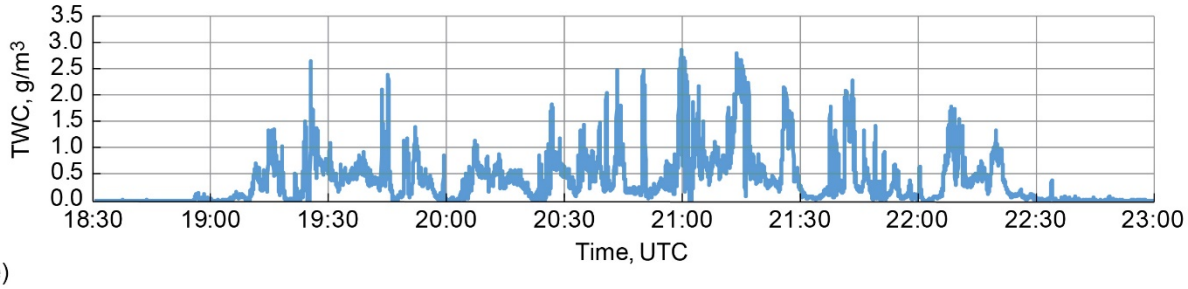

(e)

Figure 51.—August 20, 2018, flight track overlay on infrared (IR) satellite image and select time histories. (a) DC–8 flight track. TROPT/PINK = tropopause temperature. (b) Isokinetic Probe (IKP2) total water content (TWC) 5 s average versus static air temperature (SAT). (c) Pressure altitude using the meteorological measurement system (MMS). (d) SAT and updraft velocity (MMS). (e) IKP2 TWC.

Appendix B.—Nomenclature

2D–S	two-dimensional stereo
3D	three dimensional
ADC	air data computer
ALPHA	Algorithm for the Prediction of HIWC Areas
ARAC	Aviation Rulemaking Advisory Committee
ATC	air traffic control
BHS	background humidity system
CDP–2	Cloud Droplet Probe (DMT)
CFR	Code of Federal Regulations
CS	certification specification
DLH	diode laser hygrometer
DMT	Droplet Measurement Technologies
EASA	European Aviation Safety Agency
EDT	eastern daylight time
EHWG	Engine Harmonization Working Group
EUROCAE	European Organization for Civil Aviation Equipment
FAA	Federal Aviation Administration
FAR	false alarm rate
FIR	flight information regions
GOES	Geostationary Operational Environmental Satellites
GPS	Global Positioning System
HAIC	high altitude ice crystal
HIWC	high ice water content
I&Q	in-phase and quadrature
IAS	indicated airspeed
I_D	index of dispersion
IKP2	Isokinetic Probe (SEA)
IR	infrared
IWC	ice water content
KFLL	Fort Lauderdale-Hollywood International Airport
KPMD	Palmdale Regional Airport
LIDAR	Light Detection and Ranging
LWC	liquid water content
MCS	mesoscale convective system
MMS	meteorological measurement system
MOPS	minimum operational performance standards
MSD	mass size distribution
NCAR	National Center for Atmospheric Research
NEXRAD	next generation weather radar
NOAA	National Oceanic and Atmospheric Administration
NRC	National Research Council Canada
OID	optical ice detector (Collins Aerospace)
PIP	precipitation imaging probe (DMT)

POD	probability of detection
PPI	plan position indicator
PSD	particle size distribution
RASTA	radar system airborne
R–IWC	radar-identified ice water content
RRF	radar reflectivity factor
RTCA	Radio Technical Communications for Aeronautics
SAFIRE	Service des Avions Français Instrumentés pour la Recherche en Environnement
SAT	static air temperature
SC	subcommittee
SEA	Science Engineering Associates, Inc.
SLD	supercooled large drop
SP2	HAIC subproject 2
SPEC	Stratton Park Engineering Company
TAT	total air temperature
TWC	total water content
WG	working group
WVSS–II	Water Vapor Sensing System (SpectraSensors)

References

1. Mazzawy, Robert S.; and Strapp J. Walter: Appendix D—An Interim Icing Envelope. SAE Transactions Journal of Aerospace, vol. 116, 2007, pp. 634–642.
2. Mason, Jeanne G.; Strapp, J. Walter; and Chow, Philip: The Ice Particle Threat to Engines in Flight. AIAA 2006–206, 2006.
3. Mixed-Phase/Glaciated Icing Technology Plan. Version 1.1, Engine Harmonization Working Group, 2005.
4. Strapp, J.W., et al.: The High Ice Water Content Study of Deep Convective Clouds: Report on Science and Technical Plan. DOT/FAA/TC–14/31, 2016. http://www.tc.faa.gov/its/worldpac/techrpt/tc14-31.pdf Accessed Sept. 20, 2019.
5. Dezitter, Fabien, et al.: HAIC—High Altitude Ice Crystals. AIAA 2013–2674, 2013.
6. Leroy, D., et al.: Ice Crystal Sizes in High Ice Water Content Clouds. Part I: On the Computation of Median Mass Diameter From In Situ Measurements. J. Atmos. Ocean. Technol., vol. 33, 2016, pp. 2461–2476.
7. Leroy, D., et al.: Ice Crystal Sizes in High Ice Water Content Clouds. Part II: Statistics of Mass Diameter Percentiles in Tropical Convection Observed During the HAIC/HIWC Project. J. Atmos. Ocean. Technol., vol. 34, 2017, pp. 117–136.
8. Protat, A., et al.: The Measured Relationship Between Ice Water Content and Cloud Radar Reflectivity in Tropical Convective Clouds. J. Appl. Meteor. Climatol., vol. 55, 2016, pp. 1707–1729.
9. Strapp, J.W., et al.: Isokinetic TWC Evaporator Probe: Development of the IKP2 and Performance Testing for the HAIC–HIWC Darwin 2014 and Cayenne Field Campaigns. AIAA 2016–4059, 2016.
10. Davison, Craig R., et al.: Isokinetic TWC Evaporator Probe: Calculations and Systemic Uncertainty Analysis. AIAA 2016–4060, 2016.
11. Korolev, Alexie; Emery, Edward; and Creelman, Kirk: Modification and Tests of Particle Probe Tips to Mitigate Effects of Ice Shattering. J. Atmos. Oceanic Technol., vol. 30, 2013, pp. 690–708.
12. Korolev, A., et al.: Small Ice Particles in Tropospheric Clouds: Fact or Artifact? Airborne Icing Instrumentation Evaluation Experiment. Bull. Amer. Met. Soc., vol. 92, no. 8, 2011, pp. 967–973.
13. Bedka, Kristopher M.; and Khlopenkov, Konstantin: A Probabilistic Multispectral Pattern Recognition Method for Detection of Overshooting Cloud Tops Using Passive Satellite Imager Observations. J. Appl. Meteor. Climatol., vol. 55, 2016, pp. 1983–2005.
14. NASA Langley Satellite Support for High Ice Water Content (HIWC) Radar 2015 FL Campaign. 2015. https://cloudsway2.larc.nasa.gov/cgi-bin/site/showdoc?docid=4&cmd=field-experiment-homepage&exp=HIWC-PR-2015 Accessed Feb. 28, 2019.
15. Duviver, Eric: High Altitude Icing Environment. International Air Safety and Climate Change Conference, Cologne, Germany, 2010. https://www.easa.europa.eu/conferences/iascc/doc/Workshop%201%20Presentations/Workshop1_DAY%202/1_Duvivier_EASA/IASCC_E%20Duvivier.pdf Accessed Sept. 25, 2019.
16. Lawson, R. Paul; Angus, Leigh J.; and Heymsfield, Andrew J.: Cloud Particle Measurements in Thunderstorm Anvils and Possible Weather Threat to Aviation. J. Aircraft, vol. 35, no. 1, 1998, pp. 113–121.
17. Harrah, S., et al.: Radar Detection of High Concentrations of Ice Particles—Methodology and Preliminary Flight Test Results. SAE Technical Paper 2019–01–2028 (NASA/TP—2019-220433 and DOT/FAA/TC–19/29), 2019. http://ntrs.nasa.gov

18. National Center for Atmospheric Research: HIWC–RADAR: High Ice Water Content (HIWC) Radar Study 2015. https://data.eol.ucar.edu/project/HIWC-RADAR Accessed Feb. 28, 2019.
19. National Center for Atmospheric Research: HIWC–RADAR: High Ice Water Content (HIWC) Radar Study 2018. http://data.eol.ucar.edu/project/HIWC-RADAR-2018 Accessed Feb. 28, 2019.
20. Feasibility Study: Weather Radar for Ice Crystal Detection. EUROCAE WG95, Long-Range Awareness Subgroup, RTCA SC–230, 2017.
21. Strapp, J.W., et al.: An Assessment of Cloud Total Water Content and Particle Size From Flight Test Campaign Measurements in High Ice Water Content, Mixed Phase/Ice Crystal Icing Conditions: Primary In-Situ Measurements. DOT/FAA/TC–18/1, to be published, 2020.
22. Proctor, Fred H., et al.: High Ice Water Concentrations in the 19 August 2015 Coastal Mesoconvective System. AIAA 2017–4370, 2017.
23. Grandin, Alice, et al.: AIRBUS Flight Tests in High Total Water Content Regions. AIAA 2014–2753, 2014.
24. Diskin, Glenn S., et al.: Open-Path Airborne Tunable Diode Laser Hygrometer. Proc. SPIE, vol. 4817, 2002, pp. 196–204.
25. NASA Airborne Science Program: Diode Laser Hygrometer (DLH). 2019. https://airbornescience.nasa.gov/instrument/DLH Accessed Feb. 28, 2019.
26. NASA Meteorological Measurement System. 2018. https://earthscience.arc.nasa.gov/mms Accessed Feb. 28, 2019.
27. Gaines, Steven E., et al.: Comparisons of the NASA ER–2 Meteorological Measurement System With Radar Tracking and Radiosonde Data. J. Atmos. Ocean. Tech., vol. 9, 1992, pp. 210–225.
28. Strapp, J. Walter; MacLeod, James; and Lilie, Lyle L.: Calibration of Ice Water Content in a Wind Tunnel/Engine Test Cell Facility. 15th International Conference on Clouds and Precipitation, Cancun, Mexico, 2008.
29. Lilie, Lyle E.; Sivo, Christopher P.; and Bouley, Daniel B.: Description and Results for a Simple Ice Crystal Detection System for Airborne Applications. AIAA 2016–4058, 2016.
30. Ray, M.; and Anderson, K.: Analysis of Flight Test Results of the Optical Ice Detector. SAE Int. J. Aerosp., vol. 8, no. 1, 2015, pp. 1–8.
31. Anderson, K.J.; and Ray, Mark D.: SLD and Ice Crystal Discrimination With the Optical Ice Detector. SAE Technical Paper 2019–01–1934, 2019.
32. NASA Langley Satellite Support for High Ice Water Content (HIWC) Radar 2018 Campaign. 2018. https://cloudsway2.larc.nasa.gov/cgi-bin/site/showdoc?docid=4&cmd=field-experiment-homepage&exp=HIWC-2018 Accessed Feb. 28, 2019.
33. Yost, Christopher R., et al.: A Prototype Method for Diagnosing High Ice Water Content Probability Using Satellite Imager Data. Atmos. Meas. Tech., vol. 11, no. 3, 2018, pp. 1615–1637.
34. Bedka, K., et al.: Analysis and Automated Detection of Ice Crystal Icing Conditions Using Geostationary Satellite Datasets and In Situ Ice Water Content Measurements. SAE Technical Paper 2019–01–1953, 2019.
35. Rugg, Allyson, et al.: Recent Updates to the Algorithm for the Prediction of High Ice Water Content Areas (ALPHA). Presented at the SAE International Conference on Icing of Aircraft, Engines, and Structures, Minneapolis, MN, 2019.